# Chapter 6

# MOMENT LOADING OF CAISSONS IN SATURATED SAND


## Abstract

This chapter focuses on the study of monotonic and cyclic moment loading of suction caisson foundations installed into saturated sands. Firstly, a water-saturated sand was used to study drained conditions. Results of moment capacity tests under low vertical load from caissons installed by pushing and by suction are presented and compared. Caissons installed by suction had lower moment capacity than caissons installed by pushing. Furthermore, it was observed that more uplift occurred in caissons installed by pushing than in caissons installed by suction. However, no substantial differences in foundation stiffness and plastic deviatoric displacement increments were found. Secondly, a series of moment loading tests in oil-saturated sand were preformed to study the effect of undrained and partially drained conditions. It was found that the caisson moment capacity was drastically reduced under undrained conditions due to large pore pressure build-ups. The caisson moment capacity under partially drained conditions was found to be similar to that under drained conditions due to the presence of suction, especially under tensile or very low vertical loads. The caisson vertical movement observed was small compared with results under drained conditions.

## 6.1 EXPERIMENTS IN WATER-SATURATED SAND

### 6.1.1 Load paths

It has been pointed out in Chapters 3 and 4 that the loading experienced by the soil due to the caisson installation can influence the in-service performance. The results shown in Chapter 5 correspond to caissons installed into dry sand by pushing. The aim of this chapter is to study the performance of caissons installed by suction due to the importance that this installation method may have on the subsequent loading response. Before presenting the experimental results it is useful to show a simple conceptual analysis of the load paths followed by a caisson installed using the two different methods.

Possible load paths in a pushed installation, including subsequent moment loadings, are illustrated in Figure 6.1. It is assumed that drained conditions prevail, however, excess pore pressures (not featured in the figure) can appear even under slow penetration rates ($\dot{h} < 1$ mm/min) in soils with very low permeability ($k < 2{\cdot}10^{-7}$ m/s). The sign of the excess pore pressures developed will depend on the initial specific volume and stress level. For example, in a dense sand the excess pore pressures will be negative, resulting in the short term in the increase of the shear strength and stiffness. Therefore, the penetration resistance will be higher in a dense sand, but higher resistance will imply a better performance once installed and subjected to combined loads during operation.

Figure 6.1(c) depicts the load-penetration curve during pushed installation, also called self-weight or jacking installation. The final caisson penetration at $V_c = V_o$ is prior to subsequent unloading at $V_3 > V_2 > V_1$, resulting in the maximum vertical load which establishes the size of the yield surface, as shown in dashed lines in Figure 6.1(a). Because the unloading reaches a very low value of $V_3$ compared with $V_o$, the yield surface contracts due to relaxation. A moment loading event under constant $V_3$ generates the $\frac{M}{2R} - 2R\theta$ and $w - 2R\theta$ curves as depicted in Figure 6.1(b). The $\frac{M}{2R} - 2R\theta$ curve is at the top, resulting in the highest yield point $\frac{M_y}{2R}$, whilst the $w - 2R\theta$ curve is at the bottom, resulting in zero vertical displacement. Since no vertical movement occurs the resultant flow vector is

parallel to the $\frac{M}{2R}$ and $H$ axis, which is denoted as the parallel point as depicted in Figure 6.1(a). The hardening shown in the $\frac{M}{2R} - 2R\theta$ curves is illustrated in Figure 6.1(a) as an isotropic expansion of the internal yield surface to the external yield surface (dashed line). According to Byrne and Houlsby (2001) this hardening should be attributed to the deviatoric displacements since no vertical displacement occurred.

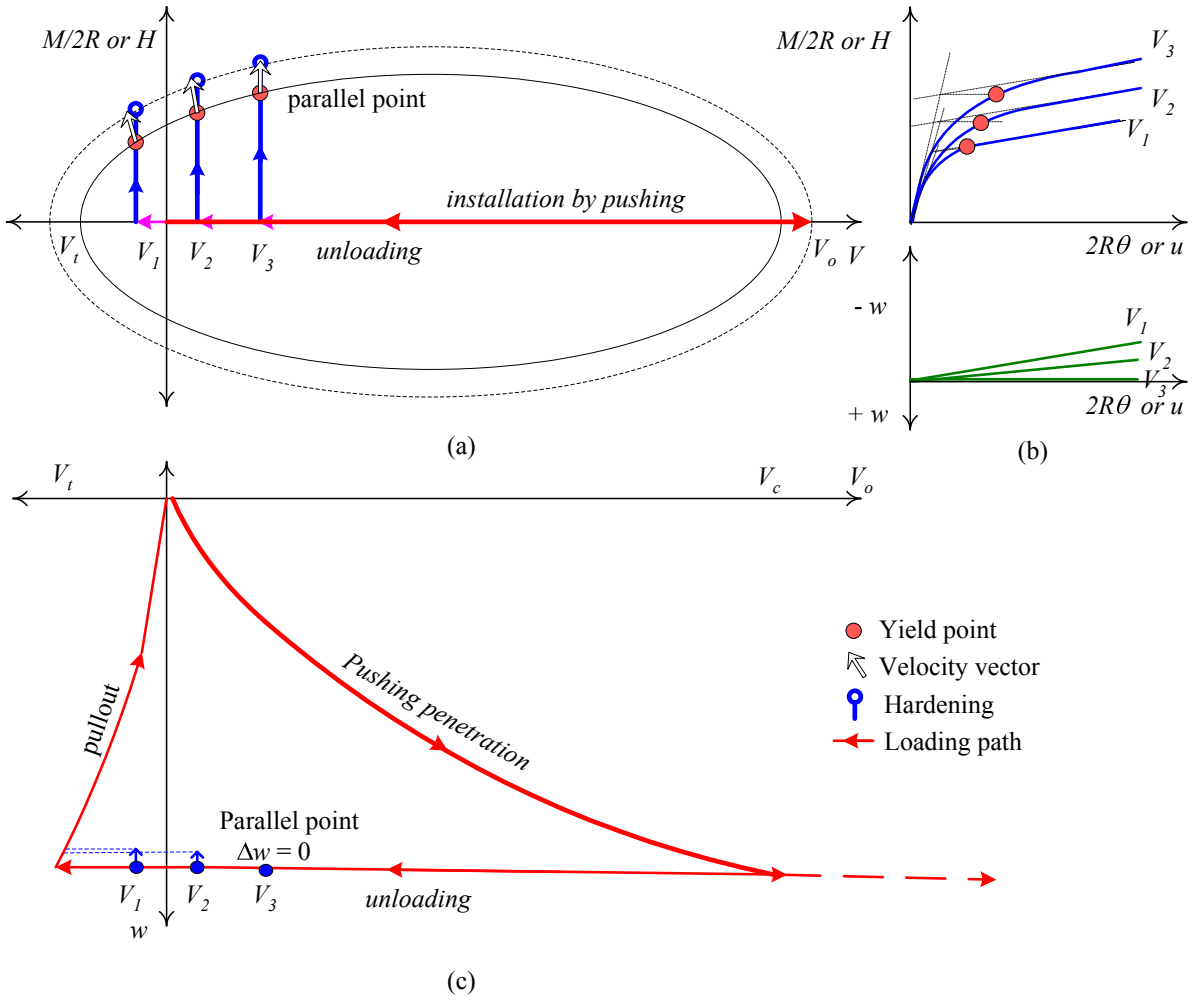


Figure 6.1: Pushing installation: (a) load paths for monotonic moment loading events under low vertical load and the resulting yield surface, (b) load-displacement curves and vertical-rotational displacement curves, and (c) installation curve, including unloading and pullout

Unloading to $V_2 < V_3$ and the subsequent moment loading event under constant $V_2$ results in a lower moment capacity with a reduced value of $\frac{M_y}{2R}$. The $w - 2R\theta$ curve for $V_2$ shows an upward movement of the caisson, resulting in the tilted flow vector on the yield point in Figure 6.1(a). The deviatoric displacements contribution to the hardening is evident since negative vertical displacement (caisson upward movement) generates softening, *i.e.* the contraction of the yield surface.

The last example illustrates the case of unloading to a tensile load $V_1$, followed by a moment loading event under the constant tension $V_1$. The $\frac{M}{2R} - 2R\theta$ curve and $\frac{M_y}{2R}$ value are the lowest and the $w - 2R\theta$ curve is the highest which represents the largest caisson uplift. The hardening assumed based on experimental evidence becomes smaller.

It is important to note that in the pushed installation unloading and the subsequent moment loading event at constant $V'$ is analogous to a triaxial test of a soil sample that is normally consolidated to $p' = p'_o$, unloaded to a certain overconsolidation ratio $\frac{p'}{p'_o}$ and then sheared at a constant $\sigma'_v$. The displacement flow vectors at yield in the footing correspond to the strain flow vectors at yield in the triaxial test. This analogy was first established by Houlsby and Martin (1992) following the work by Tan (1990).

Possible load paths followed by a caisson installed by suction are illustrated in Figure 6.2. The moment loading events are exactly the same as for the pushing installation. However, the $\frac{M}{2R} - 2R\theta$ and $w - 2R\theta$ curves as well as the $\frac{M_y}{2R}$ values are not necessarily identical to those obtained in the pushed installation examples. The load-penetration curve is definitely different since the initial pushed penetration stops at a value that represents the applied self weight (for example $V_2$ or $V_3$). Subsequently, the caisson penetrates assisted by the suction applied inside the caisson compartment. Therefore, $V_o$ becomes a function not only of the vertical displacement, but also of the suction, which defines a surface in the $(V_o, w, s)$ space. This allows penetration at low $V'$ with high suction $s$, but when $s$ reduces $V_o$ increases. In analogy with a triaxial test the foundation is in a normally consolidated condition since $V_o$ has not been experienced by the foundation.

The fluid flow taking place owing to the suction is responsible for the reduced penetration resistance. This is caused by the gradient of excess pore pressures within the soil, which reduces the effective stresses and hence the soil strength. As a consequence, the resulting yield surface is smaller, since at the end of a suction installation $V_o$ is smaller than that at the end of a pushed installation. However, the small yield surface starts to

grow as long as the flow regime ceases. Note that for the suction installed caisson the yield surface will significantly expand due to excess pore pressure dissipation.

Despite the complex changes in effective stresses that occur during the suction assisted penetration, once the combined loading is applied, the caisson can be assumed to have 'recovered' the potential bearing capacity $V_o$ corresponding to the final penetration of a pushed installation (shown in Figure 6.2(c) as the $V_o$ curve with $s = 0$). Whether the recovery is complete or partial will depend mainly on the time given to the excess pore pressures to dissipate. The hypothesis of complete recovery of $V_o$ assumes that modifications in the soil index and mechanical properties due to the suction installation do not affect the value of $V_o$. The validity or not of this hypothesis and its consequences on the

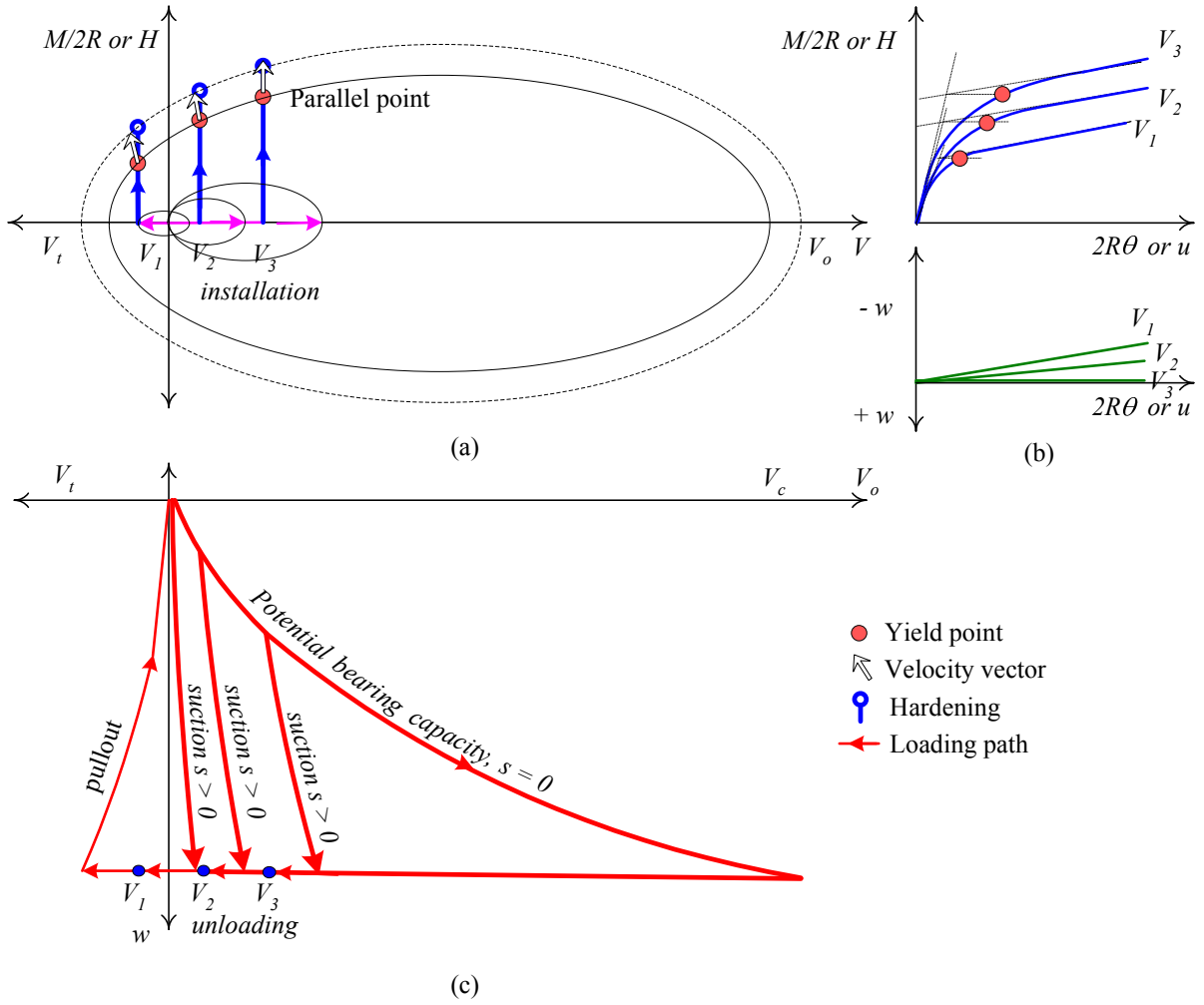


Figure 6.2: Suction installation: (a) load paths for monotonic moment loading events under low vertical load and the resulting yield surface, (b) load-displacement curves and vertical- rotational displacement curves and (c) installation curve, including potential bearing capacity

subsequent caisson response was investigated and presented subsequently.

### 6.1.2 Response of caissons installed by pushing and by suction

The use of dry sands has the advantage of easier and faster sample preparation than if the sand were saturated. This allows a larger number of tests to be carried out at different densities. To mitigate the effects of scale, the tests beds were chosen to be relatively loose as discussed in Chapter 2. However, using pushed installation by applying increasing vertical loads is different from the procedure that has to be used in the field, *i.e.* the suction assisted installation method. The different installation techniques may impose different stress paths on elements of soil around the caisson, which in turn affect the caisson load path as described above. Therefore, it is necessary to carry out experiments similar to those in the dry sand, but on caissons installed by suction, to observe if there are any fundamental differences in foundation behaviour.

In a fully saturated ground the resistance of shallow foundations is reduced since in general the effective unit weight of a submerged soil is about half that of a dry soil. Because of submergence, the bearing capacity of shallow foundations (section §3.2) may become significantly smaller, even assuming that $N_\gamma$ does not reduce due to saturation (Ausilio and Conte (2005) suggest a reduction of 40% for $\phi' = 20°$, $30°$, and $40°$). Moreover, influence of the water flow through the soil may add seepage forces to the gravity forces. However, this component may increase or decrease the bearing capacity depending on whether positive or negative excess pore water pressure is developed.

The moment loading tests are similar to those reported by Byrne *et al.* (2003) and Villalobos *et al.* (2004), and consist of rotation and translation of the footing at a specified load ratio $\frac{M}{2RH}$ and constant $V'$. The submerged vertical load $V'$ was directly obtained from the rig load cell, *i.e.* without subtracting the excess pore pressure or the suction underneath the lid multiplied by the lid section area $sA$ (refer to sections §4.3.3 and §7.1.2 for discussions about the definition of $V'$).

According to the scaling rule $n_t = n^{\alpha-2}$ determined from expression (6.7), the time of dissipation of any excess pore pressure is one thousand times faster in the laboratory when compared with a caisson one hundred times larger in the field. If $\alpha = 0$ implies that no attempt of considering stress level is made, which scales the time of dissipation to ten thousands times faster agreeing with the consolidation dimensionless time equation (6.6). Tests were carried out at a rotational velocity $2R\dot{\theta} = 0.01$ mm/s to obtain drained conditions as in the dry sand tests. Using this rotational velocity, water as the pore fluid, sand type and caisson sizes a fully drained condition is obtained. To verify this, a non-dimensional footing velocity used by Finnie (1993) for studying spudcan footings in calcareous soils suggests that for the following expression:

$$v_n = \frac{vL}{c_v} \tag{6.1}$$

from which an undrained footing response is obtained for $v_n > 10$ and a drained footing response is obtained for $v_n < 0.01$. The caisson skirt length $L$ is taken as the relevant dimension for drainage since the caisson is laterally loaded (for this series of tests the caissons have $L = R$). Taking the Redhill sand coefficient of consolidation $c_v = 0.19$ m$^2$/s (Kelly *et al.*, 2004) results in a non-dimensional footing velocity $v_n$ of $5{\cdot}10^{-6}$. Despite some differences between Finnie's test conditions ($R$ as the relevant dimension, soil type, density, vertical loading instead of rotational) drained conditions are deduced. Although offshore loading conditions can induce partially or even undrained conditions, the study of drained conditions provides a reference to compare the caisson moment resistance. Moreover, results from both installation methods can be more difficult to interpret for partially drained conditions. The study of the combined loading of suction caissons in undrained and partially drained conditions will be presented in section §6.2.

Table 6.1 summarises the data from moment loading tests, and further data about initial conditions can be found in Chapter 4 ($V_o$, initial $R_d$ and $\gamma'$, *etc.*). The test label FV6_5_2CS refers to the sample 6, site 5, test 2 within site 5, caisson C and installation

Table 6.1: Summary of moment capacity tests in Redhill sand

| Test | $V'$ N | $K_{mi}$ $\frac{N}{mm}$ | $K_{hi}$ $\frac{N}{mm}$ | $\frac{M_y}{2R}$ N | $H_y$ N | $K_{mf}$ $\frac{N}{mm}$ | $K_{hf}$ $\frac{N}{mm}$ | $\Delta u'$ kPa | $G$ MPa | $\frac{\delta u^p}{2R\delta\theta^p}$ | $\frac{\delta w^p}{2R\delta\theta^p}$ |
|---|---|---|---|---|---|---|---|---|---|---|---|
| FV6_5_2CS | 5.5 | 146 | 89 | 6.5 | 5.0 | 5 | 12 | -0.35 | 2.5 | 0.444 | -0.376 |
| FV7_5_2CP | 6 | 120 | 120 | 14.1 | 12.9 | 2 | 4 | -0.2 | 2.5 | 0.529 | -0.436 |
| FV6_2_2CS | 40 | 120 | 85 | 12.0 | 11.1 | 5 | 9 | -0.16 | 2.5 | 0.515 | -0.110 |
| FV6_3_2CP | 40 | 197 | 204 | 24.1 | 21.7 | 4 | 9 | -0.25 | 3.0 | 0.503 | -0.281 |
| FV6_8_2CS | 60 | 197 | 120 | 17.7 | 16.3 | 5 | 9 | -0.06 | 3.0 | 0.534 | -0.046 |
| FV7_1_2CP† | 60 | 250 | 250 | 29.0 | 27.0 | 4 | 7 | 0.4 | 3.5 | 0.528 | -0.273 |
| FV8_1_2AS | 10 | 181 | 253 | 14.8 | 15.1 | 6 | 17 | -0.4 | 2.5 | 0.314 | -0.400 |
| FV8_2_2AP | 10 | 220 | 220 | 33.6 | 32.7 | 4 | 6 | -0.45 | 2.5 | 0.583 | -0.575 |
| FV7_3_2AS | 60 | 340 | 350 | 30.9 | 27.7 | 13 | 33 | -0.34 | 2.5 | 0.453 | -0.276 |
| FV7_4_2AP | 60 | 240 | 260 | 41.5 | 40.3 | 7 | 15 | -0.42 | 2.5 | 0.459 | -0.496 |
| FV7_1_4AS | 120 | 647 | 406 | 40.2 | 39.0 | 16 | 42 | -0.2 | 4.0 | 0.385 | -0.119 |
| FV7_2_2AP | 120 | 652 | 290 | 55.4 | 50.8 | 15 | 33 | -0.36 | 4.0 | 0.544 | -0.288 |

All tests carried out at $\frac{M}{2RH} = 1$, †air valve open

by suction S. The parameter values were determined following the procedures presented in Chapter 5. Figures 6.3(a) and 6.3(b) show for the two different installation methods the $\frac{M}{2R} - 2R\theta$ curves and $H - u$ curves of caisson C under a constant $V' = 40$ N and load ratio $\frac{M}{2RH} = 1$. It is clear from these figures that the installation method has a strong effect on the load-displacement behaviour. The load-displacement curves have been interpreted by fitting linear expressions to the initial elastic and final plastic components of the curve (Chapter 5). The intersection of the lines represents a yield point. The yield points and the fitted straight lines are shown on the figures, and the values of the yield loads and the initial and final stiffness are collected in Table 6.1. In terms of yield it was found that suction installation reduces the yield loads as can be observed in Figure 6.4(a). This reduction is more pronounced for caisson C, possibly as a consequence of the smaller thickness ratio.

The displacements paths are shown in Figures 6.3(c) and 6.3(d), where the elastic component of the total displacement has been subtracted to obtain the plastic displacement. Values of the shear modulus $G$ used and the ratios obtained between plastic horizontal and rotational displacement increments $\frac{\delta u^p}{2R\delta\theta^p}$ and between plastic vertical and rotational displacement increments $\frac{\delta w^p}{2R\delta\theta^p}$ are summarised in Table 6.1. The vertical displacement variation during the caisson rotation is shown in Figure 6.3(d). Whilst $\frac{\delta u^p}{2R\delta\theta^p}$ values from suction and push installed caissons are very similar, values of $\left|\frac{\delta w^p}{2R\delta\theta^p}\right|$ are larger for cais-

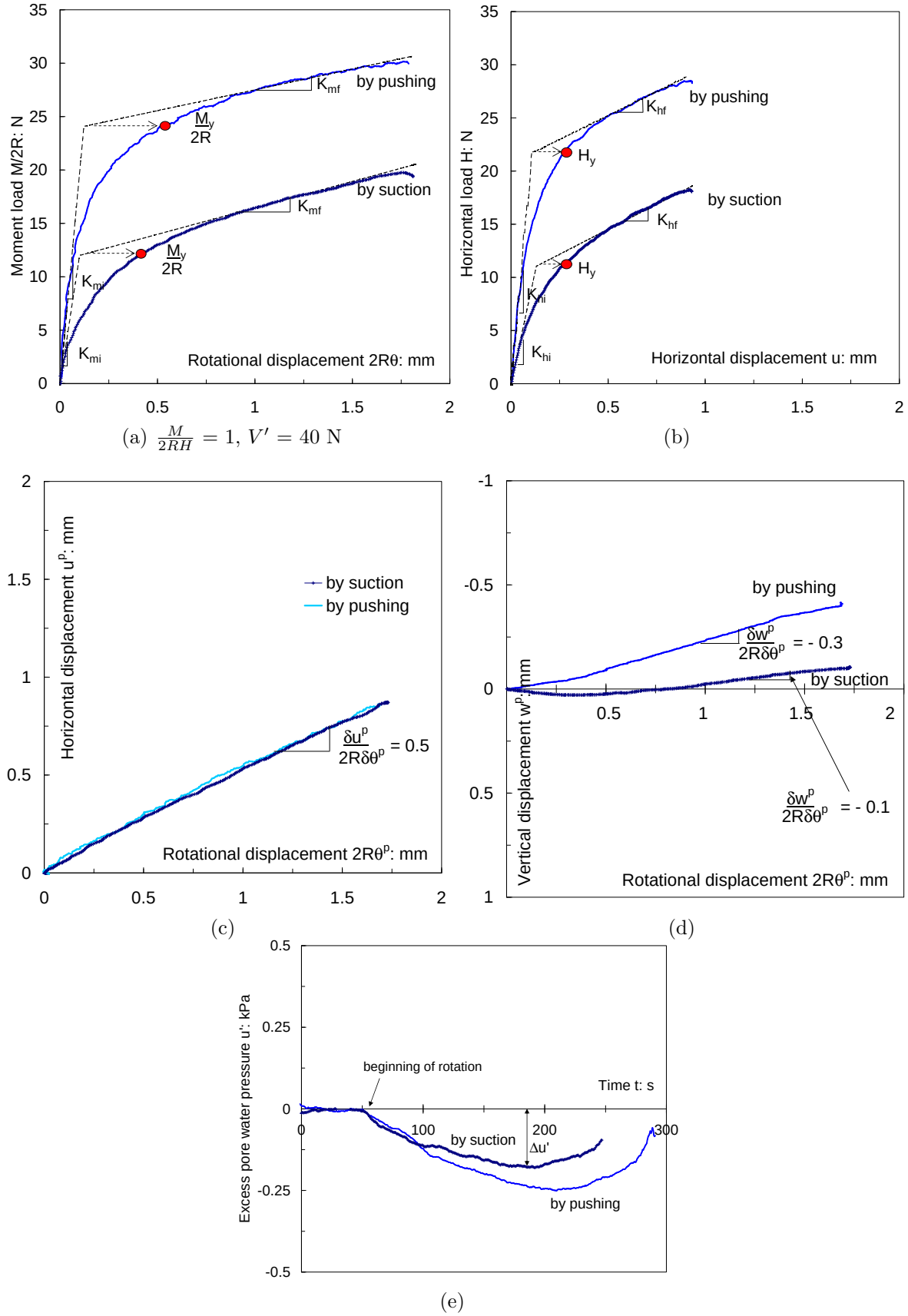


(a) $\frac{M}{2RH} = 1$, $V' = 40$ N (b)

(c) (d)

(e)

Figure 6.3: Comparison between the response of a caisson installed by suction, test FV6_2_2CS and by pushing, test FV6_3_2CP

sons push installed as can be observed in Table 6.1 and Figure 6.4(b). This indicates that suction installed caissons experience a lower magnitude of uplift compared with caissons installed by pushing. Moreover, the parallel point is reached for the caissons installed by suction at a value of $\frac{V'}{V_o} \approx 0.16$, which is close to value obtained for cyclic tests in dry sand. Although from Figure 6.4(b) the point of intersection of the pushing data with the $\frac{V'}{V_o}$ axis is less evident, it is likely a value of $\frac{V'}{V_o} \geq 0.3$, closer to value obtained from monotonic tests in dry sand.

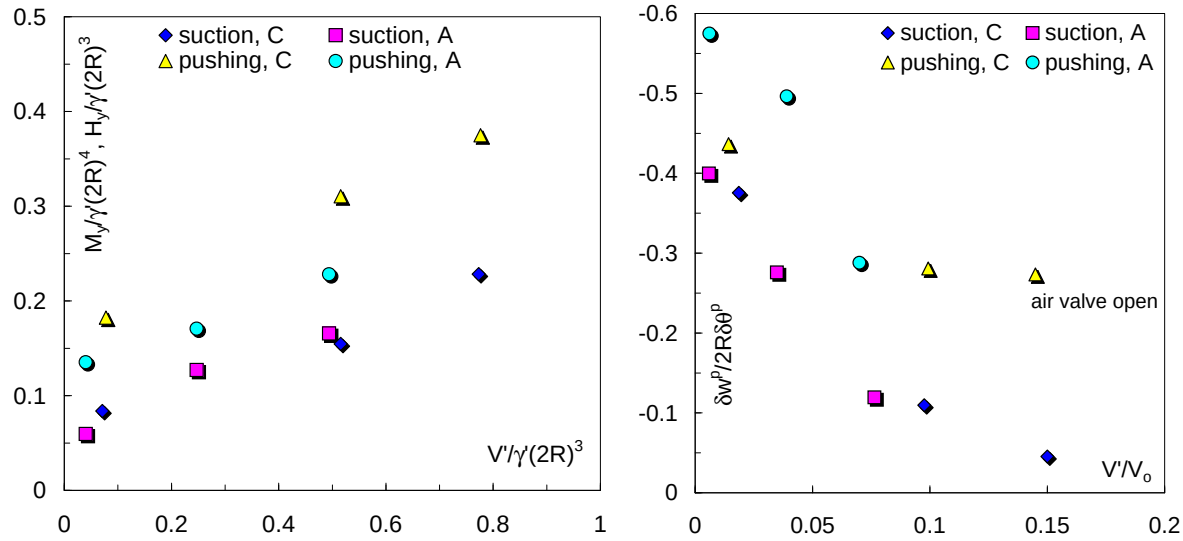


(a) $\frac{M}{2RH} = 1$ (b) $\frac{M}{2RH} = 1$

Figure 6.4: (a) Normalised yield loads as a function of $\frac{V'}{\gamma'(2R)^3}$, (b) plastic increment ratio between vertical and rotational displacements as a function of $\frac{V'}{V_o}$

The excess pore pressure variation in excess of the hydrostatic pressure $\Delta u'$ measured underneath the caisson lid is shown in Figure 6.3(e) for both moment capacity tests. Negative values of $u'$ were caused by the upward movement of the caisson, being slightly higher for the caisson push installed due to the larger uplift. Note that at the end of the tests a considerable percentage of the suction generated under the caisson lid has dissipated. Although $u'$ underneath the caisson lid does not necessarily represent the variation $u'$ around the caisson skirt, it can be interpreted as a reference for further analysis.

### 6.1.3 Foundation stiffness

The straight lines fitting the initial and final slopes of the load-displacement curves represent the foundation stiffness. Dimensionless expressions of the foundation stiffness

were obtained dividing the normalised load by the normalised displacement (equation (6.4)) as proposed by Kelly *et al.* (2006a), resulting in:

$$\frac{K_m}{(\gamma' p_a)^{0.5}(2R)^{1.5}}; \quad \frac{K_h}{(\gamma' p_a)^{0.5}(2R)^{1.5}} \tag{6.2}$$

Figures 6.5(a) and 6.5(b) show that there is no consistent difference between results from both installation methods. In Figure 6.5(a) is hard to differentiate the data, and in Figure 6.5(b) the pushing data is in between the suction data showing a separation between data from caisson A and C. For caisson A the dimensionless value of $K_{hi}$ is higher for the suction case, in contrast to the case for caisson C. It is worth pointing out that the initial stiffness determined for push installed caissons covered a larger range of load for a same displacement than for suction installed caissons. In other words, the initial linear response is larger for the caissons installed by pushing than for the caissons installed by suction. The final foundation stiffness determined at the end of the load-displacement curves are plotted in Figures 6.5(c) and 6.5(d) using the normalisations in (6.2). An enormous reduction in stiffness occurs as a consequence of progressive yielding. In Figure 6.5(c) no considerable difference is observed between suction points and pushing points, although slightly higher values for suction points appear. In Figure 6.5(d) suction points are located above the pushing points (except for one point), but again no systematic difference can be established. In conclusion, foundation stiffness was not significantly affected by the installation method.

### 6.1.4 Yield surface and velocity vectors

The yield loads $\frac{M_y}{2R}$ summarised in Table 6.1 were initially used to trace the yield surface in the $\frac{M}{2R} - V'$ plane for low vertical loads as illustrated with squares in Figure 6.6. Also, calculated yield surfaces are shown in Figure 6.6 using the expression (5.43), which is reproduced here:

$$y = \left(\frac{H}{h_o V_o}\right)^2 + \left(\frac{M}{2Rm_o V_o}\right)^2 - 2e\frac{H}{h_o V_o}\frac{M}{2Rm_o V_o} - \beta_{12}^2 \left(\frac{V'}{V_o} + t_o\right)^{2\beta_1} \left(1 - \frac{V'}{V_o}\right)^{2\beta_2} = 0 \tag{6.3}$$

in which $h_o, m_o, t_o, e, \beta_1$ and $\beta_2$ are the parameters that define the shape of the yield surface and $\beta_{12} = \beta_1^{-\beta_1}\beta_2^{-\beta_2}(\frac{\beta_1+\beta_2}{t_o+1})^{\beta_1+\beta_2}$. The values of these parameters can be found in Table 5.6. These values were determined from a series of moment loading tests performed with caisson aspect ratios of 1 and 0.5 in dry sand. It is then not surprising that the calculated yield surface gives a good prediction of the experimental yield points for the pushing method. On the other hand, the yield loads are reduced by the suction application. Therefore, the calculated yield surface does not give a good prediction for the suction installation case. A second yield surface was calculated exactly as before, but including the lower tensile load. Nevertheless, the experimentally obtained yield loads are still overestimated. Also shown on Figure 6.6 are the directions of the plastic displacement increment vectors. The installation method had also an effect on the flow vectors. For

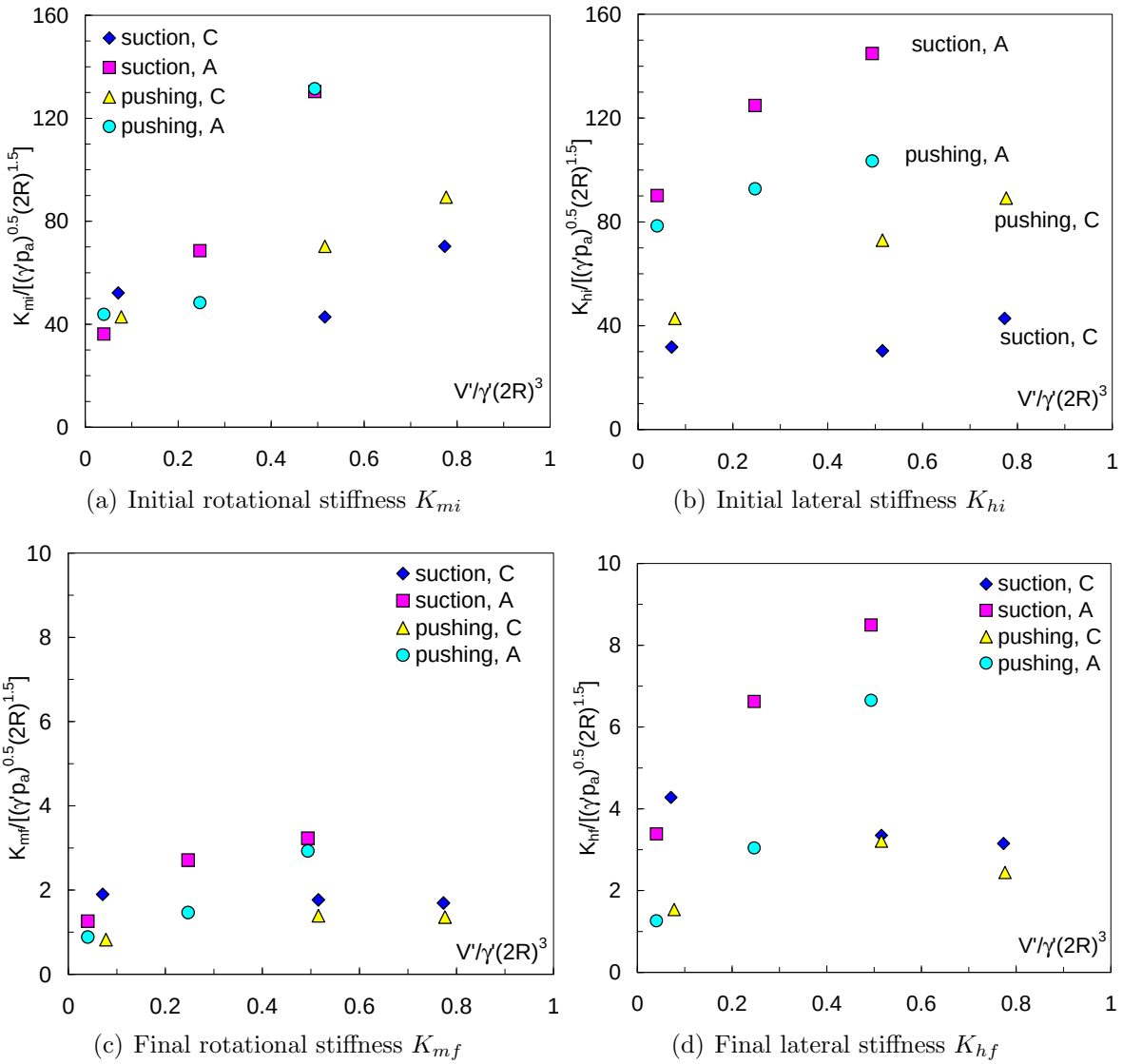


(a) Initial rotational stiffness $K_{mi}$

(b) Initial lateral stiffness $K_{hi}$

(c) Final rotational stiffness $K_{mf}$

(d) Final lateral stiffness $K_{hf}$

Figure 6.5: Normalised foundation stiffness

example, different directions can be observed for $V' = 40$ N and 60 N (see Figure 6.4(b) to compare the vertical and rotational ratio of plastic displacement increments for all the tests).

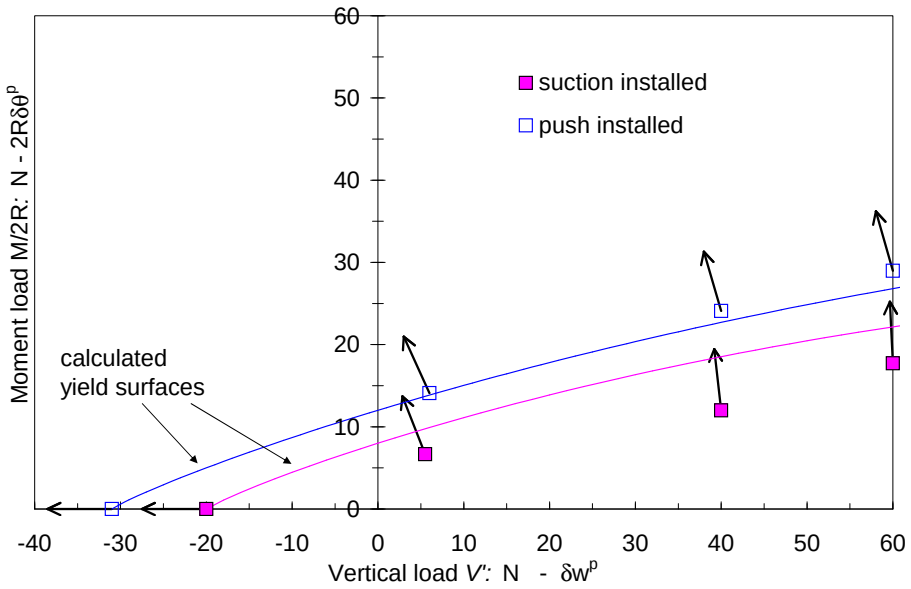


Figure 6.6: Yield points, velocity vectors and calculated yield surfaces comparing the installation method for caisson C

Results from both caisson diameters can be presented together by normalising with respect to $V_o$, the maximum applied vertical load. Figure 6.7 shows the normalised experimental yield points and the calculated yield surfaces. Equation (6.3) has been included in this plot with a value of $t_o = 0.064$ for the smaller footing and 0.040 for the larger footing. It is necessary to use different values of $t_o$ in this plot because the tensile capacity scales with $2RL^2$ (equation §4.4) whilst the $V_o$ value scales principally with $2RtL$ as discussed in section §4.3. Since the two footings have the same value of aspect ratio $\frac{L}{2R}$ but different value of thickness ratio $\frac{t}{2R}$ their tensile capacities differ on the normalised plot. However, the normalisation by $V_o$ merges the two curves shown in Figure 6.6 for caisson C, thus suction or pushing installation has only a minor effect on the normalised curve. In more detail, however, the yield surfaces presented in Figure 6.7 serve as lower bounds for the moment capacity in the case of a caisson installed by pushing. On the other hand, it represents an upper bound for a suction installed caisson. The differences are thought to be due to disturbance in the installation process due to suction.

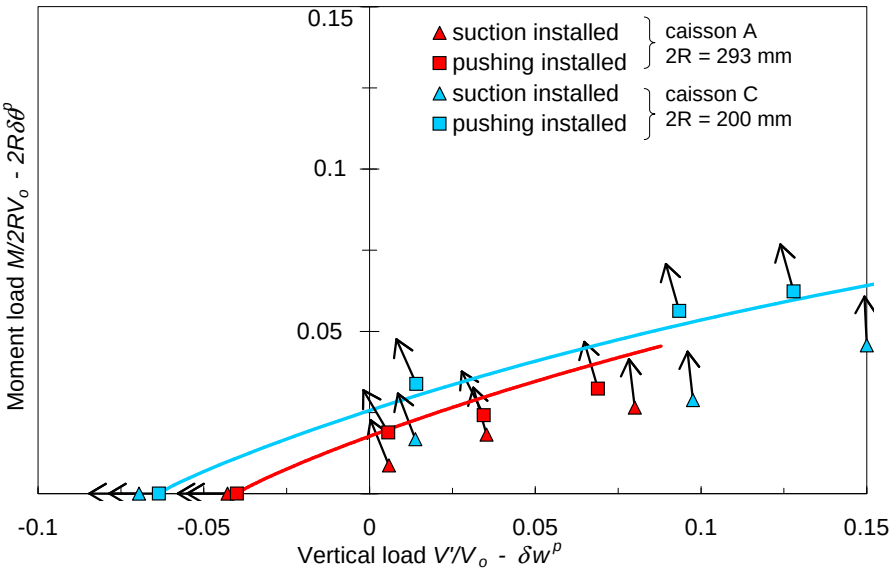


Figure 6.7: Velocity vectors, normalised yield points and calculated yield surfaces for caissons installed by pushing and by suction

The flow vectors obtained from suction installed caissons had a smaller component in the $w$-direction compared with the velocity vectors obtained from push installed caissons (see last column in Table 6.1). In other words, there was less uplift during the rotation of a caisson when the suction was used. This possibly implies that the soil is looser after a suction installation, and therefore dilates less when sheared.

### 6.1.5 Swipe tests of caissons installed by suction

Constant $V'$ tests are analogous to critical state soil mechanics interpretation of drained triaxial testing (Martin, 1994). This analogy was first established by Tan (1990) for the case of undrained triaxial testing, from which he deduced the load path of a 'side-swipe' test. The zero specific volume change corresponds to zero vertical displacement. As a consequence, the yield surface obtained from swipe tests of footings is analogous to the yield locus of Modified Cam Clay model. A swipe test can also be compared with an undrained simple shear test; since no dilation is allowed the normal load is free to vary during shearing.

Swipe tests are used to trace the yield surface along different load paths and constant $V'$ tests are conducted as probe tests to verify one point of the yield surface already traced

by a swipe test (Tan, 1990; Martin, 1994; Gottardi *et al.*, 1999; Byrne, 2000). Swipe tests have the advantage that only one swipe event is required to trace a part of the yield surface that would take several probe tests to achieve. To illustrate this, load paths of swipe tests are sketched in Figure 6.8 (compare with Figure 6.2). The fact that swipe tests are carried out under constant vertical displacement makes the flow rule analysis more complex. In this section swipe events were performed to assess the results from previous constant $V'$ tests. Additionally, swipe tests allowed for the insertion of data not covered by the constant $V'$ tests.

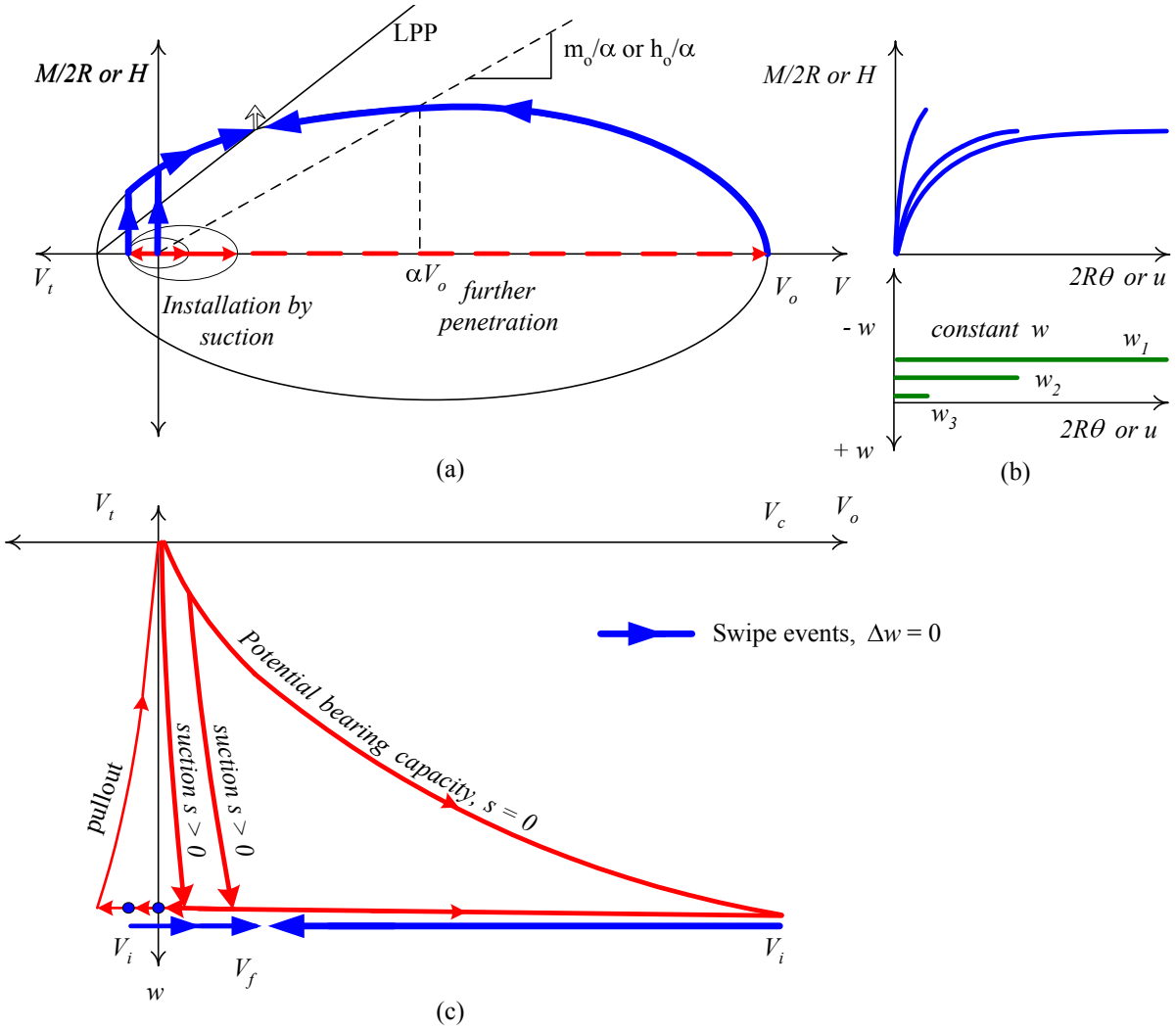


Figure 6.8: Suction installation: (a) load paths followed in swipe tests showing the line of parallel points LPP, (b) load-displacement curve and the resultant constant vertical displacement curve, (c) installation curve, including unloading and pullout

Rotational swipe tests were performed on caissons installed by suction. Details of the swipe tests are summarised in Table 6.2. Figure 6.9 shows normalised moment-rotation

Table 6.2: Summary of swipe tests in Redhill sand of caissons installed by suction

| Test | $V_i'$ N | $V_f'$ N | $\frac{M}{2RH}$ | $2R\theta_t$ mm | $h_f$ mm | $V_o$ N | $\frac{\delta u^p}{2R\delta\theta^p}$ |
|---|---|---|---|---|---|---|---|
| FV10_1_2A | -27 | 365 | 1 | 4.8 | 133 | 2400 | 0.542 |
| FV9_3_3C | -5 | 24 | 1 | 2 | 99.7 | 480 | 0.501 |
| FV9_3_4C | -1 | 87 | 1 | 5 | 100 | 480 | 0.451 |
| FV9_4_4C | -10 | 140 | 1 | 10 | 91 | 420 | 0.484 |
| FV9_1_2C | 420 | 180 | -1 | 0.7 | 98.8 | 450 | -0.282 |

curves obtained from the swipe tests, where a wide range of applied rotational displacement $2R\theta_t$ can be observed. Note the much stiffer response of the swipe event starting close to $V_o$ (test FV9_1_2C) compared with the other tests starting close to $V_t$. Figure 6.10 shows results from the swipe tests together with yield points from the constant $V'$ tests (Figure 6.7) in the deviatoric-vertical load plane normalised by $V_o$ (axes not scaled). The deviatoric load $Q$ was introduced in section §5.2.4 and $\frac{Q}{V_o}$ corresponds to the square root of the three first terms in equation (6.3). The curve of test FV10_1_2A progresses very close to the yield points obtained in the constant $V'$ tests for caissons installed by suction (the triangular points). Test FV10_1_2A was conducted immediately after the suction installation.

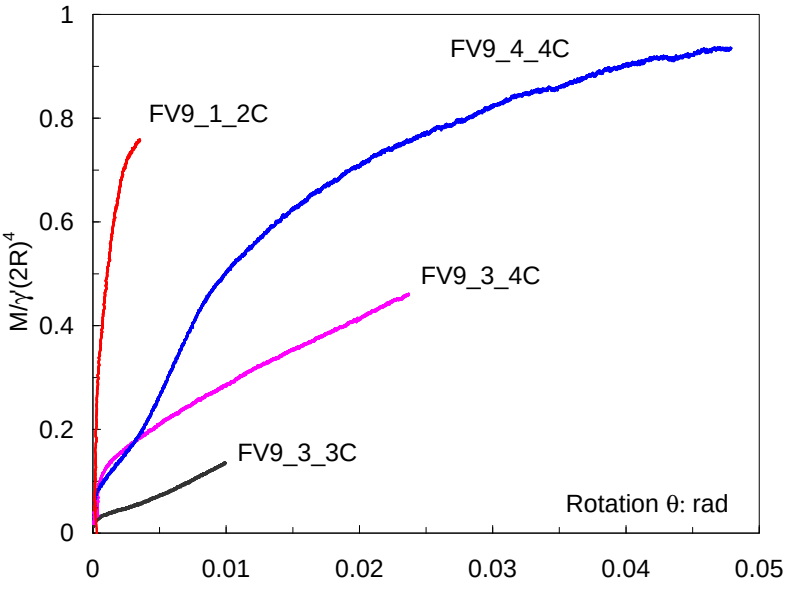


Figure 6.9: Normalised moment-rotation curves from swipe tests

Three other swipe tests using caisson C were also performed starting from low $V'$. The curve of test FV9_3_3C follows the triangular yield points along its short path. In addition, the curve of test FV9_3_4C initially follows the triangular yield points but from

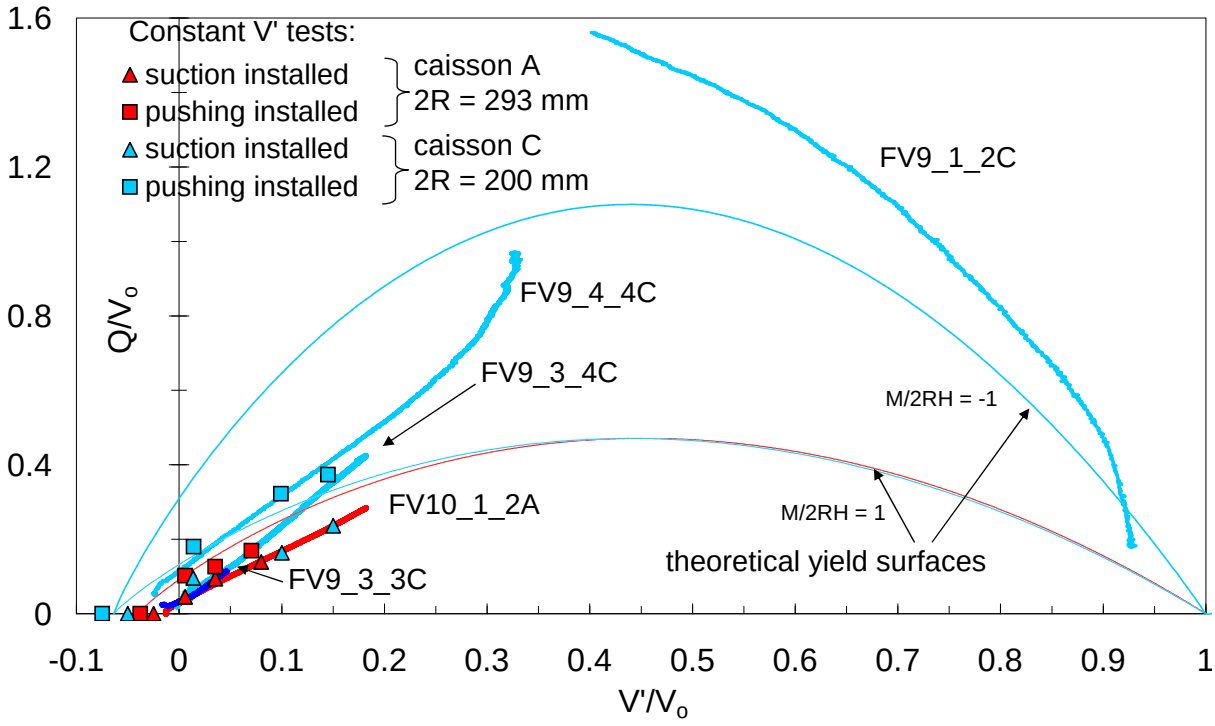


Figure 6.10: Swipe tests in the normalised deviatoric and vertical load plane comparing with results from constant $V'$ tests and calculated yield surfaces for $\frac{M}{2RH} = 1$ and -1

half way through follows a steeper path close to the square yield points that represent caissons installed by pushing. The curve of test FV9_4_4C has higher moment capacity following clearly the square points. A reason for this disparity may be due to disturbance (densification) of the sand sample after a previous test (the last number 3 or 4 represents a second or third test in the same site after installation). Time between the end of the suction and the beginning of the rotation may induce an ageing effect, which causes recovery of the soil strength lost during the suction installation. Another reason can be the effect of the skirt wall thickness as commented previously in Figure 6.4(a). For a thicker skirt wall, more soil is disturbed during penetration, which reduces the influence of the installation method.

To be applicable to offshore loading conditions of wind turbines, swipe tests were carried out for low vertical loads as for the constant $V'$ tests. However, swipe test FV9_1_2C was performed to explore the yield surface from $V'$ close to $V_o$. This is equivalent to the application of a very large vertical load on the caisson after the suction installation. The moment-rotation curve of this test in Figure 6.9 shows that large moment loads were

obtained at small rotations. Because this test was carried out under a load ratio of -1, another yield surface was calculated, which underestimates that tracked by the swipe event. A load ratio of -1 can represent for instance the case where the wind blows in opposite direction to tidal currents. Note that a curved yield surface was traced by this swipe event. Conversely, the yield surface shape traced by the low vertical load swipe events can be approximated by straight lines. These lines might seem to represent a steady load state or lines of parallel points LPP in analogy with the critical state line CSL (Tan, 1990). However, from Figure 6.9 a convergence of moment loads as rotation progresses under fixed vertical movement is not possible to observe.

It is worth pointing out that a variation of the initial value of $V_o$ occurs during a swipe event when $V'$ diminishes (Gottardi *et al.*, 1999; Byrne, 2000; Martin and Houlsby, 2001). Although the vertical displacement remains constant, the elastic vertical displacement is negative and as a consequence appears an identical positive plastic vertical displacement. This increase in the plastic vertical displacement induces an increase in $V_o$. To account for this increase the elastic vertical stiffness of the foundation $K_v^e$ and the plastic vertical stiffness of the foundation $K_V^p$ should be assessed. $K_V^e$ can be obtained from the caisson unloading-reloading response. For caisson C the order of magnitude of $K_V^e$ was around 1600 N/mm. Whilst $K_V^p$ was in the order of 10 N/mm before the caisson lid made full contact with the sand ($h < L$), and around 100 N/mm when the caisson lid is in full contact with the sand ($h \geq L$). However, for these stiffness values a negligible variation of $V_o$ is obtained as $\frac{K_V^p}{K_V^e} << 1$.

### 6.1.6 Cyclic loading tests under constant vertical load

The purpose of carrying out cyclic moment loading tests was to investigate the effect of different soil conditions and caisson geometries on the cyclic response of suction caissons. To this end, this section will continue the analysis performed in section §5.5. To compare appropriately results from different soil conditions and caisson geometries normalised quantities will be extensively used. For that reason, prior to exploring the

experimental results, the dimensionless quantities used to scale loads and displacements will be reviewed.

The dimensionless quantity of the moment $\frac{M}{\gamma'(2R)^4}$ or horizontal load $\frac{H}{\gamma'(2R)^3}$, can be compared only if similarity of $\frac{V'}{\gamma'(2R)^3}$, $\frac{L}{2R}$ and $\frac{M}{2RH}$ is achieved. From results of moment loading tests, the yield points in the moment-vertical load plane were found to follow a linear relationship for low vertical loads. Figure 6.11 shows for four load ratios the straight lines fitted. In the straight line y = $a$ + $b$x shown in Figure 6.11, $a$ is the intersection with the ordinate, $b$ is the slope and the intersection with the abscissa corresponds to the maximum dimensionless tensile load $\frac{V_t}{\gamma'(2R)^3}$ = -0.2, so that $\frac{a}{b} = 0.2$. From this linear relationship is possible to compare results at yield from different $\frac{V'}{\gamma'(2R)^3}$ and similar $\frac{M}{2RH}$ or vice versa. For example, data with load ratio of -1 can be multiplied by $\frac{y_1}{y_{-1}}$ to compare with data having a load ratio of 1 and similar value of $\frac{V'}{\gamma'(2R)^3}$. Extrapolations to scale different vertical loads and load ratios are limited to $\frac{V'}{\gamma'(2R)^3} < 0.3$ and $\frac{L}{2R} = 0.5$.

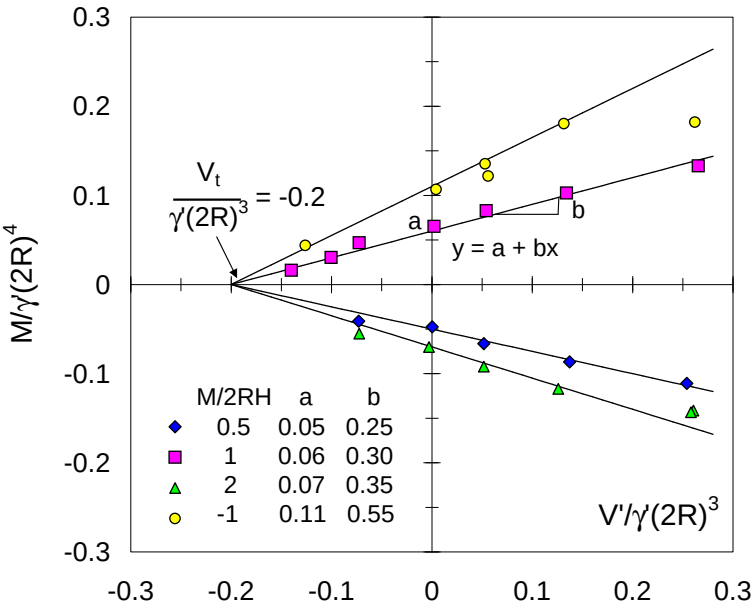


Figure 6.11: Straight lines fitted to the yield points for caissons with $\frac{L}{2R}$, showing two set of information above the abscissa and two below for clarity

A dimensionless displacement quantity that allows for comparisons from different sand unit weights and caisson diameters is suggested by Kelly *et al.* (2006a). For the vertical displacement $w$, the rotational displacement $2R\theta$ and the horizontal displacement $u$,

dimensionless quantities can be expressed as follows:

$$\frac{w}{2R}\left(\frac{p_a}{2R\gamma'}\right)^{0.5}; \qquad \theta\left(\frac{p_a}{2R\gamma'}\right)^{0.5}; \qquad \frac{u}{2R}\left(\frac{p_a}{2R\gamma'}\right)^{0.5} \tag{6.4}$$

Expressions in (6.4) were derived by Kelly *et al.* (2006a) from the elastic load-displacement relationship (5.9) and the exponent 0.5 comes from the elastic shear modulus in equation (5.14), which attempts to account for the stress level.

The results from cyclic moment loading tests in a saturated Redhill sand will be presented and compared with results from loose dry Leighton Buzzard sand shown in section §5.5. For details of the cyclic moment tests in saturated sand see Table 6.3 and for the tests in dry sand see Tables 5.7 and 5.8. The majority of the tests were carried out in dense sands since in several of the offshore wind farm sites around the UK coasts dense sands are expected to be found. In addition, results in dense sands are useful to compare with previous results in loose sands by assessing dimensionless expressions.

Table 6.3: Summary of cyclic moment loading tests

| Test | $V'_{average}$ N | $\frac{V'}{\gamma'(2R)^3}$ | $V_o$ N | $R_d$ % | $\gamma'$ kN/m$^3$ | $\frac{M}{2RH}$ | $w_t$ mm |
|---|---|---|---|---|---|---|---|
| FV9_3_2CS | 8 | 0.1 | 500 | 92 | 10.21 | 1 | -4 |
| FV9_2_2CS | 42 | 0.5 | 443 | 92 | 10.21 | 1 | 2.7 |
| FV6_1_2CP | 73 | 1.1 | 122 | 26 | 8.47 | 2.7 | 1.8 |
| FV6_4_3CS | 100 | 1.2 | 420 | 92 | 10.21 | 1.1 | 1.1 |
| FV9_5_2AS | 15 | 0.06 | 2616 | 92 | 10.21 | 1 | -7.3 |
| FV7_3_3AS | 60 - 200 | 0.25 - 0.82 | 1724 | 74 | 9.663 | 1.1 | 0.4 |

Test FV6_1_2C was carried out in a loose water-saturated Redhill sand, whereas test FV106_21_2A was carried out also in a loose but dry Leighton Buzzard sand. Both tests had a similarly high value of $\frac{V'}{\gamma'(2R)^3}$, but different $\frac{M}{2RH}$ values. Figures 6.12(a) and 6.12(b) show the normalised moment-rotation curves for both tests, which can be compared when the normalised rotations are similar (second and tenth cycles respectively in Figure 6.12(a)). It is observed a stiffer response of the caisson in dry sand than for the caisson in saturated sand. The amplitude of rotation applied to both caissons was the same, but due to the different soil and caisson geometry, the normalised or comparable rotation, was more than double for the smaller caisson. It is worth noticing in Figures

6.12(c) and 6.12(d) that regardless the differences between both tests a similar normalised cyclic vertical displacement $w$ was obtained. This would be expected for caissons with similar normalised vertical load, showing that the effect of submergence which affects the unit weight is covered appropriately by the normalisations for these particular conditions. Note that settlement occurs on the unloading parts of each cycle.

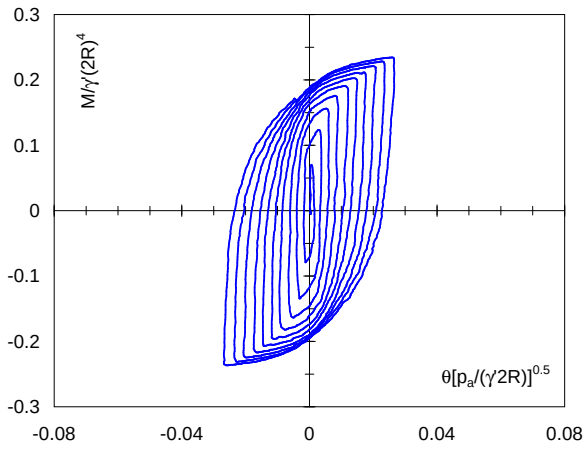


(a) $\gamma' = 15$ kN/m$^3$, $\frac{M}{2RH} = 0.5$, $\frac{V'}{\gamma'(2R)^3} = 1.0$

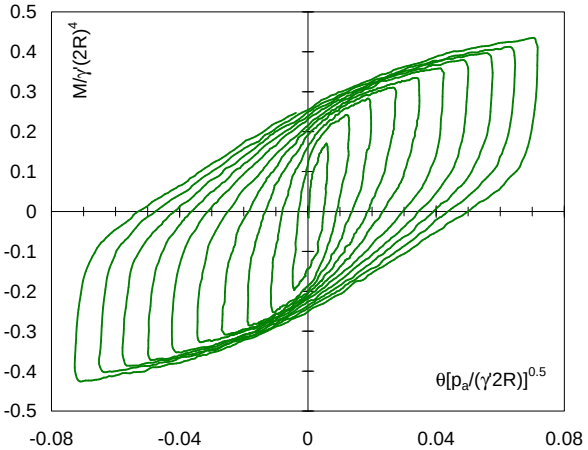


(b) $\gamma' = 8.5$ kN/m$^3$, $\frac{M}{2RH} = 2.7$, $\frac{V'}{\gamma'(2R)^3} = 1.1$

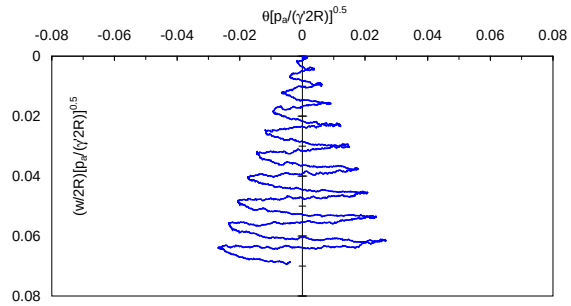


(c) Test FV106_21_2AP

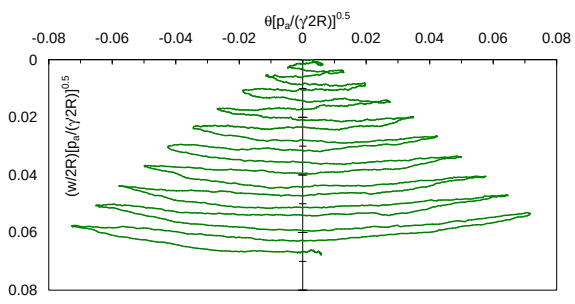


(d) Test FV6_1_2CP

Figure 6.12: Normalised moment-rotation and displacement curves

Henceforward, tests in saturated sand will correspond only to dense samples. A comparison of hysteresis loops from a test in saturated sand with backbone curves from tests in dry sand is now presented. Figures 6.13(a) and 6.13(b) show normalised cyclic load-displacement curves obtained from test FV9_5_2AS and two backbone curves from tests FV73_12_2AP and FV78_13_2AP (carried out in a loose and dry Leighton Buzzard sand), where $\frac{M}{2R}$ is interchangeable with $H$ because the tests were conducted at $\frac{M}{2RH} = 1$. The moment backbone curves of tests FV78_13_2AP and the test in dense saturated sand are fairly close, leading to a good agreement between normalised moment capacity, but not so good agreement for the normalised rotation. Broadly similar dissipation of energy is caused by the unloading-reloading cycles for both tests. For a caisson with aspect ratio

of 0.5 the hysteresis loops are less open, so less energy is dissipated. The horizontal load backbone curves do not compare so well as with the moment curves.

Figure 6.13(c) shows that the caisson uplift was significant in the saturated sand as that observed in test FV78_13_2AP, which had a smaller value of $\frac{V'}{\gamma'(2R)^3} = 0.01$. The $V'$ values that appear in Tables 5.7, 5.8 and 6.3 are an average of fluctuations or variations as shown in Figure 6.13(d) in the form of uniform pressure $\frac{V'}{A}$ underneath the caisson lid. Moreover, suction appears as a consequence of the upward movement following the $\frac{V'}{A}$ fluctuation. Note that there are two peaks and two troughs in the pore pressure response in each cycle. This phenomena is related with the vertical displacement of the caisson.

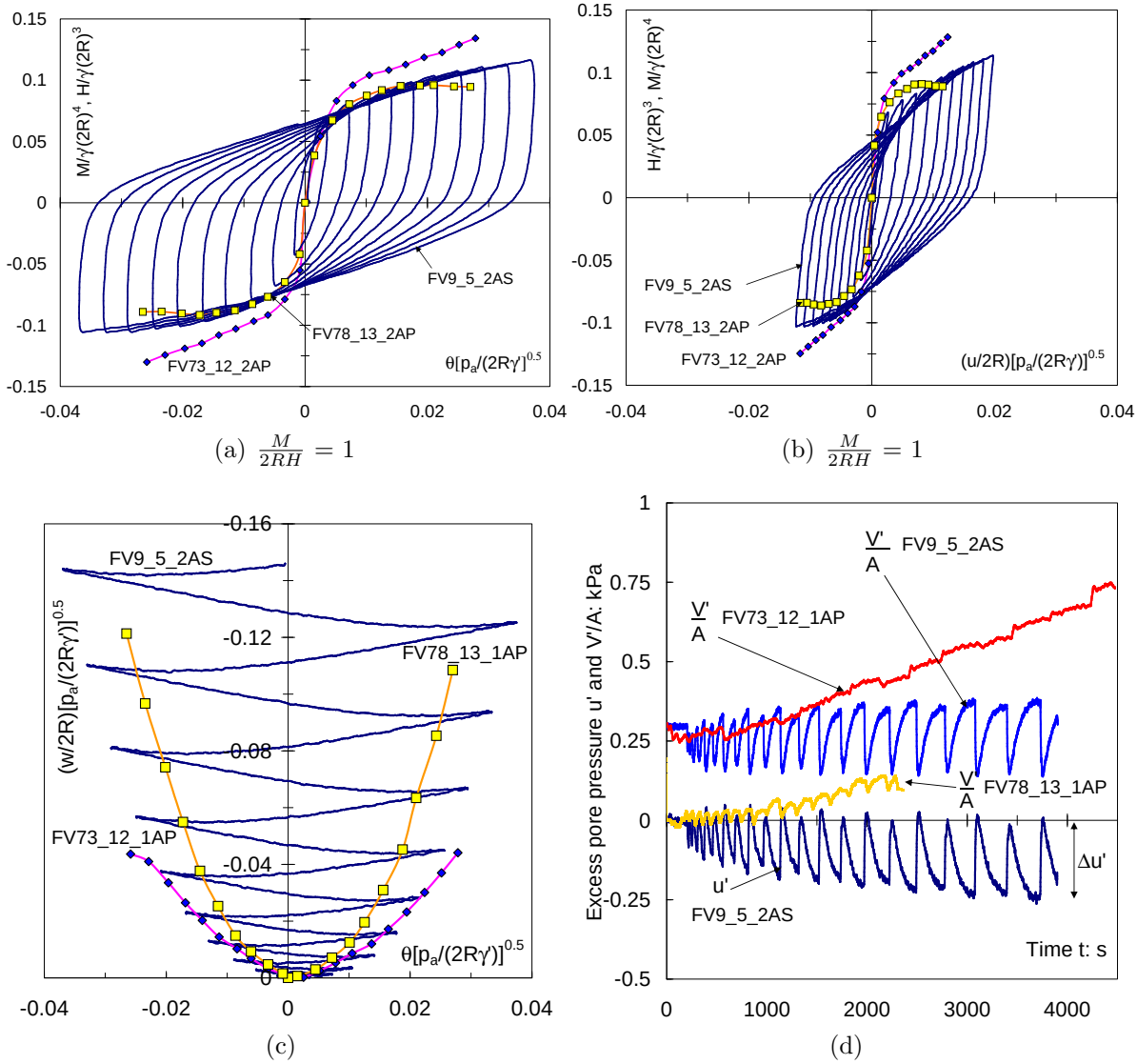


(a) $\frac{M}{2RH} = 1$ (b) $\frac{M}{2RH} = 1$

(c) (d)

Figure 6.13: Comparison of normalised backbone curves, normalised vertical displacement curves, excess pore pressure and vertical uniform pressure underneath the lid

A non-symmetric one-way cyclic rotation test was conducted at $\frac{M}{2RH} = 1$ and is compared in Figure 6.14(a) with a similar type of test as those described in section §5.5.2, but at a different value of $\frac{V'}{\gamma'(2R)^3}$. Surprisingly the normalised moment loads are comparable when the rotations are similarly scaled, despite the large difference in the value of $\frac{V'}{\gamma'(2R)^3}$. As expected the caisson under very low $\frac{V'}{\gamma'(2R)^3}$ had upward movement, whereas the caisson under high $\frac{V'}{\gamma'(2R)^3}$ exhibited settlement.

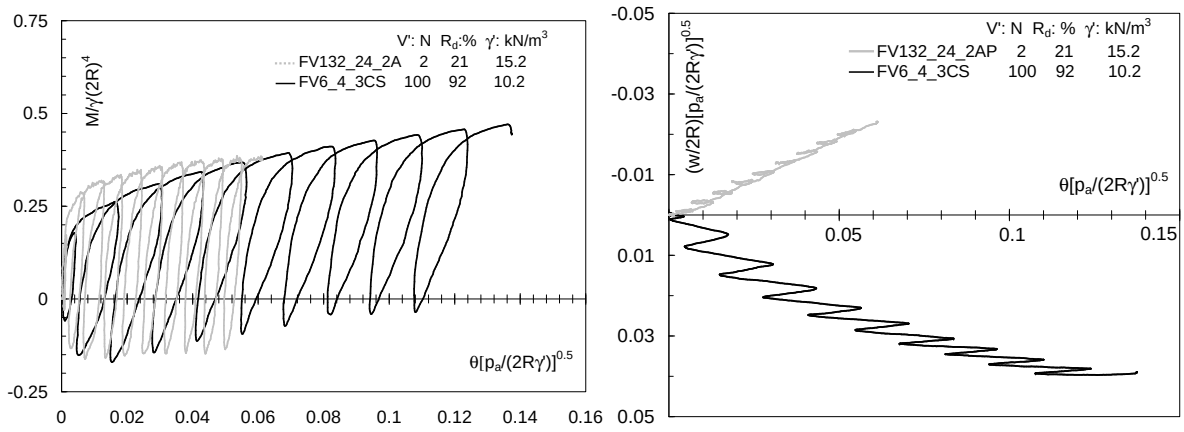


(a) $\frac{M}{2RH} = 1$ (b)

Figure 6.14: Comparison between two one-way cyclic rotation tests

It is also important to consider results from field tests (if available) to understand whether or not similar foundation response patterns are reproduced in the laboratory. Figures 6.15(a) and 6.15(b) show the moment-rotation curve and the vertical-rotational displacement curve respectively obtained in a field trial at Luce Bay by Houlsby *et al.* (2006) using a caisson 3 m diameter and 1.5 m skirt length. Kelly *et al.* (2006a) have compared the field moment resistance with laboratory tests especially programmed to scale $\frac{V'}{\gamma'(2R)^3}$ and $\theta[p_a/(\gamma' 2R)]^{0.5}$. According to Kelly *et al.* a reasonable agreement occurred only when in the laboratory the caisson was installed by pushing and subsequently rotated under small rotations ($\theta[p_a/(\gamma' 2R)]^{0.5} < 0.01$). Caissons installed by suction did not reach more than half of the moment resistance of the caisson installed by pushing due to strong sand disturbance during suction installation. Furthermore, a difference in hysteresis loop shape for higher normalised rotation was attributed to gapping in the field not observable in the laboratory tests.

A cyclic moment-rotation curve was obtained in the laboratory without the particular intention of replicating the field trial results and unlike Kelly *et al.*'s tests the caisson was installed by suction. Figure 6.15(a) shows this curve with the typical shape of hysteresis loops previously found. The normalised moment was amplified by a factor of 1.2 to scale the difference between $\frac{V'}{\gamma'(2R)^3} = 0.15$ in the field and 0.098 in the laboratory (following Figure 6.11, $\frac{y_{0.15}}{y_{0.098}} = \frac{0.06+0.3\cdot 0.15}{0.06+0.3\cdot 0.098} = 1.2$). It can be observed that the rotation scales relatively well, however, the moment resistance for large rotations is much lower than that in the field as also observed by Kelly *et al.*. It is important to realise that in the field CPT records showed a strong increase of cone resistance with depth (in the first 3 m). As shown in Figure 5.1, the caisson moment resistance is a function of the lateral earth pressure along the caisson wall. Therefore, a larger stress level with depth increases the caisson moment response.

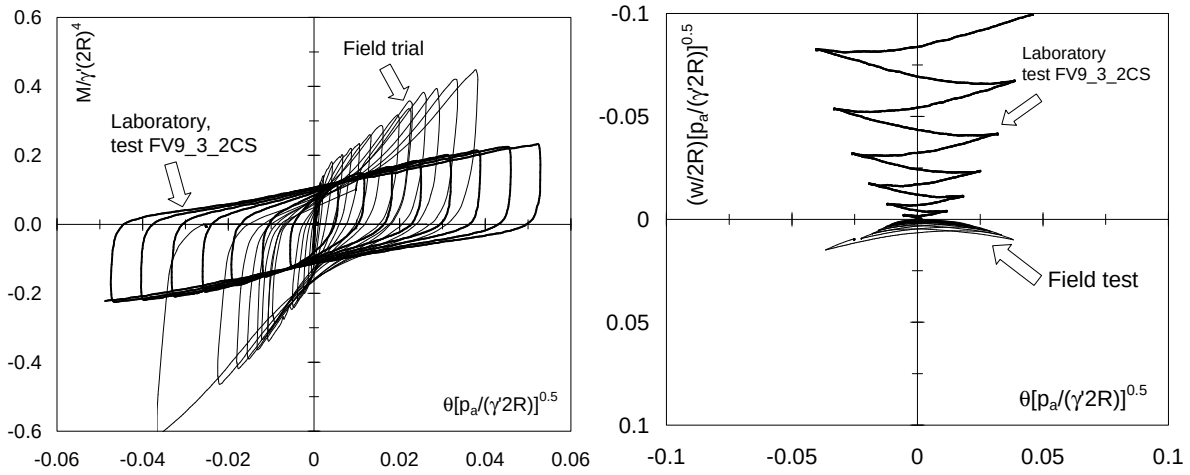


(a) $\frac{M}{2RH} = 1$ (b)

Figure 6.15: Comparison between results from the laboratory and from the field, where $2R = 3$ m, $V' = 42.4$ kN, $R_d = 80$ %, $\gamma' = 10.3$ kN/m$^3$ (taken from Houlsby *et al.*, 2006)

Figure 6.15(b) compares the normalised vertical displacement. Whilst the caisson in the laboratory moved upwards significantly, the caisson in the field rocks with very little settlement. The high stress level induces large frictional forces on the wall that restrain the vertical movement of the caisson.

A final example represents the case of a cyclic moment loading event conducted without holding constant $V'$ nor $w$, but the load ratio $\frac{M}{2RH} = 1.1$. It is observed in Figures

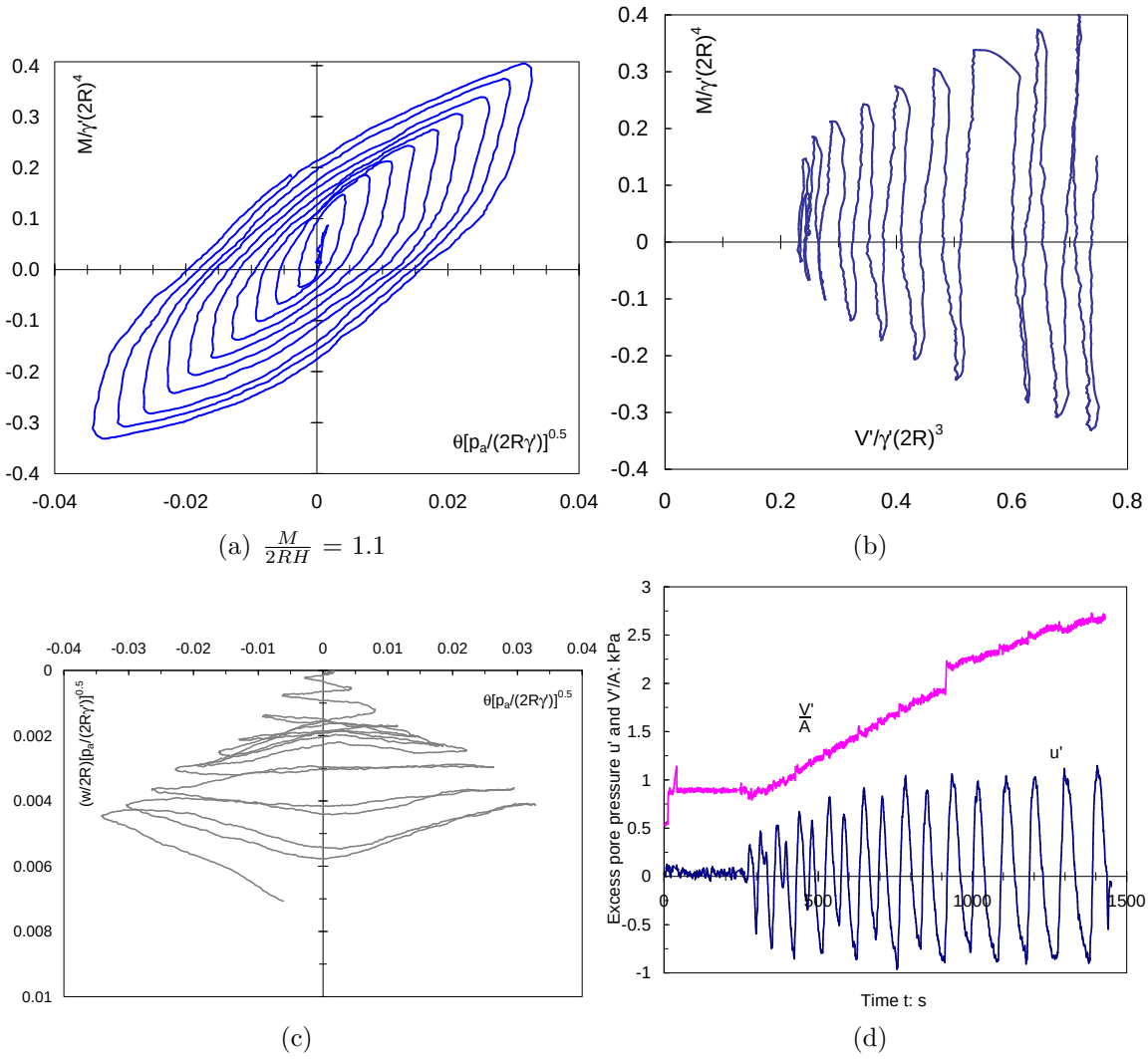


Figure 6.16: Results from test FV7_3_3AS, where only the load ratio is constant

6.16(a) and 6.16(b) that despite the pore pressure variation, the steady increase of $V'$ during cycling causes considerable enhancement of the moment resistance. Figure 6.16(c) shows that the first three small amplitude cycles cause a noticeable settlement of the caisson. There is virtually no settlement in the next four cycles of larger amplitude, but

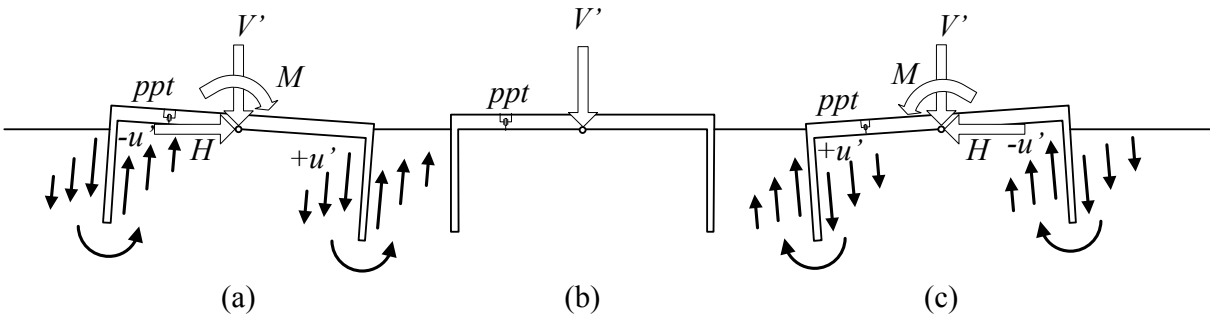


Figure 6.17: Cyclic flow caused by the cyclic rotation of the caisson

settlement occurs again in the last three largest amplitude cycles. The evolution of the excess pore pressure $u'$ and $V'$ (from 60 N to 200 N) can be seen in Figure 6.16(d), where $\frac{V'}{A}$ is the uniform pressure underneath the lid. The peaks values of $u'$ stabilizes around a value of $\pm$ 1 kPa in spite of the steady increase of $V'$. The positive and negative values of $u'$ are related to the position of the pore pressure transducer PPT. Whilst on one side of the lid settlement is occurring, on the other side uplift is occurring. This interesting feature of the variation of $u'$ gives insight into the flow directions taking place around the caisson during the cyclic moment loading. According to the negative or positive values of $u'$ the flow is assumed to be as shown in Figure 6.17. This indicates that a cyclic flow regime occurs during cycling. From the lifted side of the caisson water enters the caisson, whereas at the compressed side water leaves the caisson. A transition condition without flow occurs during unloading when the moment and horizontal loads become zero.

### 6.1.7 Cyclic swipe tests of suction caissons

The motivation of this part of the investigation relies on the fact that cyclic swipe events can represent a loading condition where moment and horizontal load vary with the vertical load. The fact that waves apply vertical loads as well as horizontal loads gives a physical interpretation of cyclic swipe tests in offshore problems. A wave train

Table 6.4: Summary of cyclic swipe tests of caissons installed by suction in Redhill sand

| Test | $V_i'$ N | $V_f'$ N | $V_o$ N | $\frac{M}{2RH}$ | $h$ mm | $\frac{\delta u^p}{2R\delta\theta^p}$ |
|---|---|---|---|---|---|---|
| FV10_2_2AS | -25 | 535 | 2472 | 1 | 138 | 0.68 |
| FV10_3_2AS | -31 | 150 | 2146 | 1 | 118 | 1.06 |
| FV10_3_3AS | -26 | 494 | 2146 | 0.98 | 118 | 1.07 |
| FV10_4_2DS | -23 | 145 | 641 | 0.48 | 138 | -2.40 |
| FV10_4_3DS | -22 | 180 | 641 | 0.52 | 138 | -2.42 |

same sand sample: $R_d = 89\%$, $\gamma' = 10.1$ kN/m$^3$

induces pressure oscillation on the seabed, then the difference between this pressure and the pressure underneath a skirted footing resting in the seabed will induce a fluctuation of the vertical load. The wave-induced pressure oscillation has a downward maximum at the peak, compressing the footing and an upward maximum at the trough, pulling out the footing. These pressures are not negligible since maximum pressures may range between 1 kPa and 6 kPa according to Sassa and Sekiguchi (2001) from a study of wave-induced

liquefaction of sand beds. In practical terms 1 kPa would induce a variation of the vertical load for caisson A of approximately $V'_{weight} \pm$ 67 N. Note that if the bleed valve is open the pressure difference is drastically reduced and such a vertical load fluctuation is minimal.

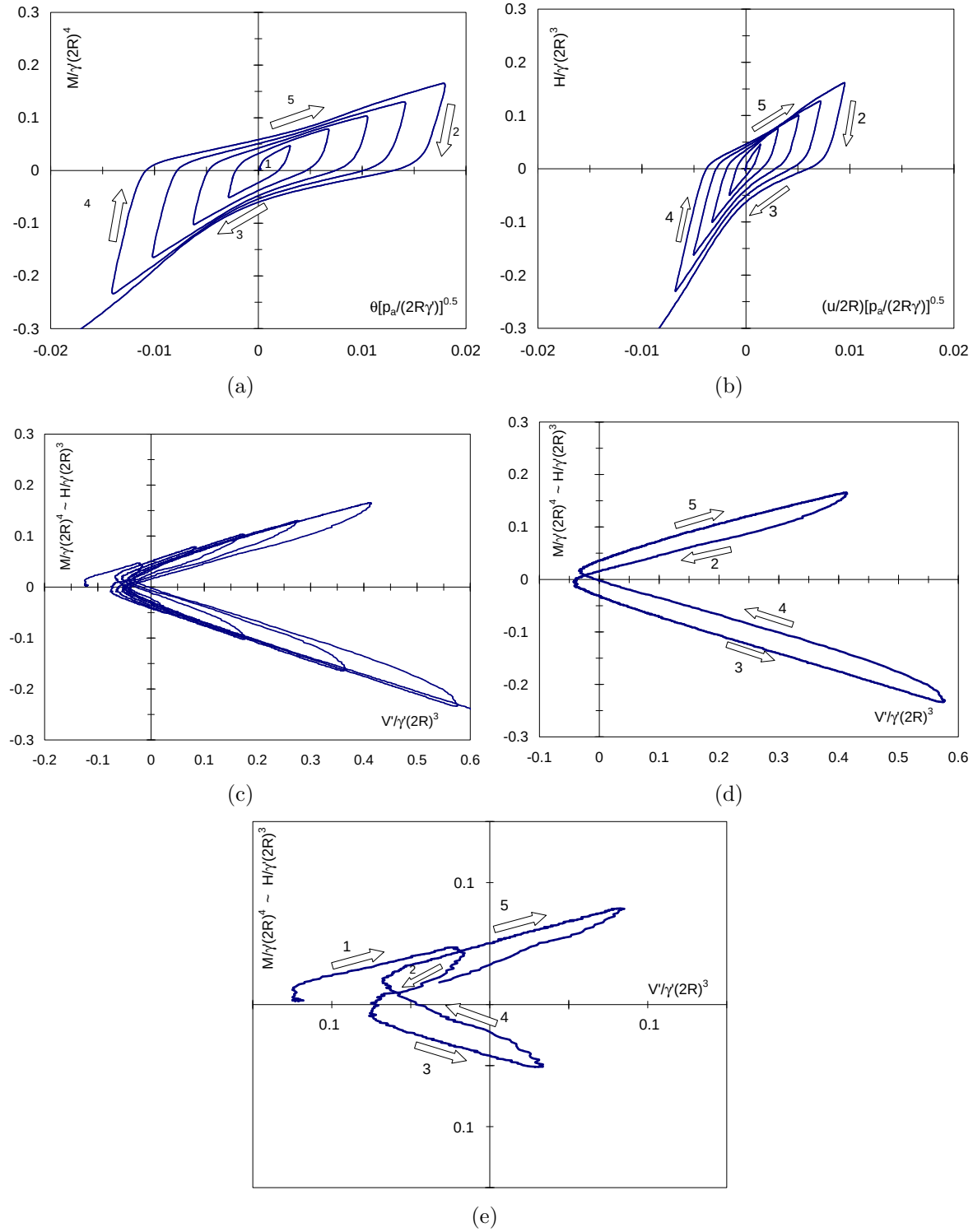


Figure 6.18: Cyclic swipe test FV10_2_2AS showing details of initial and final load path

Table 6.4 summarises details of the cyclic swipe tests performed. For example, in test

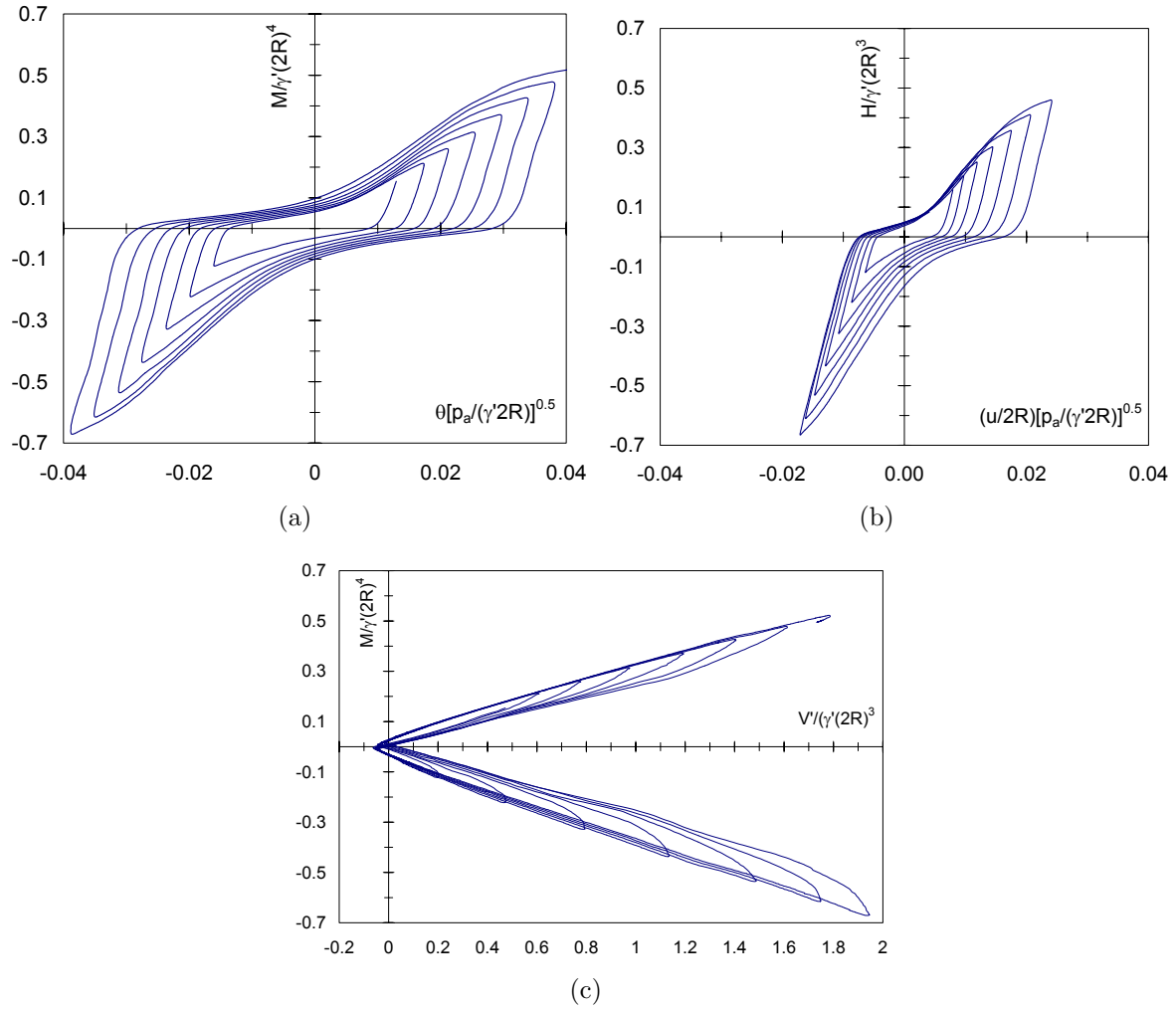


Figure 6.19: Cyclic swipe test FV10_3_3AS

FV10_3_2AS the caisson was installed by suction under a constant $V' = 16$ N until a final penetration $h = 118$ mm, following immediately a cyclic swipe event under increasing amplitudes at $\frac{M}{2RH} = 1$ (from $V_i' =$ -31 N and keeping the caisson penetration constant at 118 mm). Figures 6.18(a) and 6.18(b) show the normalised curves of $\frac{M}{2R} - 2R\theta$ and $H - u$, where it can be observed that the hysteresis loops are slightly flattened on top and at the bottom (arrows 3 and 5). This shape of the reloading and unloading curves becomes most visible for the largest rotation amplitude cycles. This is a consequence of the $V'$ variation as shown in Figure 6.18(c). Figures 6.18(d) and 6.18(e) depict the first and final cycles respectively, in which arrow 1 corresponds to the first loading, arrows 2 and 3 unloading and arrows 4 and 5 reloading. As a consequence of the fixing of the caisson in the vertical direction during rotation and translation $V'$ increases with the rotation amplitude. This causes the moment and horizontal load to increase too. However, at every reversal

$V'$ returns to a value close to the initial $V'$. Figures 6.18(d) and 6.18(e) show that the normalised value of $V'$ at reversal is around -0.05. Due to the drastic reduction of $V'$ the cyclic loop tends to close in the middle of unloading and in the middle of reloading. The hysteresis loop shape is hence different from that obtained previously in constant $V'$ tests. The pore pressure observed was negligible because, despite the caisson rotation, the vertical fixity does not induce significant pore pressure variations underneath the lid.

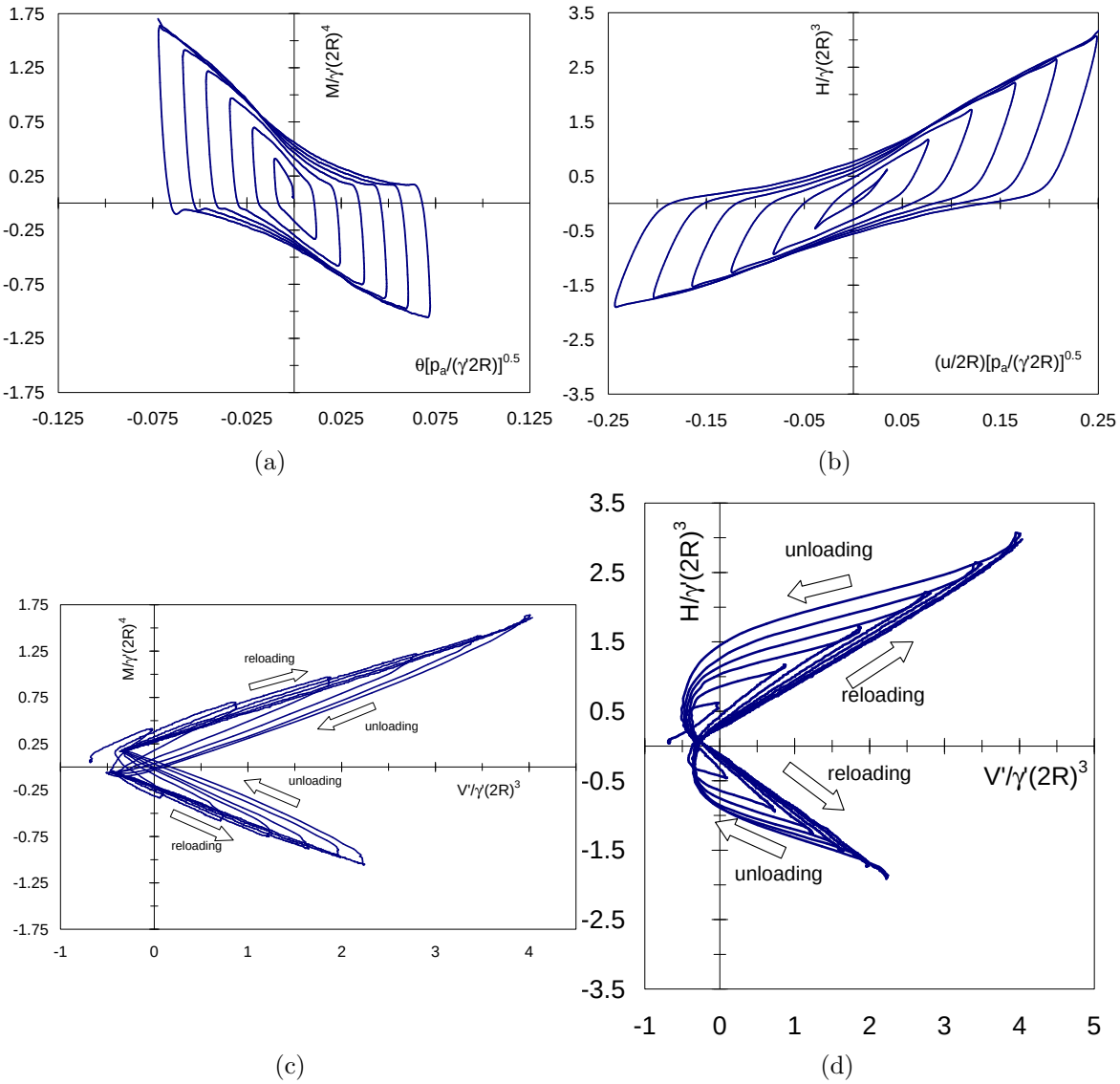


Figure 6.20: Cyclic swipe test FV10_4_2DS

A similar test but for larger rotation amplitudes is shown in Figures 6.19(a) and 6.19(b), where the characteristic shape of the hysteresis loops is clear. This test resembles the field moment-rotation response. However, in the field trial this loop shape was associated

with gapping, whereas in these tests is attributed to the strong vertical load fluctuation. If gapping occurred, they were not visible. Figure 6.19(c) shows that the response in the normalised moment-vertical load plane follows the same trend shown in Figure 6.18(c) for increasing values of vertical load. A slight curvature during reloading at the top (arrow 5) and during unloading at the bottom (arrow 3) can be observed. As before no excess pore water pressure was observed.

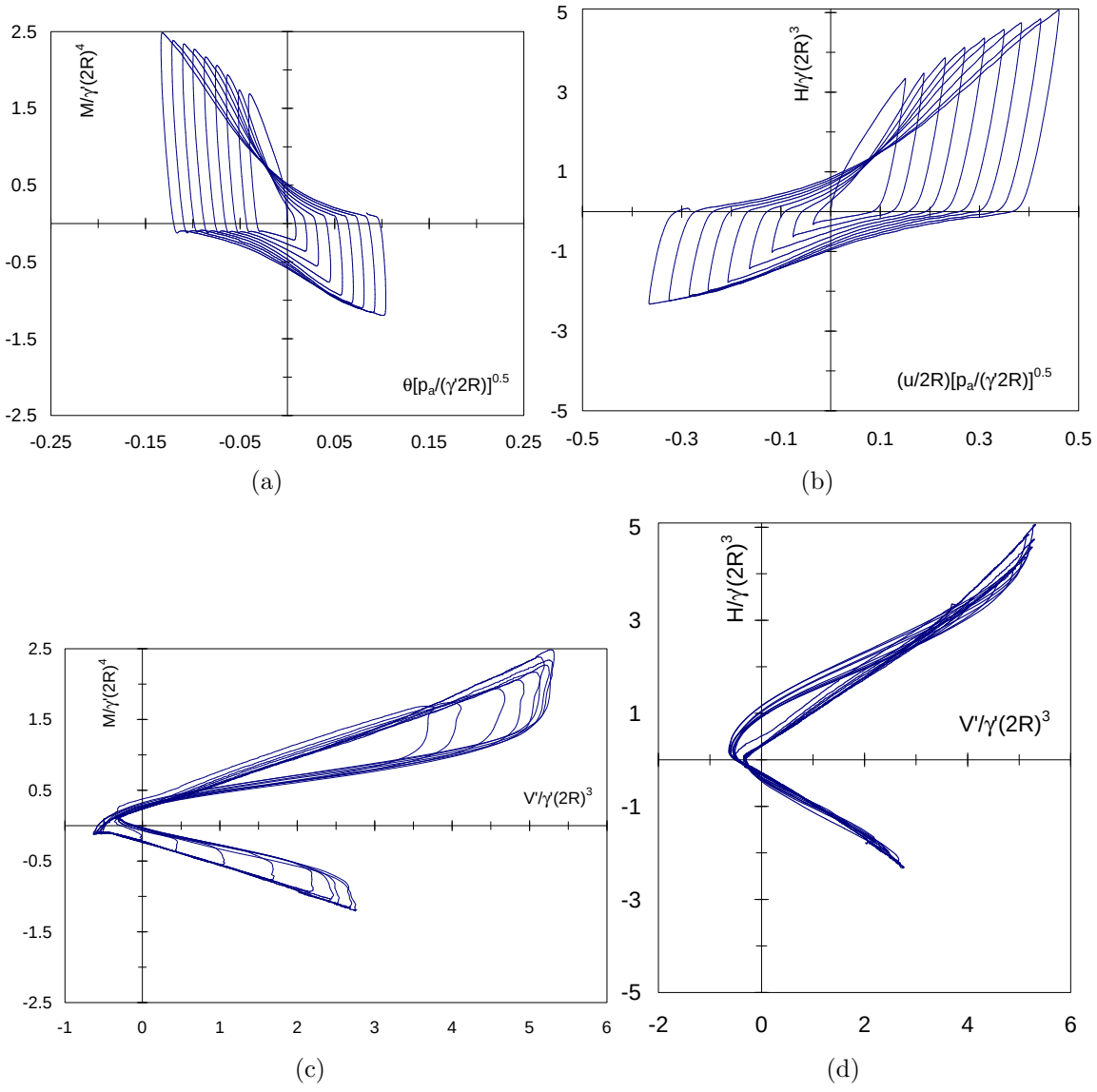


Figure 6.21: Cyclic swipe test FV10_4_3DS

Cyclic swipe tests were also performed using caisson D ($2R = 150$ mm and $\frac{L}{2R} = 1$) under a load ratio $\frac{M}{2RH} = 0.5$. In Chapter 5 it was found that the moment capacity increases with the aspect ratio. This can be confirmed looking at Figures 6.20(a) and 6.20(b), where normalised load-displacement curves are shown. Moreover, it is interesting to observe that

the normalised horizontal displacement is 3.5 times larger than the normalised rotation and the direction of rotation and horizontal displacement are opposite. Both issues are the contrary to what was shown in Figures 6.18(a) and 6.18(b) or in Figures 6.19(a) and 6.19(b). Again, the characteristic shape of the hysteresis loops with large rotation amplitude is observed. Additionally, a more pronounced asymmetry is observed after each cycle. Comparing Figures 6.20(c) and 6.20(d), different load paths during reloading and unloading are observed.

Figures 6.21(a) and 6.21(b) show that test FV10_4_3DS extends the cycling further, showing more pronounced asymmetry in the load-displacement curves and more difference in the magnitude of normalised rotation and horizontal displacement. However, the unloading curves shown in Figure 6.21(d) are not following the same trend as in Figure 6.20(d).

## 6.2 EXPERIMENTS IN OIL-SATURATED SAND

Monotonic moment loading tests of suction caissons in water-saturated sand did not cause a significant variation of the excess pore pressure $u'$. When variations of pore pressure were measured, for instance in cyclic loading tests, no noticeable effects on the caisson response were observed. In addition, dissipation of $u'$ occurred quickly due to the high soil permeability. It was deduced that fully drained conditions were prevalent in the water-saturated sand tests. However, offshore loading conditions can be partially drained or even undrained. Therefore, it was considered important to study the moment loading response of suction caissons in events where $u'$ can become a relevant parameter.

Scaling laws in the form of scale factors are useful in the study of physical geotechnical modelling, since relationships involving representative physical quantities can link prototype conditions with model conditions in the laboratory.

### 6.2.1 Scaling laws in partially drained physical models

The purpose of this section is to illustrate the effects of the use of a silicon oil as a pore fluid 100 times more viscous than water. Scaling relationships will be used to compare the relative effect of using water or oil. This will allow the scaling of time when studying partially drained phenomena.

The loading of a soil in the presence of fluid in the soil pores introduces a transfer effect between the soil grains and the fluid. In soil mechanics this loading transfer phenomenon is referred as consolidation (Terzaghi, 1943). From the normalisation of the one dimensional consolidation equation the following dimensionless time expression appears:

$$T_v = \frac{c_v t}{H^2} \tag{6.5}$$

where the coefficient of consolidation can be written as $c_v = \frac{k}{m_v \gamma_{fluid}}$; $m_v$ is the coefficient of volume compressibility, which can be obtained from standard oedometer tests as the inverse of the stiffness in a load-settlement curve, referred to as the constrained modulus $M_o$. The soil permeability $k$ is related to the absolute or specific permeability $K$, and the viscosity of the fluid $\mu$ as presented in Chapter 2. Therefore, the dimensionless time can also be expressed as:

$$T_v = \frac{K M_o t}{\mu H^2} \tag{6.6}$$

Introducing scale factors for the physical quantities in (6.6) it is possible to scale the consolidation time from the prototype to a model or *vice versa*. Muir Wood (2004) introduces the following expression:

$$n_t = \frac{n_\mu n_L^2}{n_G} \tag{6.7}$$

where the physical quantities correspond to diffusion time $n_t$, fluid viscosity $n_\mu$, length $n_L$ and soil stiffness $n_G$. Muir Wood (2004) also points out that expression (6.7) can also be derived from the analogy between the flow volume (according to the Darcy's law equal to $kiAt$, permeability, hydraulic gradient, area, time) and the strain volume ($\epsilon V$, strain,

volume), both caused by a change in stress. Then (6.7) can be applied for any problem involving diffusion time where consolidation is one possible phenomenon. For a model $n$ times smaller than the prototype the length scales linearly as $n_L = 1/n$; $n_G$ is the stiffness quantity that represents the variation of stress level between the geotechnical model in the laboratory and the prototype. A compromise is assumed by adopting the relationship for $G$ in equation 5.9, where $G \propto \sigma^{\alpha}$ ($n$ has been used before, but to not confuse with the scaling $n$ term $\alpha$ is used instead), hence $n_G = 1/n^{\alpha}$. If the same fluid is used in the model and the prototype $n_\mu = 1$, on the contrary $n_\mu = \frac{\mu_{model\,fluid}}{\mu_{prototype\,fluid}}$. If the prototype fluid is water, $\mu_{prototype\,fluid} \approx 1$ mm$^2$/s, then an option appears to increase the drainage time in sandy soils by increasing the fluid viscosity. Choosing in this particular case the model viscosity as the length scale $n$ the diffusion time gives:

$$n_t = n^{\alpha-1} \tag{6.8}$$

For sands $\alpha \approx 0.5$, thus assuming for instance a model 100 times smaller as well as a model fluid 100 times more viscous the diffusion time becomes ten times faster. To determine the velocities in the laboratory that correspond to the velocities in the field a similar analysis can be carried out in terms of the soil permeability $n_k$ instead of the viscosity $n_\mu$, resulting in the diffusion time as $n_t = \frac{n_L^2}{n_k n_G}$. From this expression the diffusion time can be obtained using the parameters for the model and the prototype as follows (Kelly *et al.*, 2006b):

$$\frac{t_m}{t_p} = \frac{k_p}{k_m}\left(\frac{2R_p}{2R_m}\right)^{2-\alpha} \tag{6.9}$$

Expression (6.9) will be used in the next section to interpret the experimental results in terms of the response of a prototype caisson.

### 6.2.2 Moment loading tests

The procedure to prepare low permeability Baskarp cyclone sand samples using silicon oil was described in Chapter 2. The suction assisted installation was carried out as described in Chapter 4. When the caisson penetration had finished the bleed and fluid

Table 6.5: Summary of moment loading tests in oil-saturated sand using caissons C

| Test | $\frac{M}{2RH}$ | $2R\frac{d\theta}{dt}$ mm/s | $h$ mm | $V'$ N | $\frac{V'}{A}$ kPa | $u_i'$ kPa | $\Delta u_i'$ kPa | $\Delta u_f'$ kPa |
|---|---|---|---|---|---|---|---|---|
| FV2_2_2S | 1.3 | 0.01 | 100 | 20 | 0.6 | 0.0 | 0.7 | 0.7 |
| FV2_3_2S | 1.4 | 0.005 | 100 | 50 | 1.6 | 0.0 | 1.5 | 1.3 |
| FV2_4_2P | 1.4 | 0.004 | 92.6 | 50 | 1.6 | 0.0 | 0.6 | 0.6 |
| FV3_1_9S | 1.0 | 0.0007 | 107.5 | 50 | 1.6 | -1.0 | 0.4 | 0.2 |
| FV3_1_5S | 1.5 | 0.04 | 105.9 | 100 | 3.2 | 1.8 | 0.9 | 0.4 |
| FV3_1_7S | 1.0 | 0.007 | 107.2 | 100 | 3.2 | 1.8 | 0.9 | 0.6 |
| FV3_1_4S | 1.5 | 0.007 | 105.6 | 100 | 3.2 | 1.8 | 0.9 | 0.7 |
| FV3_1_6S† | 1.6 | 0.007 | 106 | 200 | 6.4 | 1.8 | 2.2 | 2.2 |
| FV3_1_3S | 1.6 | 0.007 | 105.4 | 200 | 6.4 | 2.2 | 1.7 | 1.7 |

| Test | $K_{mi}$ N/mm | $K_{hi}$ N/mm | $\frac{M_y}{2R}$ N | $H_y$ N | $K_{mf}$ N/mm | $K_{hf}$ N/mm | $G_M$ MPa | $\frac{\delta u^p}{2R\delta\theta^p}$ | $\frac{\delta w^p}{2R\delta\theta^p}$ |
|---|---|---|---|---|---|---|---|---|---|
| FV2_2_2S | 3 | 1 | 0.8 | 1.2 | 1 | 1 | - | 0.479 | -0.009 |
| FV2_3_2S | 2 | 2 | 0.6 | 0.6 | 2 | 2 | - | 0.558 | 0.040 |
| FV2_4_2P | 51 | 20 | 4.0 | 2.2 | 0.4 | 0.4 | 1.0 | 0.817 | 0.014 |
| FV3_1_9S | 550 | 600 | 8.5 | 8.1 | 15 | 17 | 6.5 | 0.932 | -0.025 |
| FV3_1_5S | 48 | 10 | 2.8 | 0.3 | 10 | 8 | 0.7 | 0.916 | -0.005 |
| FV3_1_7S | 308 | 200 | 10.5 | 9.0 | 9 | 9 | 3.5 | 0.936 | -0.012 |
| FV3_1_4S | 100 | 30 | 2.6 | 0.9 | 7 | 5 | 2 | 0.945 | 0.020 |
| FV3_1_6S† | 200 | 100 | 12.6 | 7.1 | 10 | 6 | 3 | 0.935 | 0.101 |
| FV3_1_3S | 200 | 120 | 9.1 | 5.0 | 4 | 3 | 3 | 1.018 | 0.022 |

†cyclic test

valves were closed. Once the suction was stopped the recovery of a hydrostatic condition underneath the caisson lid was almost instantaneous. However, a pore fluid pressure above or below the hydrostatic pressure can be easily induced by changes in the vertical load, different from that used during the installation. Because the dissipation takes 100 times longer for the silicon oil than for water, the initial excess pore pressure $u_i'$ did not always dissipate completely as shown in Table 6.5.

The use of silicon oil in a very fine and dense sand reduces considerably the soil permeability making the loading rate a very important parameter. The tests were displacement controlled with the rotational displacement rates $2R\frac{d\theta}{dt}$ listed in Table 6.5. The initial test conditions were very similar, *e.g.* $\frac{M}{2RH}$, $R_d = 64\%$ for sample 2 and 80% for sample 3, and installation by suction (except test FV2_4_2CP, push installed). A second series of tests was carried out with slower rotation rates (Table 6.6). Selected tests from both series are shown on Figure 6.22(a), from which the dramatic effect of the rotation rate $2R\frac{d\theta}{dt}$ on the caisson moment-rotation response is clear.

The moment capacity is very small for the tests with $2R\frac{d\theta}{dt}$ = 0.01 mm/s and 0.005 mm/s. Figure 6.22(b) shows that underneath the caisson lid the fluid has taken the loading instead of the soil grains. Although there is no measurements of $u'$ around the caisson skirt, this lack of moment resistance is an indication of a loss of soil strength at the points where the soil was loaded by the caisson. However, the single measurement of $u'$ appears to capture a general pattern of response. In addition, the foundation stiffness is drastically diminished ($K_{mi}$ = 2 - 3 N/mm; $K_{hi}$ = 1 - 2 N/mm) and as a consequence, a reduction in resistance is observed no matter the amount of rotation applied. Undrained loading conditions were reached under these relatively high rotation rates. This proved to be detrimental to the suction caisson moment response.

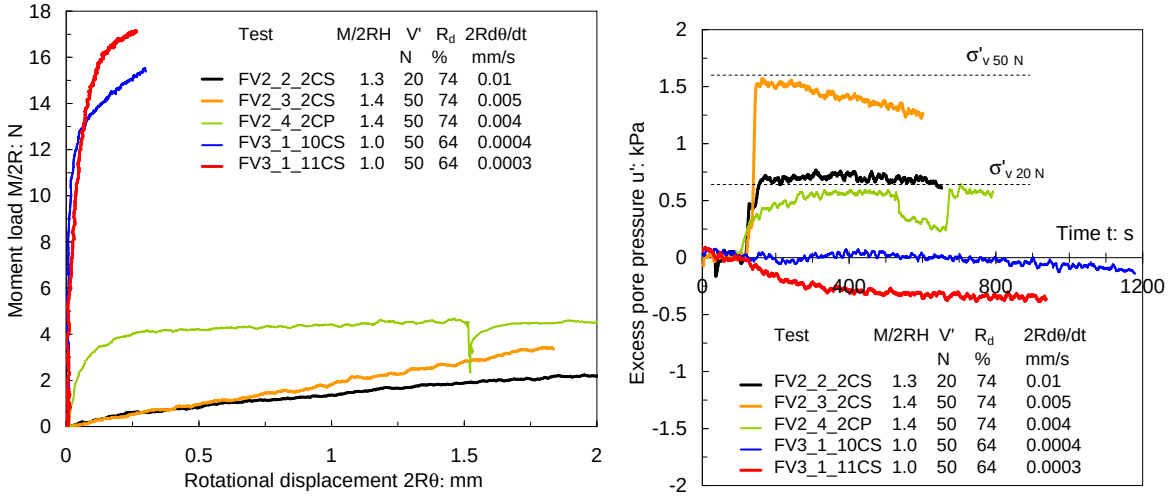


(a) Moment-rotation curves

(b) Excess pore pressure-time response

Figure 6.22: Moment loading tests showing effect of rate on the caisson moment capacity

Test FV2_4_2CP was carried out under $2R\frac{d\theta}{dt}$ = 0.004 mm/s, but the caisson was pushed into the ground instead of being installed by suction. This difference in installation method has an effect on the initial foundation stiffness response ($K_{mi}$ = 51 N/mm; $K_{hi}$ = 20 N/mm). However, as can be observed in Figure 6.22(a) there is not a significant improvement in the moment resistance. This can be also attributed to the build up of $u'$ shown in Figure 6.22(b).

Tests conducted at one order of magnitude less of rotational velocity, shown also in Figures 6.22(a) and 6.22(b), presented a much better moment response. At these rates more

time for the same rotation is allowed, leading to a 'partially' drained condition. Indeed, test FV3_1_10CS performed under $2R\frac{d\theta}{dt} = 0.0004$ mm/s shows a substantial recovery of the foundation response ($K_{mi} = 850$ N/mm; $K_{hi} = 400$ N/mm; $\frac{M_y}{2R} = 13$ N). This was a consequence of the partially drained conditions underneath the caisson lid which are highly likely to have occurred in the soil loaded by the caisson skirt too. Figure 6.22(a) shows another test with also a very slow rotational velocity $2R\frac{d\theta}{dt} = 0.0003$ mm/s with an even better moment response. Although the foundation stiffness was reduced, a slightly higher moment resistance was obtained ($K_{mi} = 400$ N/mm; $K_{hi} = 160$ N/mm; $\frac{M_y}{2R} = 16$ N). Negative values of $u'$ shown in Figure 6.22(b) reflect the beneficial effect of the suction.

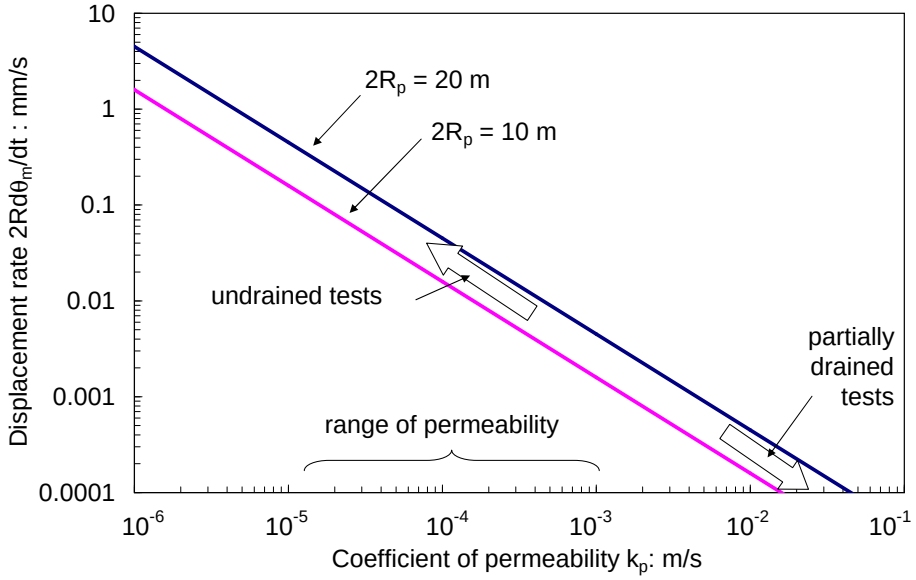


Figure 6.23: Rotational velocity of the model caisson as a function of the field permeability and prototype caisson diameter

To interpret these test results in terms of drainage conditions in the field, estimations of the scaling of rotational velocity is attempted with expression (6.9). In this expression the dissipation time is a function of the permeability and the caisson diameter. Assuming for the model a coefficient of permeability $k_m = 1.8 \cdot 10^{-7}$ m/s (Chapter 2), and for the field diameters $2R_p$ of 10 m and 20 m, $\alpha = 0.5$, and a diffusion time $t_p = 10$ s as the period of an extreme wave, the diffusion time $t_m$ can be determined. The rotational velocity $2R\dot{\theta}$ of a model caisson of 0.2 m diameter can be obtained dividing a common rotational displacement $2R\theta_m = 0.25$ mm by the diffusion time $t_m$. Figure 6.23 shows the rotational

velocity varying with the field permeability $k_p$ for two caisson diameters. For the likely range of permeability encountered in the field (bracketed in the figure) the rotational velocities of the model caisson results higher than 0.001 mm/s representing an undrained condition in the field. Therefore, only for very permeable soils and small caissons a better moment capacity would be expected. In conclusion, for extreme conditions the moment capacity of a prototype is small according to the model caisson test results.

The effect of letting the bleed valve open (Figure 2.13) during the caisson rotation is shown in Figures 6.24(a) and 6.24(b), where the two slowest tests shown in Figures 6.22(a) are included and compared with test FV3_1_16CS. The open bleed valve test shows a slightly lower moment capacity, but a similar $u'$ variation is observed. Whilst no variations in vertical displacements was observed in the two former tests with closed bleed valve, the caisson with open bleed valve exhibited uplift, as shown in Figure 6.24(c).

The moment capacity of caissons installed by suction was significantly reduced as pointed out in section §6.1.2. These moment loading tests were carried out immediately after the installation (around 10 minutes). Figure 6.25(a) shows the results from moment loading tests conducted around 48 hours after the suction installation. Only a minor difference exists between the moment capacity of the caisson installed by suction and by pushing. The improvement in the caisson response was not caused by the suction, since no suction was recorded during the moment loading tests. This suggests that time plays an important role in the recovery of the strength lost by the soil during the penetration. Figure 6.25(b) shows that the vertical movement was very small and there was no significant effect on $w$ from the installation methods.

Although the main interest of this research is the study of moment loading of caissons under low vertical load, it is important to know whether the rate effect modifies or not the response under higher constant $V'$. Figures 6.26(a), (b) and (c) show the moment-rotation response under a much higher constant vertical load ($V' = 200$ N) for cyclic and monotonic tests. The initial caisson response is very similar for the three tests in terms of

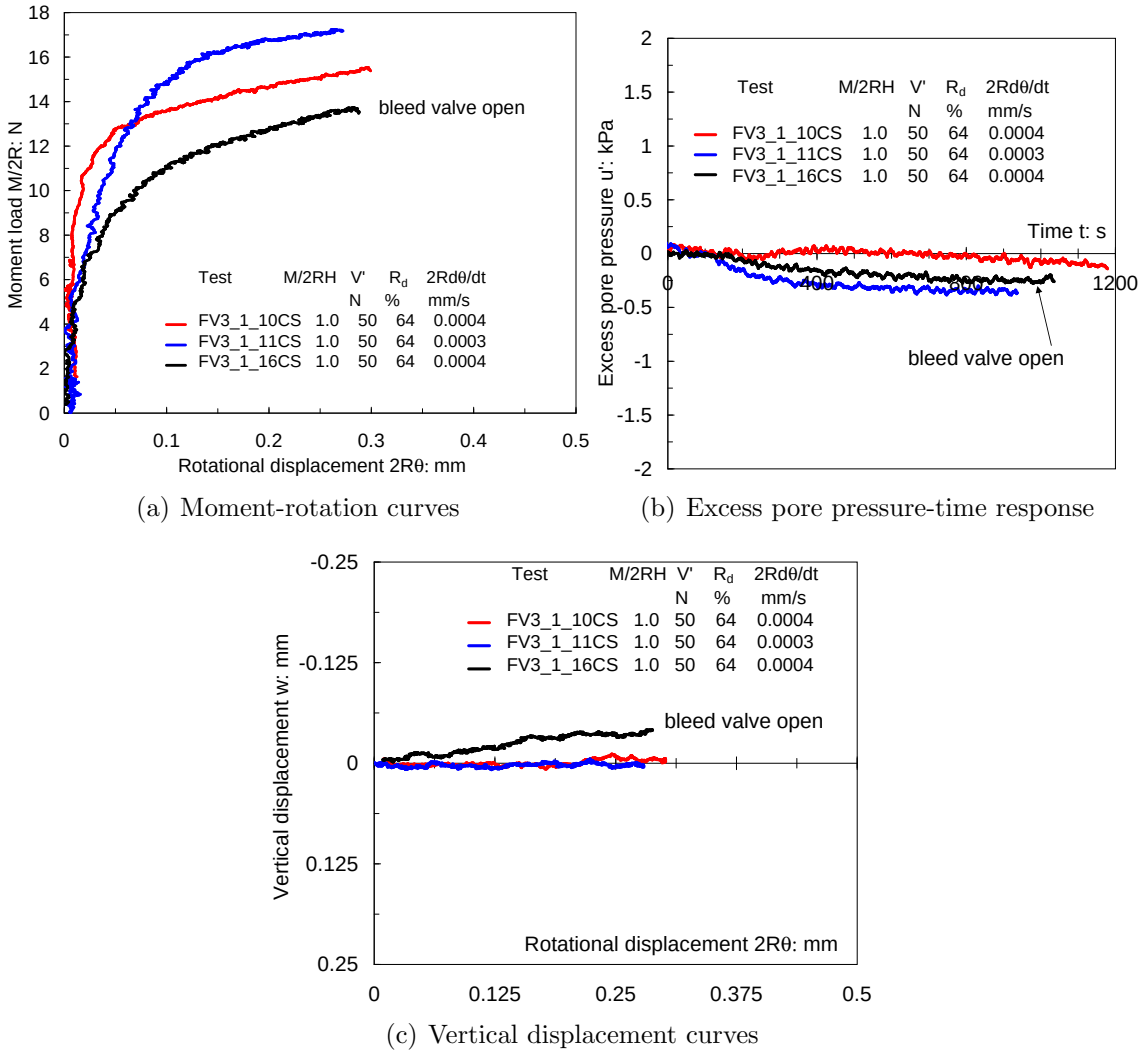


(a) Moment-rotation curves

(b) Excess pore pressure-time response

(c) Vertical displacement curves

Figure 6.24: Effect of the bleed valve open on the caisson response

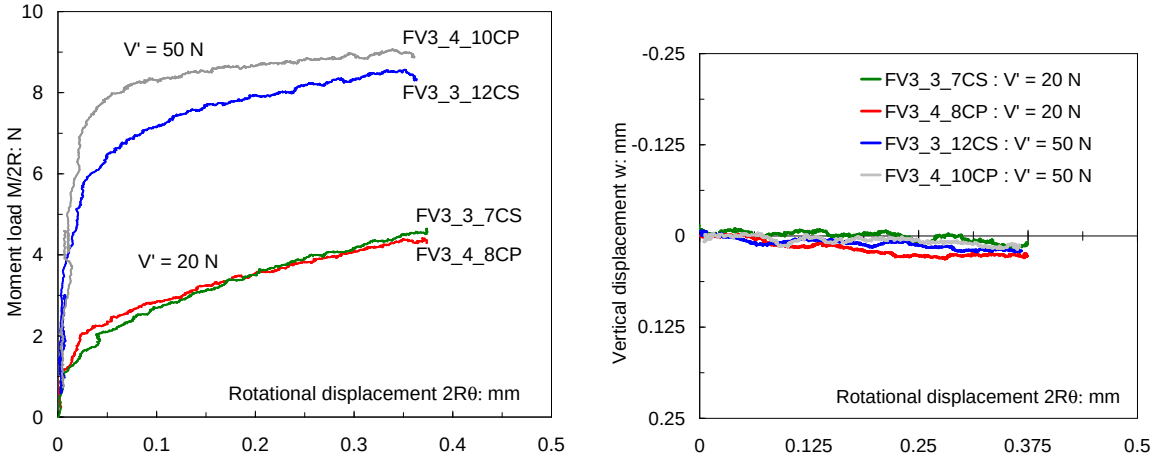


(a) Moment-rotation curves

(b) Vertical displacement curves

Figure 6.25: Comparison of moment capacity of a caisson installed by pushing and by suction

normalised moment, $\Delta u'_i$ and total $w_t$. However, the subsequent response differs specially for the cyclic tests. The excess pore pressure increases and a cyclic fluctuation $\Delta u'_{cyclic}$

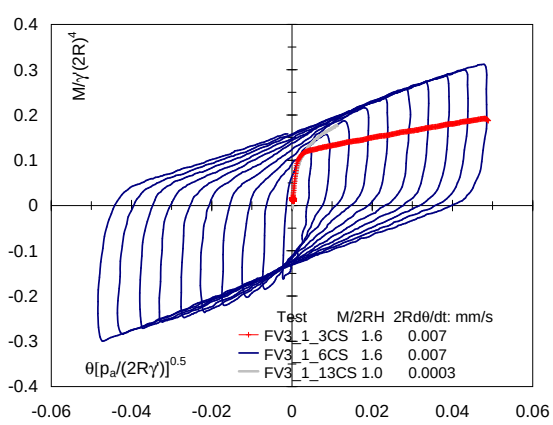


(a) Moment-rotation curves

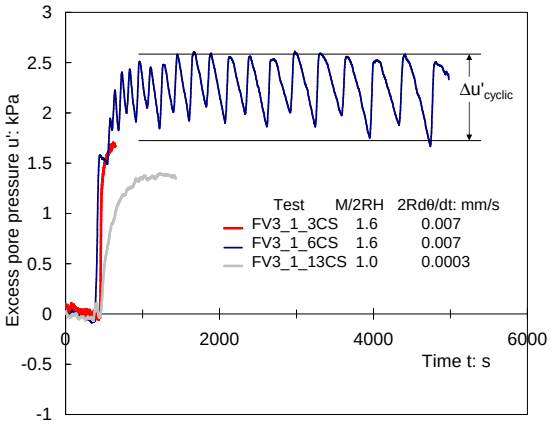


(b) Excess pore pressure curves

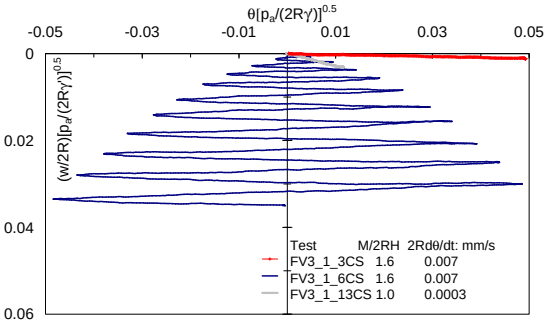


(c) Vertical displacement curves

Figure 6.26: Monotonic and cyclic response of a caisson under a very high value of $\frac{V'}{\gamma'(2R)^3} \approx 2.5$

occurs as well as a much larger caisson settlement (see Figures 6.26(b) and 6.26(c)). However, the level of $u'$ reached did not appear to be a detrimental to the monotonic nor to the cyclic moment response.

### 6.2.3 Yield points

In the previous section it was found that unless a large $V'$ is applied, high rotational velocities cause an unfavourable undrained response of the caisson foundation. Furthermore, high rotational velocities are more representative of the field condition for a certain range of permeability values. To generate fluid draining in the soil loaded by the caisson, it was necessary to rotate the caisson at a velocity $2R\frac{d\theta}{dt}$ between 0.0003 and 0.0004 mm/s. This allowed the identification of yield in the moment-rotation curves. To study partially drained conditions a second series of tests was performed, thereby yield loads ($\frac{M_y}{2R}$, $H_y$) were determined as defined in section §5.4, and are presented in Table 6.6.

Table 6.6: Summary of constant $V'$ moment loading tests installed by suction

| Test | $h$ mm | $V'$ N | $\frac{V'}{A}$ kPa | $u'_i$ kPa | $\Delta u'_i$ kPa | $\Delta u'_f$ kPa |
|---|---|---|---|---|---|---|
| $\frac{M}{2RH} = 1$ | | | | | | |
| FV3_3_19C | 97 | -11 | -0.4 | -0.4 | -0.1 | -0.3 |
| FV3_2_5C | 106.2 | -10 | -0.3 | -0.3 | -0.1 | -0.6 |
| FV3_2_2C | 106.1 | 20 | 0.6 | 0.0 | -0.4 | -0.3 |
| FV3_3_9C | 95.9 | 20 | 0.6 | 0.0 | 0.0 | -0.3 |
| FV3_1_14C | 108.1 | 30 | 1.0 | 0.0 | -0.8 | -0.8 |
| FV3_1_10C | 107.6 | 50 | 1.6 | -1.0 | 0.1 | -0.1 |
| FV3_1_11C | 107.6 | 50 | 1.6 | -1.0 | -0.3 | -0.4 |
| FV3_1_12C | 107.6 | 100 | 3.2 | 0.0 | -0.4 | -0.2 |
| FV3_3_10C | 96 | 48 | 1.5 | 0.0 | 0.5 | 0.5 |
| FV3_1_16C‡ | 108.7 | 50 | 1.6 | 0.6 | 0.0 | -0.2 |
| FV3_2_3C | 106.1 | 50 | 1.6 | 0.1 | 0.2 | 0.3 |
| FV3_2_4C | 106.3 | 100 | 3.2 | 0.2 | 0.8 | 0.7 |
| FV3_3_21C | 105 | 100 | 3.2 | 0.7 | 0.4 | 0.4 |
| FV3_2_6C | 106.5 | 150 | 4.8 | 0.0 | 1.5 | 1.8 |
| FV3_1_13C | 107.8 | 200 | 6.4 | 1.1 | 1.4 | 1.4 |
| FV3_1_15C | 108.2 | 250 | 8.0 | 3.3 | 1.2 | 1.2 |
| FV3_3_27C | 107.7 | 250 | 8.0 | 0.0 | 0.6 | 0.9 |
| FV3_3_31C | 109 | 1000 | 31.8 | 0.0 | 1.2 | 1.0 |
| FV3_3_32C | 110.5 | 2000 | 63.7 | -0.8 | 0.5 | 0.8 |
| $\frac{M}{2RH} = 0.5$ | | | | | | |
| FV3_3_18C | 97 | -10 | -0.3 | -0.5 | -0.2 | -0.2 |
| FV3_3_4C | 95.5 | 1 | 0.0 | 0.0 | 0.0 | -0.3 |
| FV3_3_6C | 95.6 | 9 | 0.3 | 0.0 | 0.0 | -0.3 |
| FV3_3_7C | 95.7 | 20 | 0.6 | 0.0 | 0.0 | -0.2 |
| FV3_3_12C | 97.2 | 48 | 1.5 | -0.5 | 0.5 | 0.0 |
| FV3_3_20C | 104.5 | 100 | 3.2 | 0.4 | 1.4 | 1.5 |
| FV3_3_26C | 107.5 | 248 | 7.9 | 1.0 | 0.4 | 0.5 |
| FV3_3_30C | 108.2 | 500 | 15.9 | 0.5 | 0.6 | 0.5 |
| $\frac{M}{2RH}$ = -2 | | | | | | |
| FV3_2_7C | 106.5 | 50 | 1.6 | 0.0 | -0.2 | -0.4 |
| FV3_3_13C | 97.4 | 50 | 1.6 | 0.0 | 0.5 | 0.5 |
| FV3_3_23C | 105 | 100 | 3.2 | 0.0 | 0.2 | 0.6 |
| FV3_1_8C† | 107.3 | 100 | 3.2 | 0.0 | 1.3 | 0.8 |
| FV3_3_28C | 107.8 | 250 | 8.0 | 0.0 | 0.0 | 0.3 |
| $\frac{M}{2RH}$ = -0.5 | | | | | | |
| FV3_3_15C | 97.6 | 49 | 1.6 | 0.0 | 0.3 | 0.6 |
| FV3_2_8C | 106.5 | 50 | 1.6 | 0.0 | 0.3 | 0.0 |
| FV3_3_24C | 105.4 | 100 | 3.2 | 0.0 | 0.5 | 0.5 |
| FV3_3_29C | 107.9 | 250 | 8.0 | 0.0 | 0.0 | 0.0 |
| $\frac{M}{2RH}$ = -0.25 | | | | | | |
| FV3_2_9C | 106.6 | 50 | 1.6 | 0.0 | 0.2 | 0.3 |
| FV3_3_16C | 98 | 50 | 1.6 | 0.0 | 0.7 | 0.9 |
| FV3_3_25C | 105.6 | 99 | 3.2 | 0.0 | 0.1 | 0.8 |

†$\frac{M}{2RH}$ = -1.5, ‡bleed valve open

Normalised plots showing the yield points as a function of the difference $V' - u'A$ were constructed. Measured values of $u'$ are restricted to only the location of the pore pressure transducer. It is believed that during the caisson rotation $u'$ varies across the lid. The inclusion of $u'$ attempts to account the level of excess pore fluid pressure underneath the

Table 6.7: Summary of constant $V'$ moment loading tests (continuation Table 6.6)

| Test | $K_{mi}$ N/mm | $K_{hi}$ N/mm | $\frac{M_y}{2R}$ N | $H_y$ N | $K_{mf}$ N/mm | $K_{hf}$ N/mm | $G$ MPa | $\frac{\delta u^p}{2R\delta\theta^p}$ | $\frac{\delta w^p}{2R\delta\theta^p}$ |
|---|---|---|---|---|---|---|---|---|---|
| $\frac{M}{2RH}$ = 1 | | | | | | | | | |
| FV3_3_19C | 90 | 60 | 1.7 | 1.5 | 5 | 10 | 1.5 | 0.54 | 0.01 |
| FV3_2_5C | 70 | 90 | 2.4 | 2.7 | 12.5 | 15 | 1 | 0.71 | -0.12 |
| FV3_2_2C | 220 | 120 | 6.8 | 6.6 | 2 | 3.5 | 3 | 0.72 | -0.06 |
| FV3_3_9C | 222 | 70 | 4.6 | 4.9 | 8 | 9 | 3.5 | 0.81 | 0.02 |
| FV3_1_14C | 350 | 200 | 9.2 | 9.0 | 9 | 10 | 5 | 0.90 | -0.09 |
| FV3_1_10C | 850 | 400 | 12.8 | 12.6 | 10 | 11 | 10 | 0.88 | -0.01 |
| FV3_1_11C | 400 | 160 | 15.8 | 15.5 | 7 | 8 | 3 | 0.98 | -0.03 |
| FV3_1_12C | 280 | 400 | 14.5 | 15.0 | 24 | 18 | 5 | 1.07 | 0.11 |
| FV3_3_10C | 270 | 180 | 6.8 | 6.4 | 6 | 9 | 3.5 | 0.76 | 0.09 |
| FV3_1_16C‡ | 350 | 180 | 10.9 | 10.5 | 11 | 12 | 5 | 1.01 | -0.16 |
| FV3_2_3C | 350 | 180 | 8.7 | 8.7 | 2.5 | 3 | 5 | 0.74 | 0.07 |
| FV3_2_4C | 200 | 150 | 6.8 | 6.9 | 12.5 | 15 | 3 | 0.84 | 0.14 |
| FV3_3_21C | 300 | 180 | 5.7 | 5.4 | 15 | 21 | 4 | 0.70 | 0.43 |
| FV3_2_6C | 350 | 290 | 10.5 | 10.6 | 12.5 | 13 | 4.5 | 0.84 | 0.21 |
| FV3_1_13C | 280 | 200 | 9.6 | 8.8 | 15 | 15 | 4 | 1.10 | 0.31 |
| FV3_1_15C | 180 | 130 | 9.8 | 8.5 | 19 | 19 | 2.5 | 1.31 | 0.46 |
| FV3_3_27C | 1000 | 300 | 28.0 | 28.1 | 19 | 21 | 12 | 0.83 | 0.07 |
| FV3_3_31C | 320 | 520 | 23.8 | 18.7 | 80 | 65 | 6.5 | 1.30 | 0.31 |
| FV3_3_32C | 1220 | 420 | 41.5 | 35.7 | 150 | 105 | 15 | 1.65 | 0.49 |
| $\frac{M}{2RH}$ = 0.5 | | | | | | | | | |
| FV3_3_18C | 50 | 60 | 1.0 | 1.8 | 4 | 10 | 1 | 0.75 | -0.03 |
| FV3_3_4C | 180 | 190 | 2.2 | 4.1 | 5 | 13 | 3 | 0.80 | 0.04 |
| FV3_3_6C | 180 | 190 | 4.4 | 8.6 | 4 | 8 | 3 | 0.85 | 0.02 |
| FV3_3_7C | 222 | 100 | 2.2 | 5.0 | 7 | 15 | 3.5 | 0.81 | 0.05 |
| FV3_3_12C | 470 | 770 | 7.1 | 13.7 | 5 | 12 | 6.5 | 0.79 | 0.06 |
| FV3_3_20C | 150 | 250 | 6.3 | 11.8 | 5 | 14 | 2.5 | 0.83 | 0.15 |
| FV3_3_26C | 500 | 1420 | 13.2 | 25.6 | 25 | 45 | 6.5 | 1.05 | 0.23 |
| FV3_3_30C | 400 | 420 | 23.0 | 45.9 | 40 | 60 | 6.5 | 1.39 | 0.36 |
| $\frac{M}{2RH}$ = -2 | | | | | | | | | |
| FV3_2_7C | 350 | -65 | 10.5 | -5.2 | 18 | -13 | 4.5 | 0.79 | -0.07 |
| FV3_3_13C | 300 | -80 | 8.6 | -4.4 | 11 | -8 | 3.5 | 0.59 | 0.05 |
| FV3_3_23C | 300 | -50 | 9.5 | -5.0 | 15 | -12 | 3.5 | 0.69 | 0.46 |
| FV3_1_8C† | 48 | -40 | 2.3 | -2.0 | 12 | -9 | 0.7 | 0.91 | 0.00 |
| FV3_3_28C | 1200 | -85 | 40.8 | -22.3 | 50 | -50 | 12 | 0.58 | 0.03 |
| $\frac{M}{2RH}$ = -0.5 | | | | | | | | | |
| FV3_3_15C | 300 | -220 | 12.8 | -26.4 | 11 | -80 | 3.5 | 0.29 | 0.11 |
| FV3_2_8C | 130 | -175 | 13.7 | -28 | 22 | -220 | 1.5 | 0.30 | 0.13 |
| FV3_3_24C | 500 | -220 | 16.0 | -35.2 | 22 | -100 | 4 | 0.43 | 0.54 |
| FV3_3_29C | 2200 | -263 | 38.3 | -69.0 | 60 | 400 | 17.5 | -0.36 | 0.01 |
| $\frac{M}{2RH}$ = -0.25 | | | | | | | | | |
| FV3_2_9C | 230 | -400 | 10.4 | -42 | 22 | 26 | 1.5 | -3.79 | 0.05 |
| FV3_3_16C | 300 | -250 | 9.2 | -40.5 | 22 | 19 | 3.5 | -4.45 | 0.41 |
| FV3_3_25C | 300 | -357 | 16.2 | -72.0 | 32 | 40 | 2 | -3.94 | 1.71 |

†$\frac{M}{2RH}$ = -1.5, ‡bleed valve open

caisson lid. In Table 6.6 a value of initial excess pore pressure $u'_i$ is included to account for non dissipated pore pressures at the beginning of the moment loading test. The variation in excess pore pressure caused by the caisson rotation above or below $u'_i$ is $\Delta u'$. In general the value of $\Delta u'$ was fairly constant during the caisson rotation, but to account

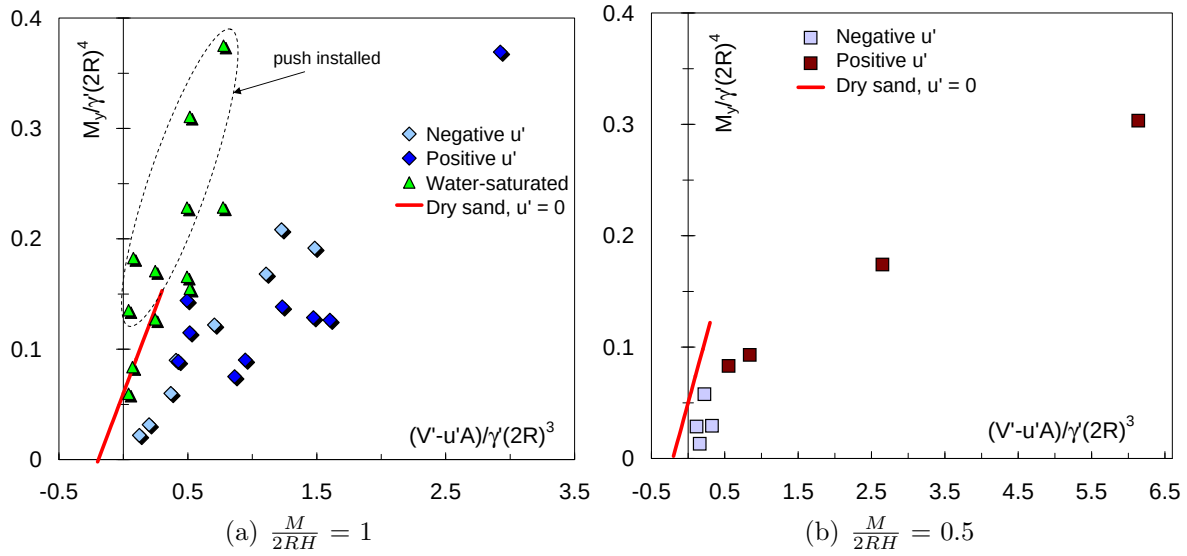


(a) $\frac{M}{2RH} = 1$ (b) $\frac{M}{2RH} = 0.5$

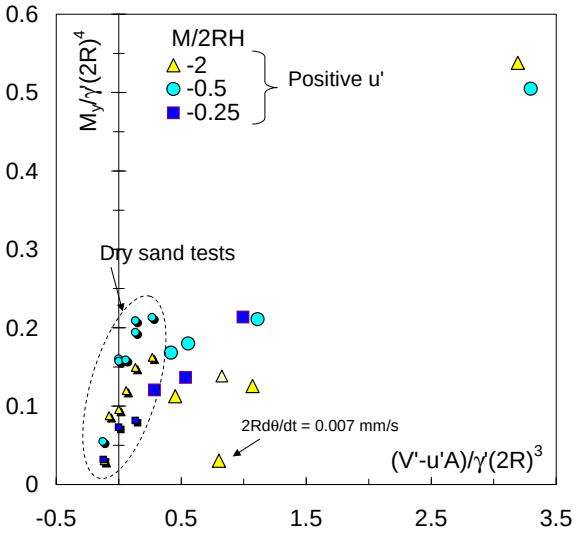


(c) $\frac{M}{2RH}$ = -2, -0.5, -0.25

Figure 6.27: Comparison of the moment capacity between partially drained and drained tests

for a possible variation a final value of pore pressure variation $\Delta u'_f$ (assuming $u'_i = 0$) was considered. In the following figures the excess pore pressure $u'$ is taken as the maximum sum of $u'_i + \Delta u'$ or $u'_i + \Delta u'_f$.

Yield points of tests conducted at $\frac{M}{2RH} = 1$ are shown in Figures 6.27(a). Results from partially drained oil-saturated sand tests can be compared with drained test results from loose dry sand (line) and from water-saturated sand (triangular yield points). A similar plot for $\frac{M}{2RH} = 0.5$ is shown in Figure 6.27(b) and for $\frac{M}{2RH}$ = -2, -0.5, -0.25 in Figure 6.27(c). It can be observed that the yield points from water-saturated sand tests follow the trend of the results from the dry tests. Yield loads from the oil-saturated tests, asso-

ciated with negative values of $u'$, represent the presence of suction during rotation. These yield points are slightly moved towards the right from the trend follow by the drained tests, owing to the inclusion of the suction in the normalised vertical load. Whilst, positive $u'$ values, generated by increasing values of normalised $V'$, shift the yield loads to the left. In view of these plots, the caisson moment capacity was reduced by the build up of $u'$ in comparison with that obtained from drained tests.

An example of the yield points projected on the $\frac{M_y}{2RV_o} - \frac{H_y}{V_o}$ plane is shown in Figure 6.28 where results of tests with $V' = 50$ N from oil-saturated sand are compared with results from the tests in dry sand for $V' = 100$ N since both $V'$ scale as $\frac{V'}{V_o} \approx 0.2$. It can be observed the favourable effect of negative $u'$ on the caisson lateral capacity, which is reflected in the increasing values of $\frac{M_y}{2R}$ and $H_y$.

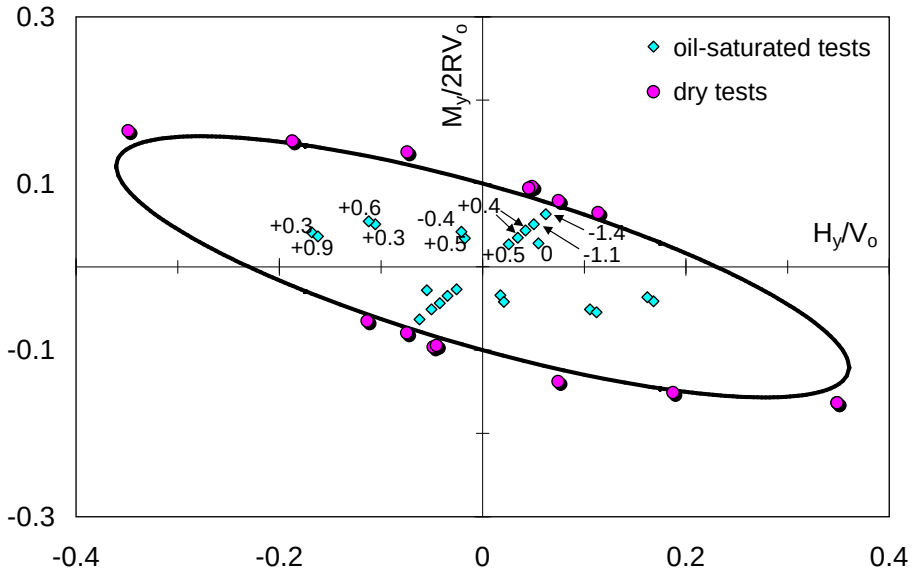


Figure 6.28: Comparison between the yield surface and yield points determined in drained condition and in partially drained conditions. Numbers next to the points indicate the maximum $u'$ in kPa

### 6.2.4 Foundation stiffness

The moment capacity can be significantly reduced if not enough suction is developed or an even more unfavourable condition if positive $u'$ build up occurs. It is important to assess the foundation stiffness before a yield condition occurs. Values of the initial and

final foundation rotational and lateral stiffness are presented in Table 6.7 as $K_{mi}$, $K_{mf}$, $K_{hi}$ and $K_{hf}$. Comparisons, in terms of a normalised $K_{mi}$ (Kelly *et al.*, 2006a), are shown in Figure 6.29(a) between results obtained in the partially drained oil-saturated tests and drained test results from dry and water-saturated sands. There is scatter in the data, but it is clear that the normalised stiffness from partially drained test follows the trend of the normalised stiffness from drained tests. It is worth noting that the foundation stiffness was even higher when suction appeared.

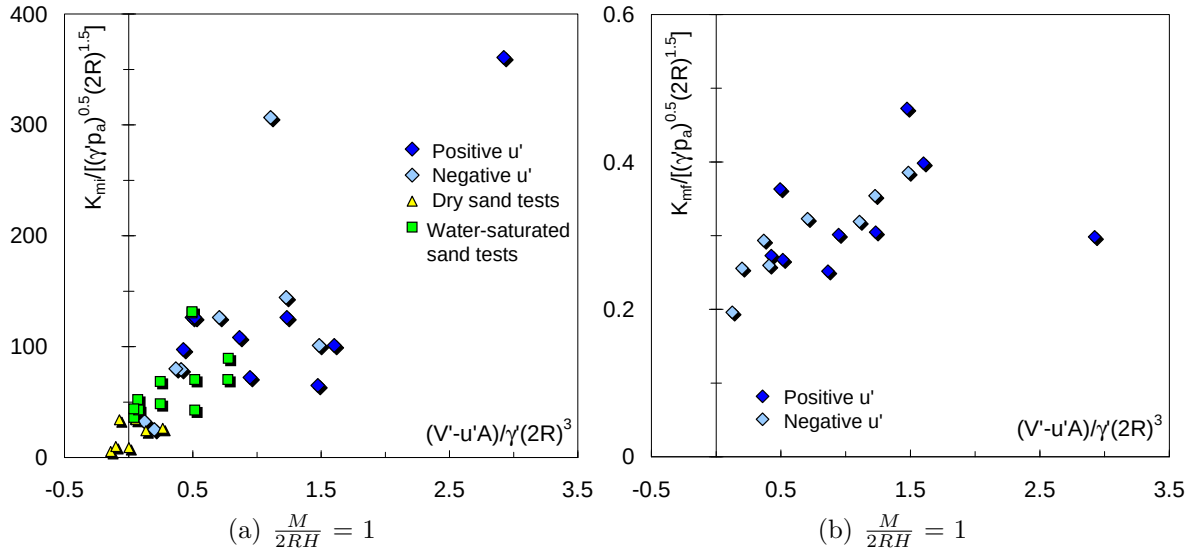


Figure 6.29: Comparison of the normalised foundation stiffness between partially drained tests and drained tests

As previously pointed out, $K_{mf}$ is practically independent of $V'$ and also independent of the excess pore pressure as can be observed in Figure 6.29(b). Values of normalised $K_{mf}$ from the drained tests are not shown because they are much higher (see Figure 6.5(c)). This is evidence that a gradual process of yield leads to a state where the foundation response is the same, no matter the combined loading applied or even the pore fluid pressures developed.

### 6.2.5 Vertical displacement

The previous analysis of the effect of $u'$ on the resultant moment load at yield is in fact a consequence of the displacements experienced by the caisson and in particular of the vertical displacement $w$. Figures 6.30(a) and 6.30(b) shows the ratio between the plastic

vertical displacement increment and the plastic rotational displacement increment $\frac{\dot{w}^p}{2R\dot{\theta}^p}$ varying with $\frac{V'-u'A}{V_o}$.

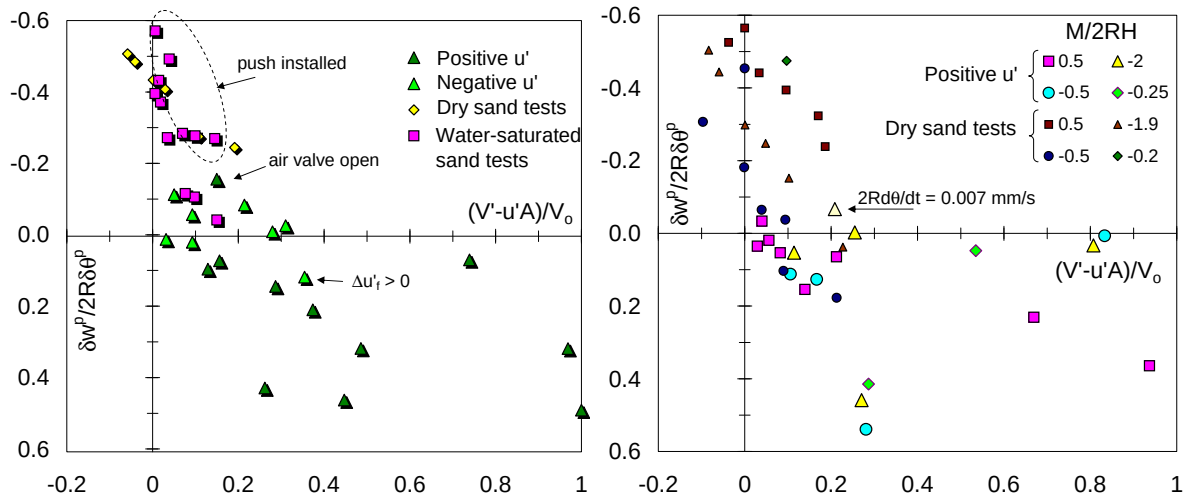


(a) $\frac{M}{2RH} = 1$ (b) $\frac{M}{2RH} = 0.5, -2, -0.5, -0.25$

Figure 6.30: Comparison of the normalised plastic vertical displacement between partially drained tests and drained tests

The suction generation during loading reduces the caisson upward movement, whereas positive $u'$ induces settlements increasing with the vertical load. There is scatter in the partially drained data, which is believed to be due to the pore pressure transducer location. Therefore, it is difficult to identify the parallel point, but rather a range of $\frac{V'-u'A}{V_o}$ values between 0.05 and 0.3. Further experiments are required to determine the $u'$ variation across the caisson lid during moment loading.

## 6.3 CONCLUSIONS

With the purpose of investigating the moment response of suction caissons under drained, partially drained and undrained conditions, two main groups of tests were performed, one in water-saturated sand and the other in oil-saturated sand.

### 6.3.1 Experiments in water-saturated sand

From experiments comparing caissons installed by suction and by pushing was found that the moment resistance of a suction caisson depends on the method of installation. The yield loads determined from suction installed caissons were approximately half of

those determined from pushing installed caissons for the case of low thickness ratio $\frac{t}{2R} = 0.5\%$. Less difference was found for $\frac{t}{2R} = 1.2\%$. The suction installation method causes a fluid flow regime around the caisson that disturbs the soil, reducing the shear strength of the soil inside the caisson. The initial foundation stiffness was significantly reduced for the case of suction installation only for the caisson with lower thickness ratio.

The ratio of plastic deviatoric displacement increments was found to be independent of the installation method. However, the ratio of plastic vertical and rotational displacement increments was reduced when the suction was used. In other words, more uplift was observed in pushing installed caissons than in suction installed caissons.

The yield surface expression was applied successfully to two different size suction caissons after normalisation by $V_o$, but requires different values of $t_o$ to account for the different thickness ratios.

Comparisons between results from laboratory cyclic tests and results from field trials showed the importance of the level of stresses on the lateral earth pressure, when assessing moment capacity and vertical displacements. Difference in the shape of the hysteresis loops for large rotation was observed due to gapping for the caisson in the field trial.

Cyclic swipe events can be used as an approach to reproduce offshore wave loading, where the vertical load varies simultaneously with the moment and horizontal loads. Masing's rules were not obeyed in these tests.

### 6.3.2 Experiments in oil-saturated sand

To study undrained and partially drained conditions moment loading tests of suction caissons were carried out in an oil-saturated sand. For a plausible range values of soil permeability in the field, it was found that the high rotational velocity tests in the laboratory which caused undrained conditions are representative of the field conditions. Undrained

conditions had a detrimental effect on the moment response of suction caissons under low vertical load.

In partially drained tests the presence of suction during combined loading under low vertical loads improves the moment capacity and reduces almost completely the caisson uplift. However, in $V' - u'A$ plots the caisson resistance appears reduced in comparison with drained test results. Positive excess pore pressures induced settlements increasing with the vertical load.

It was assumed an uniform excess pore pressure distribution from measurement in one location underneath the caisson lid. Further experiments with measurements at several locations are required to determine the excess pore pressure distribution across the caisson lid during monotonic and cyclic moment loading.

# Chapter 7

# SUCTION CAISSONS IN CLAY

## Abstract

A testing programme to study the response of a suction caisson with an aspect ratio of one in heavily overconsolidated clay was conducted. Firstly, installation of the caisson by pushing and by suction, as well as the maximum pullout capacity was studied. Secondly, three series of cyclic vertical loading tests, which are relevant to applications for multi-caisson foundations, were performed. It was found that, before failure, the caisson installed by suction had less upward movement than the caisson installed by pushing for increasing cyclic load amplitudes around a mean vertical load $V_m = 0$ N. This is attributed to the different pore water pressure variation developed and measured underneath the caisson lid, since both series of tests were performed under identical conditions. Thirdly, monotonic and cyclic moment loading tests, which are relevant to applications for monopod caisson foundations, were performed in the form of swipe events and constant vertical load events. In the cyclic tests hysteresis loop constriction appeared as a consequence of gapping, reducing the moment capacity and increasing caisson uplift when experiencing tensile load. Results from monotonic tests permitted the parameters of a mathematical expression for the yield surface to be determined. It was found that the yield surface had different shape and size depending on the ratio between the caisson load history and bearing capacity $\frac{V_o}{V_u}$. An associated flow rule was defined to suit the ratio $\frac{V'}{V_o}$. However, variations with the $\frac{V_o}{V_u}$ ratio were found.

# 7.1 INSTALLATION AND PULLOUT CAPACITY

## 7.1.1 Introduction

Suction caisson response in clayey soils has been studied more widely than for sands. Research has concentrated mostly on suction caissons as anchors, and in normally consolidated soils for a variety of offshore deep water structures, where caisson aspect ratios are commonly higher than three. Information on this application can be found in Andersen *et al.* (1993), Clukey *et al.* (1995), El-Gharbawy (1998), Andersen and Jostad (1999), House (2002), Colliat and Dendani (2002) and Aubeny *et al.* (2003) among others. Latterly, the proceedings of the conference "Frontiers in Offshore Geotechnics" held in Perth, Australia in 2005 included a state-of-the-art keynote paper by Andersen *et al.* and a section dedicated to suction caissons in deepwater developments. However, very little research of foundations for offshore wind turbines in clay has been carried out. Therefore, this study emerges as a natural and rational response to a necessity in this area of geotechnical engineering.

Recent studies by House (2002), Rauch *et al.* (2003) and Chen and Randolph (2004) have demonstrated that there is not a substantial difference (as in sands) between the net vertical load required to install caissons (with $\frac{L}{2R} \geq 4$) into normally consolidated clay by pushing ($V'$) and by suction ($V' + |S|$). However, it is not yet clear the effect that the different installation methods have on the caisson response to subsequent loading. Although, installations by pushing were mostly chosen owing to the simplicity in the use of the *VMH* loading rig, one suction installation test was performed. This allowed comparisons with theoretical estimations of the suction, as well as to assess if the net vertical load is indeed independent of the installation method. Furthermore, comparisons of subsequent short term vertical cyclic response were established.

Caisson D (diameter and skirt length $2R = L = 150$ mm, aspect ratio $\frac{L}{2R} = 1$, and skirt thickness $t = 1$ mm), shown in Figure 2.8(e), was selected for the testing programme in heavily overconsolidated kaolin clay specimens. Properties, details of the preparation

and set-up conditions of the clay specimens are presented in Chapter 2. Natural over-consolidated clays are the product of a number of geological processes such as glaciation, ground water level changes, *etc.* This type of soil is encountered in the offshore seabed at some of the sites released by Crown Estates and is commonly referred to as stiff or hard clay.

### 7.1.2 Penetration resistance

The vertical load required (without suction) to penetrate a caisson into a purely cohesive soil can be obtained from equilibrium of the acting and reacting forces involved. The frictional resistance inside and outside the caisson are calculated using adhesion factors $\alpha_i$ and $\alpha_o$. The end bearing is calculated using the cohesion bearing capacity coefficient $N_c$ for deep plane strain (strip footing). As a result, the submerged vertical load $V'$ needed to penetrate a caisson a depth $h$ can be expressed as follows:

$$V' = \alpha_o \bar{s}_u 2\pi R_o h + \alpha_i \bar{s}_u 2\pi R_i h + 2\pi R t \left(\gamma' h + s_u N_c\right) \tag{7.1}$$

where $\bar{s}_u$ is the average undrained shear strength amidst the mudline and the caisson tip, $s_u$ is the undrained shear strength at the caisson tip, $R_o$, $R$ and $R_i$ are the outside, mean and inside caisson radii, and $t$ is the skirt wall thickness (see Figure 4.2 for suction caisson outline). House (2002) and Chen and Randolph (2004) adopted a value of $N_c$ = 7.5. However, $N_c$ varies with depth between 7 and 12; for that reason a value of 9 is considered more appropriate.

The suction required to assist the installation of a caisson into clay a depth $h$ can be derived from equation (7.1), resulting in the following expression:

$$s = \frac{1}{\pi R_i^2}\left[\alpha_o \bar{s}_u 2\pi R_o h + \alpha_i \bar{s}_u 2\pi R_i h + 2\pi R t \left(\gamma' h + s_u N_c\right) - V'\right] \tag{7.2}$$

where the suction $s$ has been added as the contributing force $S = s\pi R_i^2$ to the left hand side of (7.1). It is necessary to clarify that $V'$ does not correspond to the subtraction

$V' = V - S$. The subtraction $V'_e = V' - S$, where the subscript $e$ stands for 'effective', emulates Terzaghi principle of effective stresses. Once full penetration is achieved, care should be taken in the interpretation of $V'_e$ values, since values of $s$ correspond to one point, which can be assumed uniformly distributed underneath the caisson lid. However, it has been shown in Chapter 6 that for instance, during caisson rotation $s$ can vary substantially across the caisson lid.

### 7.1.3 Pushing and suction installation test results

House (2002) employing equation (6.1) with $t$ as the relevant dimension instead of $2R$ (as originally suggested for calcareous sand by Finnie (1993)) found that in NC kaolin clay undrained conditions correspond to dimensionless footing velocities $v_n > 10$, whilst fully drained conditions will be reached for $v_n < 0.1$. In this study penetration of the caisson skirt into the ground by pushing was conducted at a rate $\dot{h}$ of 0.5 mm/s. Then, since $v_n = 1.6$, it is deduced that partially drained conditions occur, assuming vertical flow with a value of $c_v = 0.3$ mm$^2$/s for a vertical pressure $p' = 200$ kPa (de Santa Maria, 1988).

Figure 7.1(a) shows all the pushing load-penetration curves $V' - h$, in addition to the curve $(V' + |S|) - h$ of test FV7_1S, which was installed by suction assistance after 30 mm of pushing penetration. This initial pushing penetration followed the curves of tests FV2_1 and FV6_1 due to the proximity of $s_u$ values. Note that between 30 mm and 60 mm $(V' + |S|) - h$ reduces the rate of increase with penetration as a result of the starting and fluctuation of the suction. However, after 60 mm of penetration the curve of test FV7_1S undoubtedly follows again in between the pushing penetration curves of tests FV2_1 and FV6_1. Therefore, it can be concluded that the caisson penetration resistance is independent of the installation method in heavily overconsolidated kaolin clay, as previously found in NC kaolin clay and in high aspect ratio caissons by House (2002), Rauch *et al.* (2003) and Chen and Randolph (2004).

Differences observed in the curves shown in Figure 7.1(a) are due to the different val-

ues of $s_u$ and $V_c$ (contact vertical load at full penetration). Thus, those differences can be reduced normalising $V'$ (and $V' + |S|$) by $V_c$ or by $s_u(2R)^2$ as shown in Figure 7.1(b).

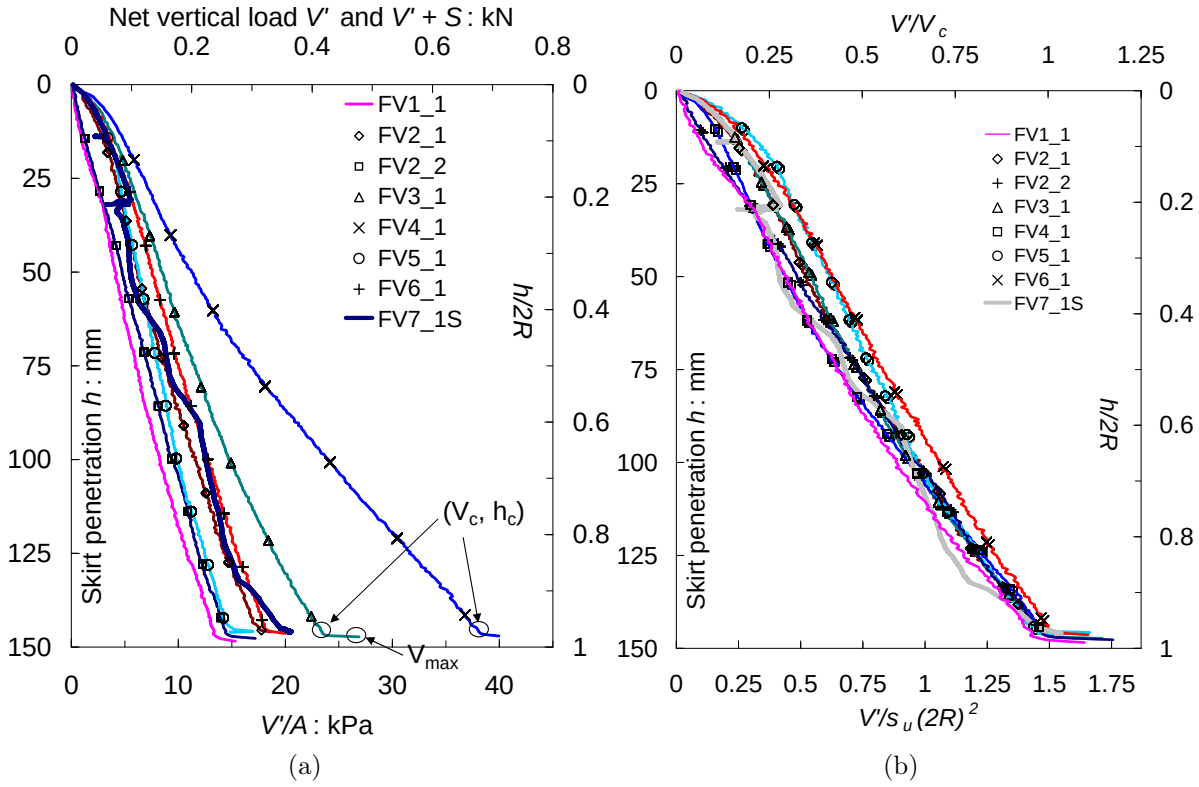


Figure 7.1: (a) Load-penetration curves, (b) Normalised load-penetration curves

From the load-displacement curves shown in Figure 7.1(a), values of contact vertical load $V_c$, contact penetration $h_c$, $V_{max}$, and back-calculated values of adhesion $\alpha_i = \alpha_o$ were obtained and are summarized in Table 7.1. It is worth pointing out that differences between the values of $h_c$ and $L = 150$ mm (4 mm in average) are due to internal soil-plug upheaval, which is caused by the soil displaced inwards by the skirt penetration. Surprisingly, the inwards flow caused by the suction did not induce more upheaval than that obtained in the pushing tests. If only inwards movement occurred the soil volume displaced by the skirt penetrating would result in a heave of 4 mm (with 1 mm wall thickness). This suggests that the volume occupied by the penetrating skirts may be fully displaced inwards, indicating the existence of a non-symmetrical shear failure mechanism. This demonstrates that the plug-heave represents a tiny 2.7% of the caisson length $L$. In caissons with higher $\frac{L}{2R}$ heave can be totally different, for instance House (2002) reported cases for $\frac{L}{2R} > 8$ (in NC kaolin) where the plug-heave percentage was as high as 30% or 40%.

Table 7.1: Parameter values obtained from the installation test results

| Test | $V_c$ N | $h_c$ mm | $V_{max}$ N | $\alpha_{io}$† | $s_u$ kPa |
|---|---|---|---|---|---|
| FV1_1 | 248 | 148 | 500 | 0.35 | 7.3 |
| FV2_1 | 316 | 146 | 998 | 0.47 | 8.1 |
| FV2_12 | 260 | 147 | 1089 | 0.42 | 7.3 |
| FV5_1 | 271 | 145 | 301 | 0.55 | 6.1 |
| FV3_1 | 417 | 146 | 478 | 0.50 | 10.2 |
| FV6_1 | 321 | 145 | 417 | 0.48 | 8.4 |
| FV4_1 | 682 | 147 | 1082 | 0.60 | 13.2 |
| FV7_1‡ | 353 | 145 | 353 | 0.40 | 9.8 |

†back calculated using $N_c = 9$

‡installation by suction, $\alpha_{io} = 0.5$ assumed for the initial pushing installation

Normalisations by $s_u$ and $V_c$ are shown in Figure 7.1(b) because a linear relationships was found between $s_u$ and $V_c$. The values of $s_u$ were obtained from shear vane measurements carried out after each test in non disturbed sites at depths of 25 mm and 125 mm (Table 2.5). Whilst, $V_c$ values were obtained directly from the load-displacement curves (Table 7.1). Figure 7.2 shows that the results of $s_u$ at 125 mm depth are more consistent than the obtained at 25 mm, since (discarding test FV5_1) more scatter occurred for measurements close to the surface. This is confirmed by the higher value of the coefficient of determination $R^2$ (closer to 1) of the fitted curve. The value of $s_{u_{125}}$ assumed as $s_u$ at the tip gives hence more consistent values for normalisation by the clay strength.

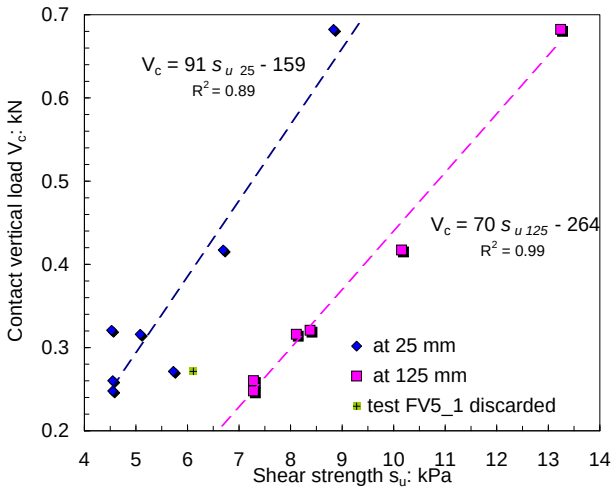


Figure 7.2: Relationships between $V_c$, measured in caisson installation tests, and $s_u$, measured at two depths: close to the surface and close to the caisson tip

The equations (7.1) and (7.2) were use to fit the load-penetration curves by back-analysing a theoretical adhesion factor, assumed to be equal inside and outside the caisson skirt ($\alpha_{io} = \alpha_i = \alpha_o$). Figure 7.3(a) shows that the values of $\alpha_{io}$ obtained correlated reason-

ably well with $s_u$ and hence with $V_c$. The expression that best fit the results is:

$$\alpha = 0.0275 s_u + 0.23 \tag{7.3}$$

It is important to mention that (7.3) is restricted to the particular conditions of the testing, namely $\frac{L}{2R} = 1$ and a heavily OC clay. The API RP2A (1993) (quoted by Kolk and van der Velde, 1996) established expressions for axial capacity of fully installed driven piles in clay (after full consolidation). For clays with plasticity index of $I_p > 20\%$, $\alpha$ can be obtained as follows

$$\begin{aligned} \alpha &= \frac{1}{2}\left(\frac{s_u}{\sigma'_v}\right)^{-0.5} \qquad \text{for} \qquad \frac{s_u}{\sigma'_v} \leq 1.0 \\ \alpha &= \frac{1}{2}\left(\frac{s_u}{\sigma'_v}\right)^{-0.25} \qquad \text{for} \qquad \frac{s_u}{\sigma'_v} > 1.0 \end{aligned} \tag{7.4}$$

Although (7.4) has been found to be adequate for piles in heavily OC clays (Kolk and van der Velde, 1996), resulting values of $\alpha$ between 0.22 and 0.26 are too conservative to be applied for caissons. This reveals that direct extrapolations from pile design may lead to wrong predictions in suction caisson analyses. Conversely, Andersen and Jostad (1999, 2002) suggest that the reduction of $s_u$ along the skirt due to penetration is caused by clay remoulding. On the grounds that by definition the clay sensitivity is a measure of the remoulded state, they define that $\alpha$ is the inverse of the sensitivity $S_t$, as defined by Terzaghi (1943), in the following form:

$$\alpha = \frac{C_t}{S_t} = C_t \frac{s_{u_{(remoulded)}}}{s_{u_{(peak)}}} \tag{7.5}$$

where $C_t$ is the thixotropy strength ratio which accounts for the capacity of a remoulded clay to return to its undisturbed state after a certain time interval (Skempton and Northey, 1952). For kaolin clay $C_t$ is close to unity, for other clays refer to Skempton and Northey (1952) and Andersen and Jostad (2002). Equation (7.5) gives an initial value of $\alpha$, which is obtained immediately after installation, hence before any dissipation of excess pore pressures. Figure 7.3(b) shows $\alpha - \Theta$ curves obtained from shear vane tests. The ma-

jority of these tests were stopped around 60° of rotation, after a peak value was reached. However, three vane tests carried out in sample 6 continued further until a remoulded condition (assumed as residual) was reached after more than 360° of rotation. It can be observed that a value of $\alpha$ around 0.4 can be obtained directly from the plot for a depth of 125 mm (slightly lower than the back-calculated 0.48), and around 0.25 for a depth of 25 mm.

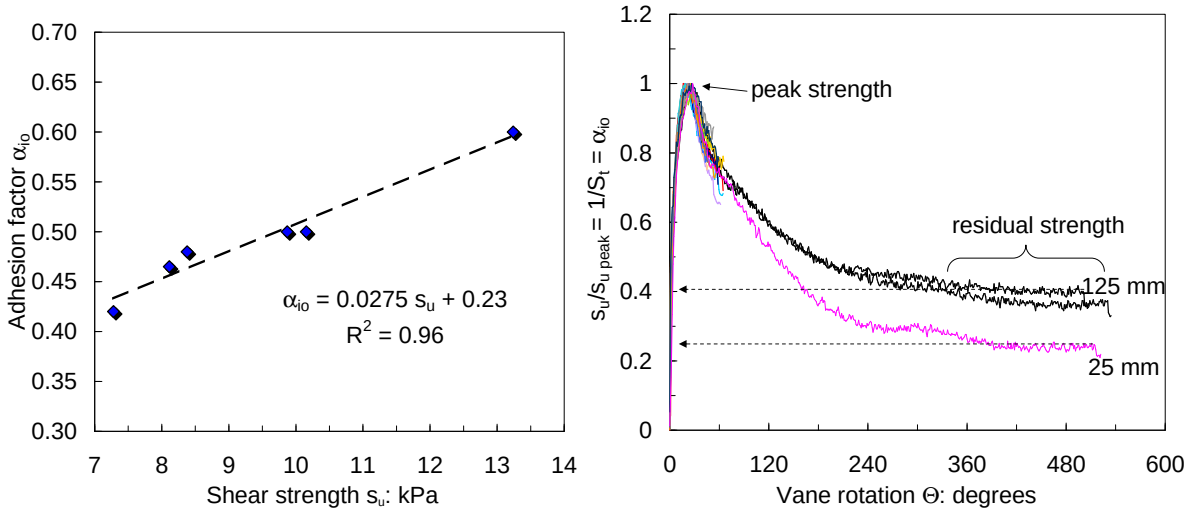


Figure 7.3: (a) Relationship between the adhesion factor and the shear strength $\alpha$ - $s_u$, and (b) adhesion factor as the inverse of the sensitivity $\alpha = \frac{s_{u(remoulded)}}{s_{u(peak)}} = \frac{1}{S_t}$ *versus* vane rotation $\Theta$

With the back-calculated $\alpha$ values an estimation of the caisson penetration resistance with depth using equation (7.1) is presented in Figure 7.4(a) for test FV2_1. It can be observed that between 5 mm to 60 mm of penetration the calculated $V'$ is lower than the measured value of $V'$. This is due to the lower shear strength assumed in the idealized distribution for that range of penetration. However, the predicted curve is fairly close to the measured curve after that initial layer was penetrated.

Figure 7.4(b) shows the measured and calculated suction-penetration curve obtained in test FV7_1. To account for the variation of strength with depth in the same plot the suction appears normalised by $\frac{s}{\rho 2R}$, where the shear strength gradient $\rho = \frac{ds_u}{dz}$ was assumed constant and equal to 23 kPa/m. This is a very high value compared with values around 1 kPa/m reported for NC clay by Chen and Randolph (2004). In OC clays much

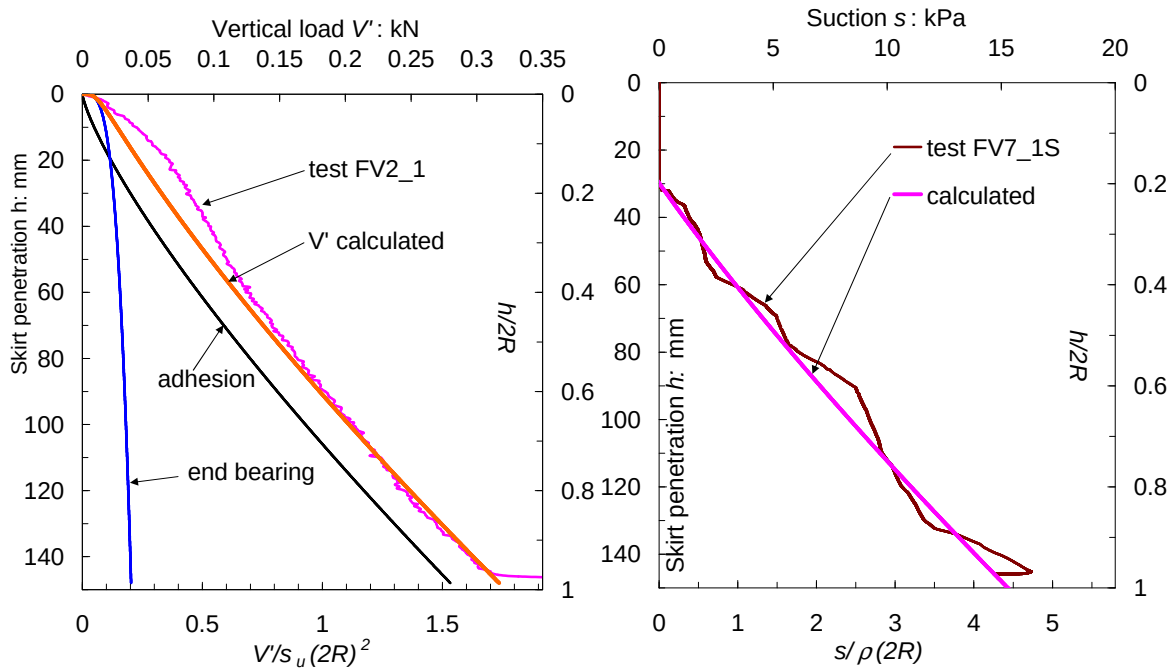


(a) Test FV2_1 (b) Test FV7_1

Figure 7.4: Measured and calculated (a) load-penetration curve, and (b) suction-penetration curve ($\rho = \frac{ds_u}{dz}$)

higher values of $\rho$ can be observed near the surface. Valuable comparisons with field values can be obtained by means of the quantity $\frac{\bar{s}_u}{\rho 2R}$. The application of suction introduced a reduction of the back-calculated $\alpha$ value from 0.5 (pushing) to 0.4. In the long term the dissipation of excess pore pressures after the caisson suction installation in a NC clay induces horizontal consolidation, therefore, a horizontal coefficient of consolidation $c_h$ should be used in the analysis (Cao *et al.*, 2002). For instance, calculation examples of $\alpha$ as a function of the dissipation time is presented by Andersen and Jostad (2002) for different type of clays.

### 7.1.4 Pullout capacity

The tensile capacity of a suction caisson with the compartment fully sealed, *i.e.* valves closed, and assuming a reversed bearing capacity failure can be expressed by (House, 2002):

$$V_{pullout} = W + (N_c s_u - \sigma_{v\,tip})\pi R^2 + \alpha_o \bar{s}_u 2\pi R_o h \tag{7.6}$$

where $V_{pullout}$ represents the pullout capacity, $W$ represents the submerged weight of the caisson plus the total soil-plug weight and plus the weight of the water column above the caisson lid. $N_c$ is the reverse bearing capacity factor, $\sigma_{v\,tip}$ is the total stress at the caisson tip, $\alpha_o$ is the outside adhesion factor and $\bar{s}_u$ is an average undrained shear strength. Equilibrium of the axial forces of the soil-plug allows the calculation of the suction developed under the caisson lid according to Fuglsang and Steensen-Bach (1991) (quoted by House, 2002) as follows:

$$s = \alpha_i \bar{s}_u \frac{2h}{R_i} - N_c s_u \tag{7.7}$$

where $\alpha_i$ is the inside adhesion factor. Using (7.6) $N_c$ can be obtained from experiments, assuming for instance that $\alpha_o$ does not change in the short term, *i.e.* the time interval for the pullout event is not long enough for consolidation to occur. In long term pullout events $\alpha_o$ in equation (7.6) may probably increase from installation values. This consolidation effect is more pronounced in NC clays as revealed by Watson (1999) and House (2002) in centrifuge tests, where days, weeks and even years of consolidation time were simulated.

Pullout tests using caisson D were performed at a rate of 2 mm/s (limited by the maximum rate of the loading rig). Taking the diameter as the relevant dimension gives a value of $v_n = 250$, which is high enough for a fully undrained condition to be assured. The pullout test FV3_8 was performed after a swipe event from $V' = 0.45$ kN to 0.18 kN and a series of five moment loading events at constant $V' = 100$ N, from which practically no vertical displacement was observed (see Tables 7.3 and 7.4). The resulting maximum pullout load recorded was -1.8 kN with a maximum pore load of -1.5 kN ($u'$ = -85 kPa) after a caisson extraction of 27 mm. Pore load is the pore pressure multiplied by the interior sectional area of the caisson lid. It was observed that the soil around the caisson sunk during extraction, implying that the soil-plug inside the caisson lost the contact with the soil at the base causing a reversed bearing capacity failure mechanism.

The response in terms of pressure $\frac{V'}{A}$ and $u'$ *versus* extraction $h$ is shown in Figure 7.5(a),

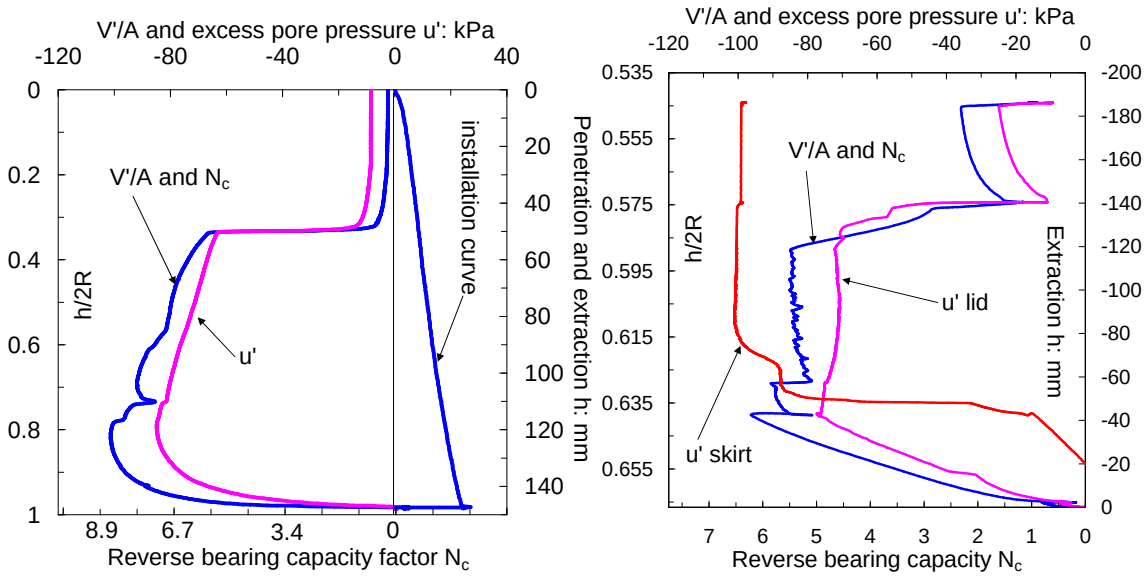


(a) Laboratory test FV3_8 (b) Field test Pull_1

Figure 7.5: Pullout test curves: (a) laboratory and (b) field (from Houlsby *et al.*, 2005)

including the installation curve and the unloading caused by the swipe test. Figure 7.5(a) also shows in the bottom abscissa the variation of $N_c$ calculated with equation (7.6) assuming $\alpha_o = 0.5$ (obtained from the installation). The maximum value of $N_c$ (at the maximum pullout load) was 8.6, which is lower than the theoretical lower bound solution of $N_c = 9.3$ determined by Martin (2001) for a caisson with identical aspect ratio, smooth skirts, but in a NC soil. A smooth condition agrees with observations after the caisson extraction, as it was found that the external skirt was very clean.

Results from large scale pullout tests carried out by Houlsby *et al.* (2005) with a caisson 1.5 m diameter and skirt length of 1 m are shown in Figure 7.5(b), where it can be seen that $u'$ was measured close to the tip and reaches the highest value. The maximum value of $N_c$ obtained was 6.4 using an adhesion factor $\alpha = 0.2$ as suggested by the same authors. Martin's (2001) lower bound solution for an aspect ratio of 0.67 and for rough and smooth skirts give values of 10.1 and 9.3 respectively. Although similarities exist between $\frac{V'}{A}$ and $u'$, measured in the laboratory and measured in the field, there is a pronounced disparity in extraction, $\frac{h}{2R} \approx 0.65$ in the laboratory, whereas $\frac{h}{2R} \approx 0.1$ in the field. The load-controlled mode applied in the field seems to be the cause for the much lower pullout capacity and extraction . In load-controlled tests it is difficult to reach and hold loads

close to failure. For that reason lower capacities are obtained without the possibility of having post failure softening.

## 7.2 CYCLIC VERTICAL LOADING TESTS

### 7.2.1 Introduction

The investigation of vertically cycled caissons is pertinent for multiple-caisson foundations for offshore wind turbines, since the tensile capacity controls the response. It is assumed that there is sufficient separation amongst the footings to reduce to a minimum any interaction effect. Therefore, the analysis of a single suction caisson is appropriate. Previous studies by El-Gharbawy (1998) and House (2002) have concentrated on cycling around high negative mean vertical loads (cyclic pullout) as well as aspect ratios relevant for anchoring applications ($\frac{L}{2R} \geq 3$). In this study, three series of tests with escalating sequences of 10 cycles per load packet were planned. The first series considered increasing load packets around the $V' = V_c$, load reached by the caisson after the pushing installation. In the second series the increasing cycling was carried out around $V' = 0$ N, after unloading from the $V_c$ value reached in the pushing installation. The third series was a repetition of the second, but employing suction instead of pushing to install the caisson, hence unloading from $V' + |S|$. In this form assessment of the effect of the installation method on the caisson cyclic response can be made. To this end, evaluation of the stiffness degradation, displacement and pore pressure variations were pursued.

Before analysing the test results, it is important to look at the load, displacement and pore pressure variation with time during a cyclic event. Pseudo-load-controlled tests were conducted by means of a feedback subroutine with a specified loading history. Examples of sinusoidal loading history inputs with a period of 12 seconds (0.08 Hz) are shown in Figures 7.6(a) and 7.6(b) as $\frac{V'}{A}$. Extreme waves have long periods, typically between 7 s to 13 s (Kühn, 2002). Byrne (2000) found in dense oil-saturated sand that for frequencies between 0.3 Hz and 0.03 Hz there is very little influence on the caisson response as long

as a failure condition is not approached. El-Gharbawy (1998) showed that in NC clay cyclic pullout close to the long term failure (drained capacity) caused the same 13 mm of displacement after: 300 cycles at 20 Hz, 2000 cycles at 2 Hz, or 10000 cycles at 0.2 Hz. These findings imply that there is a frequency effect for higher frequencies than those considered by Byrne (2000), but for cyclic pullout loads close to failure.

Tests were in reality displacement-controlled, since to achieve a specified loading history the stepper motor moves up or down the caisson attached to the rig arm until the target load is reached within a certain tolerance. It can be observed in Figures 7.6(a) and 7.6(b) that $\pm\Delta V'$ peaks of the first cycles are slightly below of the remaining peaks. This shows the effect of low gain values introduced at the beginning of the test in the feedback control subroutine; once the gain was increased $\pm\Delta V'$ peak values were closer to the nominal targets. However, even with the increase of the gain during cycling the target nominal $\pm\Delta V'$ peaks were never accurately achieved. This subtle detail did not cause any effect on the results obtained.

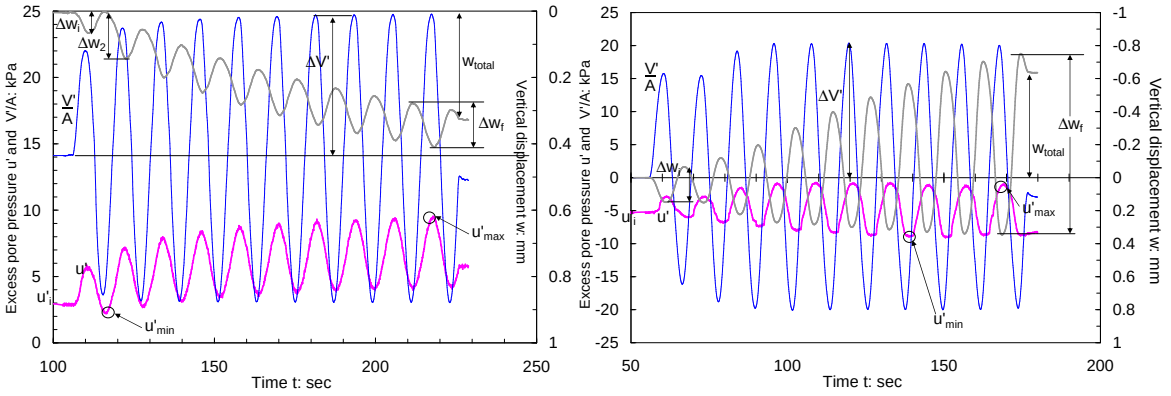


(a) Test FV5_4 (b) Test FV6_6

Figure 7.6: Loading history applied (as average pressure over the lid area $\frac{V'}{A}$), displacement $w$, and excess pore pressure $u'$ response, showing characteristic parameters used in the analysis

Figure 7.6(a) shows the displacement variation $\Delta w$ in each cycle, but because $\Delta w_2 \approx \Delta w_f$ a common value $\Delta w = \Delta w_f$ was collected for the entire cycling event (ignoring $\Delta w_i$ which corresponds to the initial half cycle). Conversely, in test FV6_6 it is not possible to claim uniformity of $\Delta w$ for all the cycles since $\Delta w$ is indeed varying cycle after cycle as can be clearly observed in Figure 7.6(b). To simplify the analysis, initial and final values of $\Delta w_i$

and $\Delta w_f$ were collected. Additionally, it was important to account for the total or net vertical movement $w_t$ of the caisson at the end of each cyclic event. A maximum and a minimum excess pore pressure value ($u'_{max}$, $u'_{min}$) during a cycling event was considered an appropriate indication of the range of variation of $u'$. The variation of $u'$ in test FV5_4 occurs mainly above the initial value $u'_i$, whereas in test FV6_6 $u'$ varies around $u'_i$. Values of $u'_{max}$ and $u'_{min}$ are able to capture these variations.

### 7.2.2 Results of cyclic loading around $V_m = V_c = 250$ N

In the first series of tests, immediately after the installation by pushing, the caisson was cyclically loaded by a series of eight loading packets of 10 cycles each. Increasing cyclic amplitudes $\pm\Delta V'$ from $\pm 47$ N for the first packet to up to $\pm 560$ N for the last packet were applied around a mean vertical load $V_m = V_c = V_o = 250$ N, *i.e.* the load required to penetrate the caisson into the ground $V_c$ was at the same time the maximum pre-load $V_o$ experienced by the caisson at $h_c = 145$ mm. The load-displacement curves of the whole sequence of cyclic events are presented in Figure 7.7(a) adopting two nor-

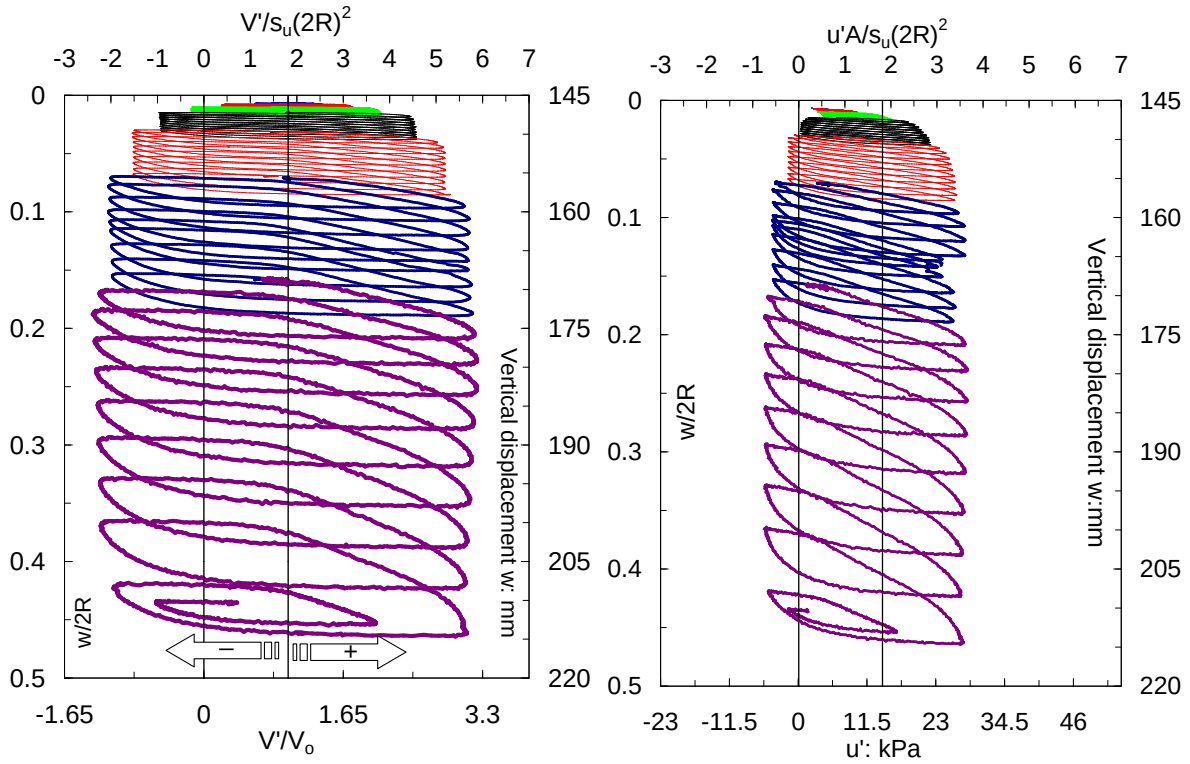


(a) Load-displacement response

(b) Excess pore pressure

Figure 7.7: Series of cyclic vertical loading events FV5 under $V_m = 250$ N

malisations: strength $s_u$ and 'pre-load' $V_o$, which are related by the relationship stated in Figure 7.2. Variation of $s_u$ with depth has not been taken into account since its profile is fairly constant as can be seen in Figure 2.4(b) (Tank 2).

Figure 7.7(b) shows the variation with depth of $u'$ and also the normalised excess pore load $U' = u'A$, where $A$ is the cross sectional area of the caisson $\pi R_i^2$. These figures allow only the inspection of events with extremely large displacements corresponding to the last two or three loading packets, where the caisson reached a settlement almost half of its length $L$. Note that there is no sign of settlement attenuation in these large displacement cycles. It is also worth observing that the positive build-up of pore water pressure accounts for almost half of $\frac{V'}{A}$.

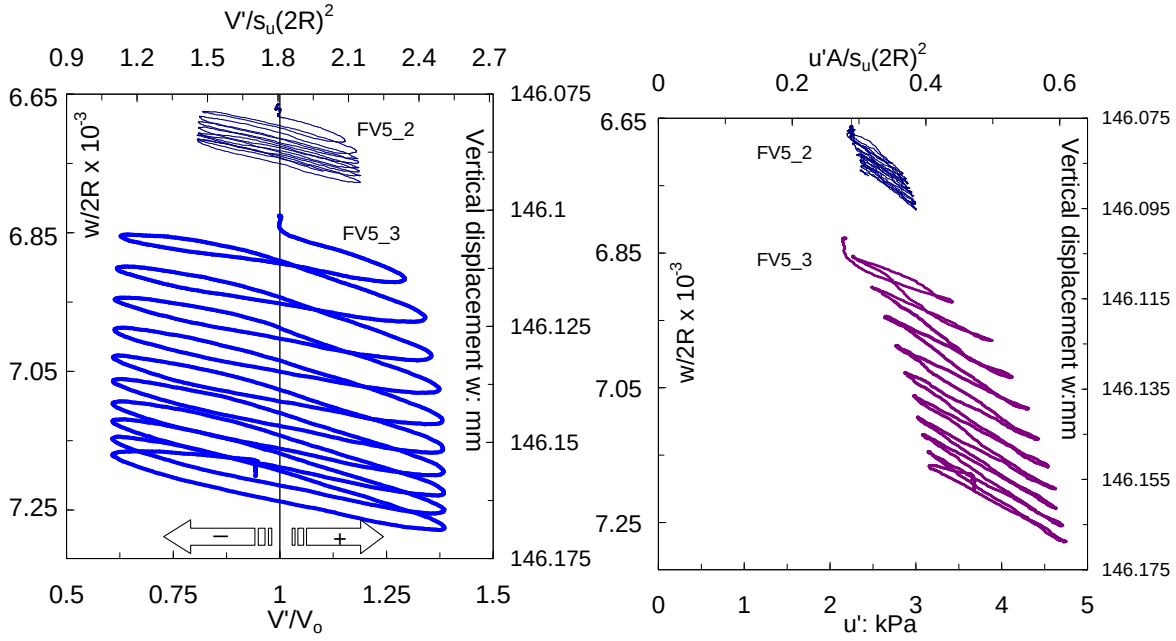


(a) Load-displacement response

(b) Excess pore pressure

Figure 7.8: Tests FV5_2 and FV5_3 under $\Delta V' = \pm 50$ N and $\pm 100$ N

Figures 7.8(a) and 7.8(b) show the load-displacement curves of tests FV5_2 and FV5_3, corresponding to the first two loading packets, *i.e* the lowest $\pm\Delta V'$ applied, which in turn resulted in the smallest displacement variations measured. The high resolution of the short LVDTs (1 $\mu$m) allowed refined displacement measurements as shown in the figures. The entire cyclic loading induced irrecoverable settlements and little build-up of pore water pressure. It is worth highlighting that the rate of settlement attenuates after

each cycle as can be clearly observed in the second loading packet, which may tend in the long term to a state where only very small settlements occur (cyclic shakedown). Furthermore, it is important to point out that this type of 'small' load-displacement response will be more often experienced by a caisson in a tetrapod foundation, but for periods probably lower than 12 s.

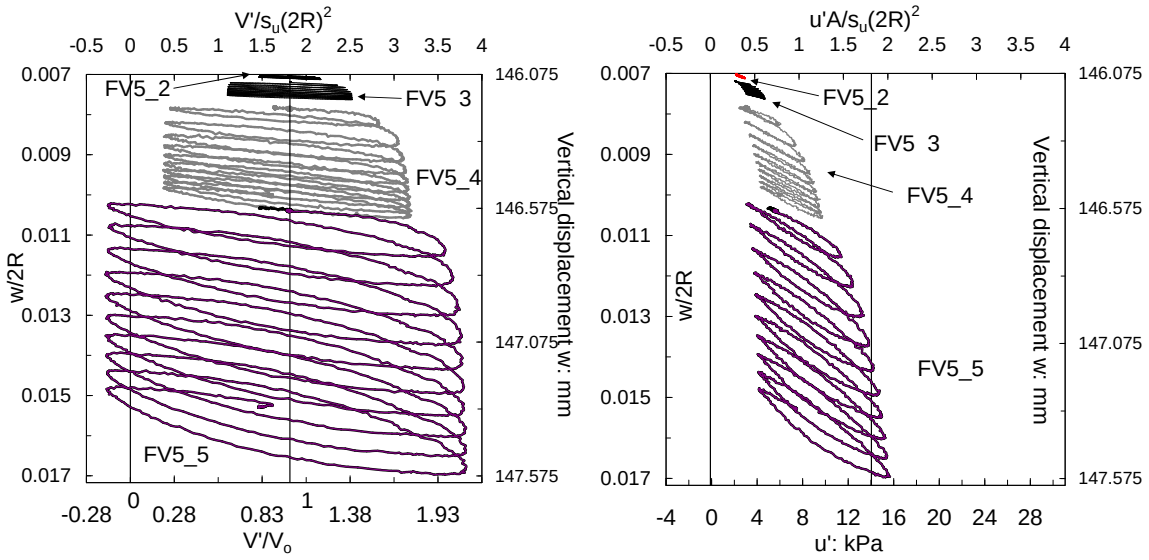


(a) Laboratory tests

(b) Laboratory tests

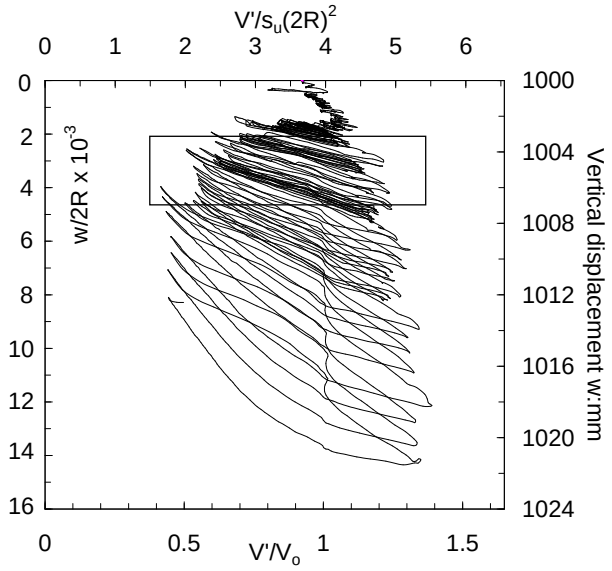


(c) Field test

Figure 7.9: Normalised curves obtained in the laboratory and in the field site at Bothkennar (taken from Houlsby *et al.*, 2005)

The next tests FV5_4 and FV5_5, shown in Figures 7.9(a) and 7.9(b), exhibit a substantial increase in settlement compared with the previous lower $\Delta V'$ tests FV5_2 and FV5_3. Moreover, excess pore water pressure variations are more significant, reaching values that

account for approximately half of the load pressure $\frac{V'}{A}$. An attempt to compare these results with results obtained in large scale tests is pursued in the following. Houlsby *et al.* (2005) carried out lateral cyclic loading tests with a caisson of 1.5 m diameter and an aspect ratio of 0.67. A vertical load-displacement response was obtained since a constant load ratio $\frac{H}{V'}$ was attempted whilst loading laterally. It was not possible to keep $\frac{H}{V'}$ constant due to difficulties in the simultaneous control of two hydraulic jacks, leading to a complex load path. Figure 7.9(c) shows the vertical load-displacement curve obtained with the large caisson. Notwithstanding the test condition disparities, the framed part of the field curve shown in Figure 7.9(c) has a resemblance to the curve of test FV5_4, since in both cases $\frac{\Delta V'}{V_o} \approx \pm 0.5$ and $\frac{\Delta w}{2R} \approx 0.002$. However, the lateral loading in the large caisson reduced drastically the vertical response by approximately a factor of three when interpreted as the normalised secant stiffness $\frac{K_v}{2Rs_u}$.

### 7.2.3 Results of cyclic loading around $V_m = 0$ N

The second and third series of cyclic tests were carried out to investigate the response of cyclic loading around $V' = 0$. The former was conducted immediately after the caisson was installed by pushing and the latter immediately after the caisson was installed by suction. Figures 7.10(a) and 7.10(b) show the load-displacement curves for the whole sequence of cyclic tests, where is only possible to observe large displacements caused by the largest $\pm\Delta V'$. A totally different load-displacement response was obtained compared with the response shown above (cycling around $V_m = V_c$). There are also differences between the curves shown in Figures 7.10(a) and 7.10(b), revealing that the installation method has an effect on the short term cyclic response. On one hand, a gradual increase of displacement with cyclic loading occurred in the pushing installation case (increasing degradation due to softer response), leading to failure for $\Delta V' = \pm 505$ N. On the other hand, the suction installation induced a much stiffer response for values of $\Delta V'$ beyond $\pm 505$ N until sudden large displacements occurred for $\Delta V' = \pm 744$ N.

Figures 7.10(c) and 7.10(d) reveal that totally different excess pore water pressure vari-

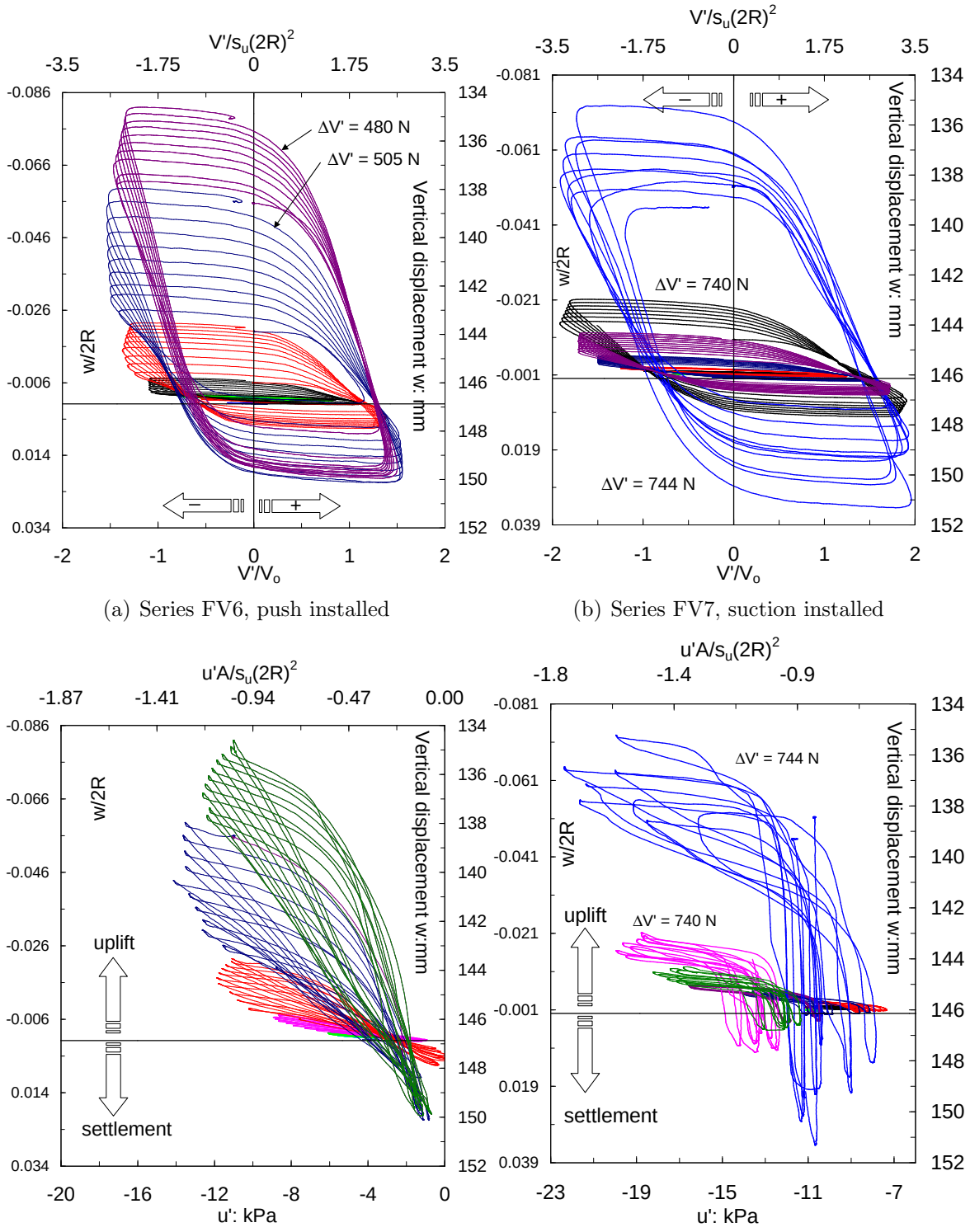


(a) Series FV6, push installed

(b) Series FV7, suction installed

(c) Series FV6, push installed

(d) Series FV7, suction installed

Figure 7.10: Sequence of vertical loading events FV6 and FV7 under $V_m = 0$ N showing: (a), (b) load-displacement response and (c), (d) pore pressure-displacement response

ations were found in these tests compared with the cycling tests around $V_m = 250$ N. Whilst only negative values were measured in the former (even under compression loads), predominant positive values were measured in the latter, although negative values were

measured under the presence of high tensile loads (Figure 7.7(b)). This is evidence of the fact that the development of excess pore water pressure is directly related to the caisson vertical movement. As a result, for cycling around $V' = 250$ N permanent settlement generated positive excess pore pressure and during cycling around $V' = 0$ N predominant upward movement generated exclusively suction. The uplift was, however, not permanent since the caisson moves up and down passing through the initial position ($\frac{w}{2R} = 0$) in each cycle.

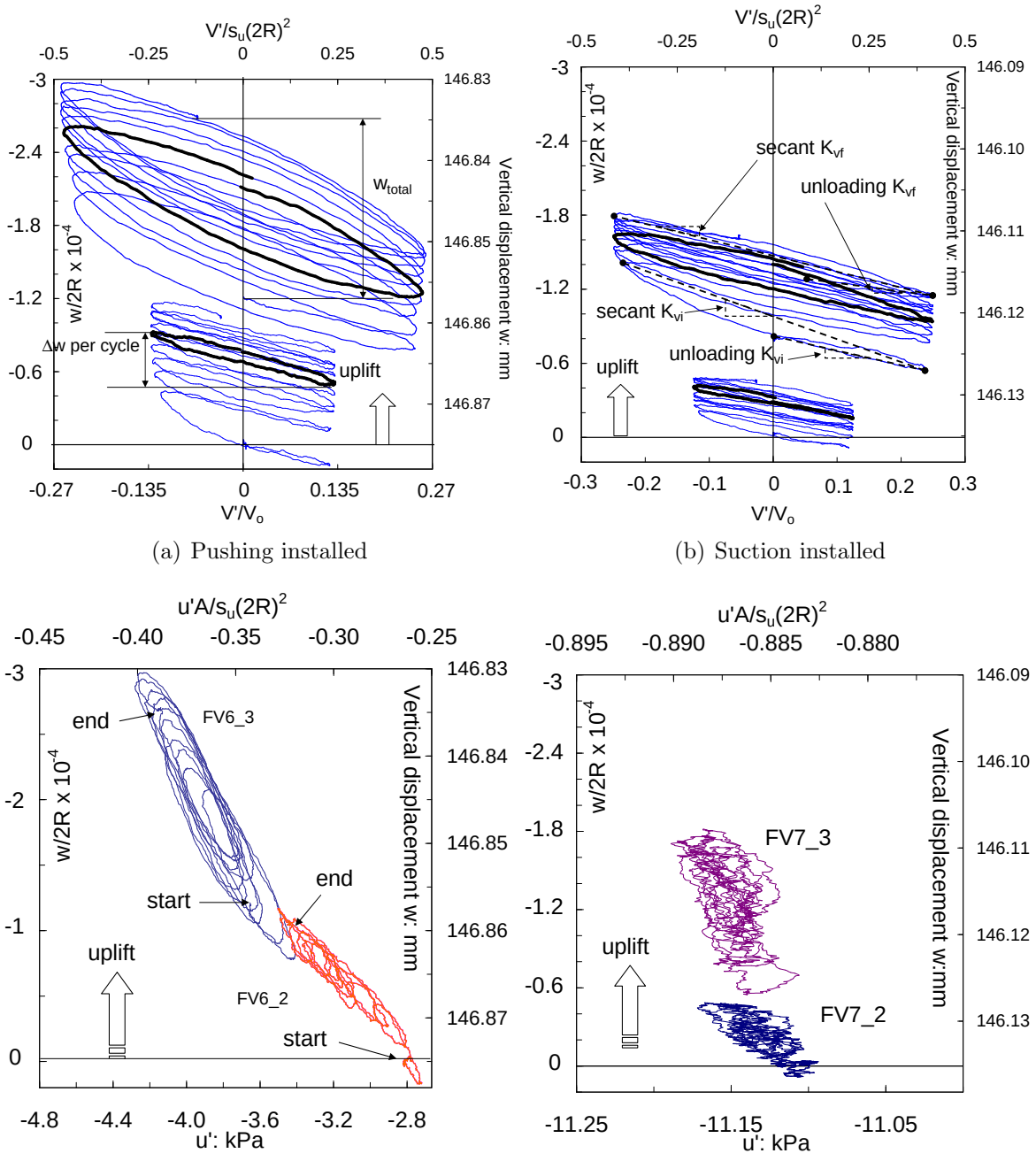


(a) Pushing installed

(b) Suction installed

(c) Tests FV6_2 and FV6_3

(d) Tests FV7_2 and FV7_3

Figure 7.11: Small displacement response showing curves of normalised load-displacement and excess pore load and excess pore pressure variation with displacement

The first two series of loading tests had very small displacements under the application of the nominal values of $\Delta V' = \pm 50$ N and $\pm 100$ N, for that reason they are not visible in Figures 7.10(a) and 7.10(b). As mentioned before, it is of fundamental importance to study the range of small displacements since they represent the expected foundation serviceability condition, with large displacements to be encountered in sporadic loading events. Previously it was found that for the same nominal load amplitudes ($\Delta V' = \pm 50$ N and $\pm 100$ N) irrecoverable settlements occurred when cycling around $V_m = 250$ N. Figures 7.11(a) and 7.11(b) show that now a permanent uplift occurs when the same cyclic load amplitude is applied around $V_m = 0$ N. It is important to highlight that displacements of the caisson installed by pushing were higher than displacements of the caisson installed by suction. An explanation for this difference can be found in the higher suction during the loading. The suction varied with the vertical movement of the caisson as can be observed in Figure 7.11(c). On the contrary, no suction variation is observed in Figure 7.11(d), where $u' = u'_i =$ -11 kPa, value that represents a great percentage of the maximum suction applied during the installation ($s \approx 16$ kPa).

### 7.2.4 Comparison of displacements and excess pore pressure

This and the next section attempt to find patterns of the caisson behaviour as a function of the displacement variation $\Delta w$ occurring in each cycle. Table 7.2 summarizes the values of the parameters to be compared.

Figure 7.12(a) shows clearly the increase of vertical displacement with vertical load in the semi-log plot. For the series of tests FV5 there was very little variation of $\Delta w$ within each loading packet of cycles (Figure 7.6(a) shows an example), for that reason the points of the first cycle are merged with the points of the last cycle. Conversely, for the series FV6 and FV7 this was not the case in all the tests, for instance, there were tests where in the last cycle $\Delta w$ was larger than for the first cycle as shown in Figure 7.6(b). The points for the series FV5 follow a fairly straight line in the semi-log plot, which is followed closely by the series FV7, except for the last packet. However, the series FV6 follows this

Table 7.2: Parameters of the series of cyclic vertical loading tests

| Test | $\pm\Delta V'$ | Secant | | Unloading | | | | $u'$ | | |
|---|---|---|---|---|---|---|---|---|---|---|
| | | $K_{vi}$ | $K_{vf}$ | $K_{vi}$ | $K_{vf}$ | $\Delta w$† | $w_{total}$ | initial | min | max |
| | N | N/mm | | N/mm | | mm | | kPa | | |
| FV5_2 | 47 | 20591 | 16249 | 17953 | 13898 | 0.015 | 0.01 | 2.25 | 2.25 | 3 |
| FV5_3 | 96 | 18453 | 12316 | 16025 | 14347 | 0.032 | 0.06 | 1.9 | 1.9 | 4.5 |
| FV5_4 | 187 | 5295 | 3841 | 11490 | 5874 | 0.14 | 0.4 | 3 | 2.2 | 9.4 |
| FV5_5 | 280 | 2794 | 1815 | 7862 | 5377 | 0.37 | 0.9 | 5.3 | 3 | 15.3 |
| FV5_6 | 380 | 1362 | 646 | 4629 | 3266 | 1.45 | 3.4 | 6.3 | 0 | 21.7 |
| FV5_7 | 460 | 563 | 344 | 3648 | 3133 | 3.3 | 8 | 5.9 | -2.1 | 26 |
| FV5_8 | 530 | 284 | 209 | 2937 | 1786 | 7.6 | 17.4 | 5 | -4.3 | 27.8 |
| FV5_9 | 560 | 198 | 140 | 963 | 1458 | 14.36 | 45.5 | 4.8 | -5.6 | 28 |
| FV6_2 | 45 | 9409 | 16722 | 19135 | 22615 | 0.009 | -0.02 | -2.8 | -3.6 | -2.7 |
| FV6_3 | 90 | 9100 | 8596 | 14469 | 17162 | 0.023 | -0.02 | -3.7 | -4.3 | -3.3 |
| FV6_4 | 180 | 5491 | 4248 | 15310 | 16280 | 0.07→0.09 | -0.07 | -4.25 | -5.8 | -3.4 |
| FV6_5 | 270 | 3749 | 2178 | 13137 | 11307 | 0.1→0.23 | -0.09 | -5.2 | -6.17 | -2.3 |
| FV6_6 | 360 | 2684 | 653 | 18284 | 7296 | 0.2→1.06 | -0.66 | -5 | -8.9 | -0.7 |
| FV6_7 | 450 | 611 | 198 | 5301 | 5738 | 1.3→3.7 | -2.3 | -7.5 | -11.8 | 0.3 |
| FV6_8 | 505 | 229 | 83 | 2090 | 1934 | 3.9→11.7 | -5.4 | -8.7 | -14.1 | -0.85 |
| FV6_9 | 480 | 87 | 58 | 1508 | 1379 | 10.3→14.5 | -3.57 | -11 | -12.5 | -0.7 |
| FV7_2 | 46 | 21190 | 26690 | 29636 | 25140 | 0.010 | -0.01 | -11 | -11.1 | -11 |
| FV7_3 | 92 | 13402 | 18854 | 22413 | 24666 | 0.016 | -0.01 | -11 | -11.1 | -11 |
| FV7_4 | 186 | 10926 | 9685 | 20272 | 22437 | 0.042 | -0.02 | -11.2 | -11.2 | -10.8 |
| FV7_5 | 275 | 8145 | 6231 | 18211 | 17725 | 0.09 | -0.01 | -11 | -11 | -10.4 |
| FV7_6 | 385 | 6312 | 4554 | 16707 | 16062 | 0.14→0.17 | -0.02 | -10.6 | -10.8 | -8.6 |
| FV7_7 | 480 | 3729 | 2468 | 8539 | 9746 | 0.28→0.39 | -0.08 | -9 | -10.7 | -7.1 |
| FV7_8 | 580 | 2057 | 1154 | 6757 | 6106 | 0.6→0.99 | -0.37 | -9 | -14 | -8.2 |
| FV7_9 | 660 | 1008 | 539 | 5588 | 4627 | 1.43 | -0.96 | -11.9 | -18.2 | -10.5 |
| FV7_10 | 740 | 501 | 294 | 4133 | 3328 | 3.26→5.31 | -1.6 | -15 | -20 | -12 |
| FV7_11 | 744 | 160 | 115 | 2584 | 1689 | 9.78→33 | -2.5 | -10.6 | -22.3 | -7.9 |

†initial and final range of vertical displacement per cycle

line in the first four loading packets after which the first cycle points deviate slightly and the last cycle points deviate even more, following a different line.

The difference between the maximum and minimum excess pore pressure normalised by $s_u$ is shown in Figure 7.12(b) as a function of $\log\frac{\Delta w}{2R}$, but for more clarity, $\Delta w$ is now presented as the average between the first and last cycle. The maximum difference was found in the series FV5 ($V_m = 250$ N), whereas the lowest differences corresponded to the suction installed caisson for $V_m = 0$ N. The excess pore pressure difference between the series FV6 and FV7 were related to the initial excess pore pressure $u'_i$. For the suction installed caisson $u'_i$ = -11 kPa (test FV7_2), giving evidence of the recent maximum suction applied (s $\approx$ 16 kPa) to install the caisson. Not surprisingly, $u'$ has not yet been dissipated due to the short time elapsed. During cyclic loadings with small $\frac{\Delta w}{2R}$ ($< 10^{-3}$), $u'$ did not move away from $u'_i$, but when larger $\Delta w$ were caused $\Delta u'$ increased significantly with $\Delta w$

from $u'_i$. No excess pore pressure accumulation was observed since at the beginning of every cyclic loading event $u' \approx u'_i$ = -11 kPa. Conversely, for the push installed caisson $u'$ at the beginning of every cyclic loading event varied after each series of cycling events from -2.8 kPa for FV6_2 to -11 kPa for FV6_9. This short term excess pore pressure response needs confirmation with long term results, *i.e.* when excess pore water pressure generated during installation has been mostly dissipated.

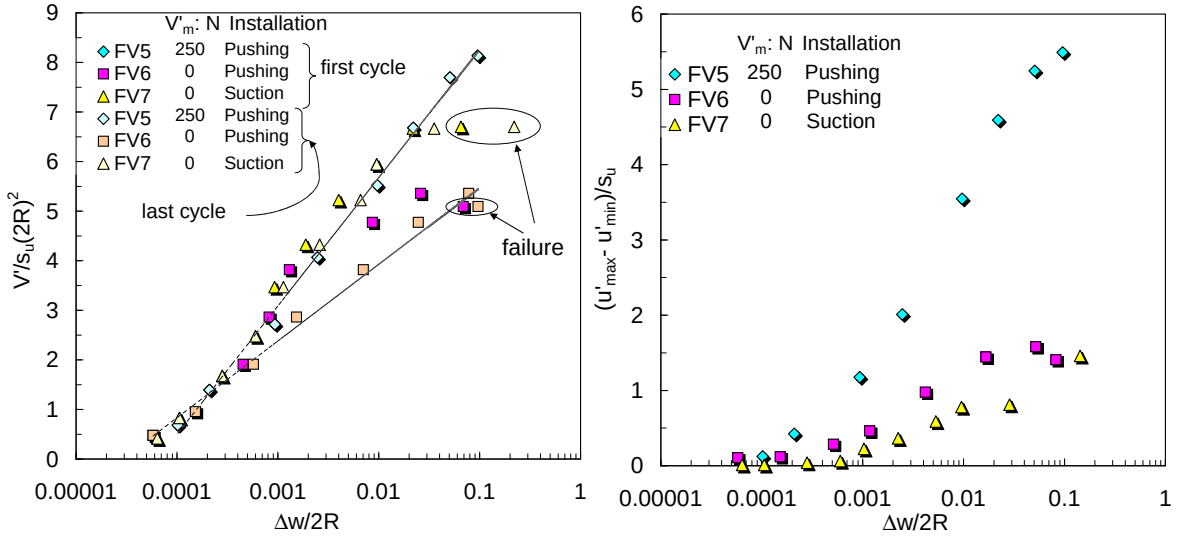


Figure 7.12: (a) Normalised load *versus* displacement variation per cycle and (b) normalised range of pore pressure variation *versus* average displacement variation

### 7.2.5 Comparison of caisson foundation stiffness

Normalised secant and unloading stiffness, determined as illustrated in Figure 7.11(b), are shown in Figures 7.13(a) and 7.13(b), respectively. Including initial and final stiffness ($K_{vi}, K_{vf}$) to reveal whether there exists or not degradation within the cycles at the same constant load amplitude $\pm\Delta V'$.

It can be observed that for all the series the secant stiffness shows a clear decrease with displacement (or load amplitude). Series FV5 presents also a stiffness decrease within each 10 cycles of loading. On the contrary, the series FV6 and FV7 have an initial stiffness lower than the final stiffness for the cycling loading with $\Delta V'$ = 46 N. This only reveals that a weak initial response occurred (larger uplift during unloading than settle-

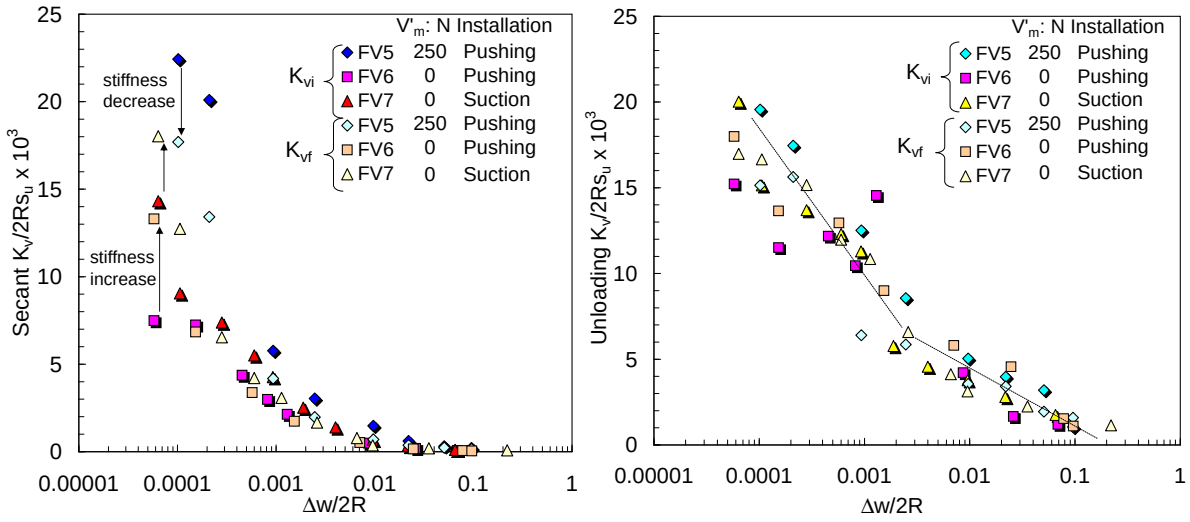


(a) Secant stiffness (b) Unloading stiffness

Figure 7.13: Normalised initial and final vertical stiffness plotted against normalised displacement variation per cycle

ment during initial loading) which is recovered immediately at the second cycle, as shown in Figures 7.11(a) and 7.11(b). Conversely, in Figure 7.13(b) is observed that the normalised unloading stiffness does not show a strong reduction at small displacements as in the secant stiffness ($6 \cdot 10^{-6} < \frac{\Delta w}{2R} < 3 \cdot 10^{-4}$), but a more regular decrease along the whole range of $\Delta w$ that could be reduced to a bilinear relationship in the semi-log plot.

# 7.3 MOMENT CAPACITY

## 7.3.1 Introduction

Combined loading of suction caisson foundations in clay has been mainly studied analytically (Bransby and Randolph, 1998; Taiebat and Carter, 2000; Gourvenec and Randolph, 2003). Although some researchers have focused on experimental studies, attention has been paid to foundations for heavy offshore structures such as oil rigs, or as mentioned before to suction anchors in deep water applications such as floating structures. One of the few studies for the former was reported by Cassidy *et al.* (2004), where swipe tests were carried out in a drum centrifuge to compare the moment response of a spudcan footing and a suction caisson ($\frac{L}{2R} = 0.5$) in a soft NC clay. For the latter, where lateral loading is applied through a chain connected to a padeye, more work has been

done (*e.g.* House, 2002; Clukey *et al.*, 2003; Aubeny and Murff, 2005). The possibility of using suction caisson foundations for offshore wind turbines has led to this study since the geometry of monopod caisson foundations, water depths, turbine weight and load paths are totally different to other previous applications.

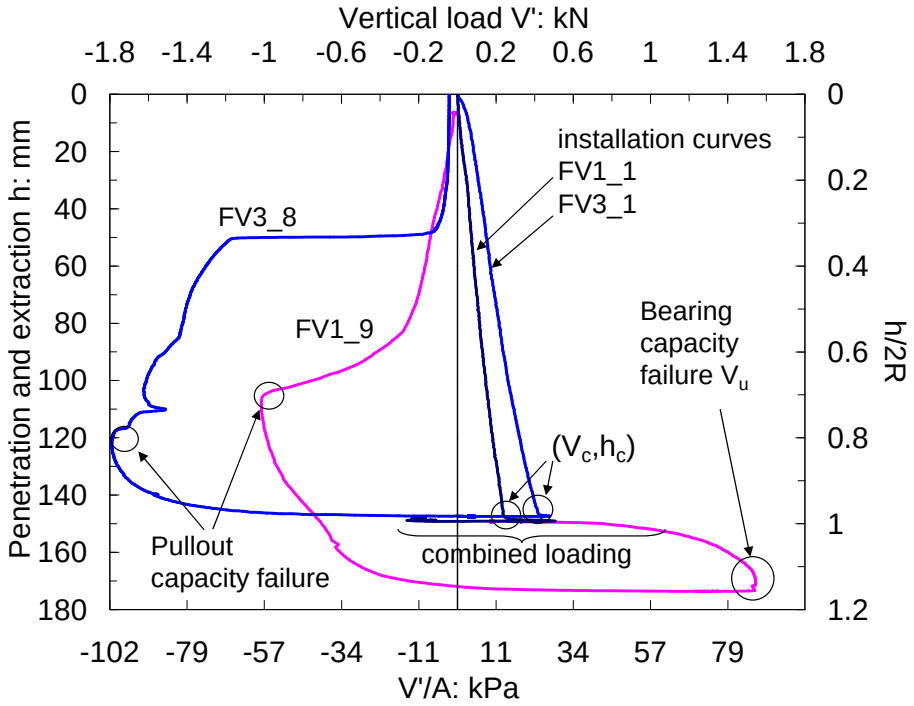


Figure 7.14: Installation, combined loading, bearing capacity failure and pullout

The experimental strategy included monotonic and cyclic swipe events as well as moment loading tests at constant $V'$, using caisson D ($2R = 150$ mm, $\frac{L}{2R} = 1$) tested in heavily OC kaolin clay. Before analysing the test results it is useful to review the global context of the combined loading with respect to the vertical loading. Figure 7.14 shows the pushing installation curves of tests FV1_1 and FV3_1 studied in section §7.1, where $V_c$ and $h_c$ are as in Figure 7.1(a) and $V_u$ is the ultimate bearing capacity. After installation combined loading events can be conducted straightaway, or further penetration, or tensile loading can be applied before any subsequent combined loading. Any of these possibilities may have important effects on the caisson response depending on the variation of $w$, the vertical displacement after installation. It is worth noting that although a bearing capacity failure occurs around $V_u = 1.5$ kN at 169 mm of penetration (test FV1_9), serious reduction of vertical stiffness started from 1 kN. Therefore, any incursion beyond that level of vertical load and penetration ($> 152$ mm) could have detrimental effects on the caisson

moment response.

Additionally, Figure 7.14 shows the pullout response following the bearing capacity failure, and the pullout response shown in Figure 7.5(a) for comparison. The reduced pullout capacity after failure compared with the pullout capacity after installation agrees with previously reported results by Byrne and Cassidy (2002). The pullout capacity reduces from 1.8 kN to 1 kN after 67 mm of extraction, but it still represents two third of $V_u$. Finally, in order to determine the size of the yield surface and normalise the loads, the maximum value of $V'$ experienced under a particular value of $h$, *i.e.* $V_o$ will be used.

### 7.3.2 Swipe test results

Swipe tests are an efficient way to obtain information of the shape and size of the yield surface. For that reason, mapping out of the yield surface was attempted by swiping from the tensile side and from the compressional side (analogous to the Cam Clay critical state terminology from the dry side of critical and from the wet side of critical). The former represents an OC condition for the foundation with an OCR = $\frac{V_o}{V'}$, whereas the latter represents a NC condition for the foundation. Swipe tests were described in section §6.1.5 for caissons installed by suction into sand. Table 7.3 summarizes the values of excess pore pressure $u'$ underneath the caisson lid (initial $u'_i$, initial and final variation $\Delta u'_i$ and $\Delta u'_f$ with respect to $u'_i$), initial and final foundation secant stiffness $K_{mi}$, $K_{hi}$, $K_{mf}$ and $K_{hf}$, yield loads $\frac{M_y}{2R}$ and $H_y$, shear modulus $G$ (back-calculated from the moment caisson response using the expressions of elastic behaviour presented in section §5.2.2), and plastic displacement increment ratios. Complementary information can be found in Table 7.1 (*e.g.* $s_u$, $V_c$ and $V_{max}$).

It can be seen in Table 7.3 that the tests were carried out with the load ratio usually $\frac{M}{2RH} = 1$. This represents a condition where wind forces are similar to wave and current forces. Conversely, jack-up rigs have a higher $\frac{M}{2RH} \approx 2.5$ (Cassidy *et al.*, 2004). They found a considerable moment and lateral capacity under tensile vertical loads and a max-

Table 7.3: Summary of swipe tests

| Test | $V_i'$ N | $V_f'$ N | $V_o$ N | $h$ mm | $\frac{M}{2RH}$ | $2R\theta_t$ mm | $u_i'$ kPa | $\Delta u_i'$ kPa | $\Delta u_f'$ kPa |
|---|---|---|---|---|---|---|---|---|---|
| FV4_2 | -563 | 268 | 682 | 147.1 | 1.01 | 3.3 | 0 | 0 | 0 |
| FV4_5 | -250 | -16 | 650 | 142.9 | 0.43 | -5.8 | -0.4 | 1 | 0.8 |
| FV1_2 | -190 | 25 | 250 | 148.2 | 1.02 | 3.9 | 0 | 0 | 0 |
| FV3_2 | 450 | 183 | 474 | 147.3 | 1.03 | 3.4 | 5.3 | 2.7 | -3.3 |
| FV6_13 | 645 | 423 | 750 | 185.6 | 1.05 | 2.6 | 9.6 | 0 | 0.8 |
| FV2_2 | 878 | 506 | 900 | 147.7 | 1.06 | 3.7 | 34 | 0 | -11 |
| FV2_7 | 899 | 633 | 900 | 148.8 | 0.65 | 4.7 | 18 | 1 | 8 |
| FV2_14† | 838 | 294 | 1100 | 153.1 | 1.05 | ±1.75 | 38 | -6 | -16 |

| Test | $K_{mi}$ | $K_{hi}$ | $\frac{M_y}{2R}$ | $H_y$ | $V_y$ | $K_{mf}$ | $K_{hf}$ | $G$ | $\frac{G}{s_u}$ | $\frac{\delta u^p}{2R\delta\theta^p}$ | $\frac{\delta w^p}{2R\delta\theta^p}$ |
|---|---|---|---|---|---|---|---|---|---|---|---|
| | N/mm | | N | N | N | N/mm | | MPa | | | |
| FV4_2 | 2000 | 400 | 203.8 | 203.2 | -300 | 25 | 24 | 30 | 2266 | 1.057 | -0.010 |
| FV4_5 | 140 | 349 | 27.7 | 65.8 | -120 | -21 | -55 | 3 | 227 | 0.940 | -0.154 |
| FV1_2 | 600 | 171 | 60.6 | 58.1 | -50 | 10 | 8 | 8 | 1099 | 1.26 | -0.083 |
| FV3_2 | 1191 | 278 | 126.4 | 120.2 | 388 | 17 | 17 | 30 | 2956 | 1.047 | 0.010 |
| FV6_13 | 1200 | 400 | 72.0 | 68.8 | 528 | 24 | 24 | 20 | 2387 | 0.964 | -0.026 |
| FV2_2 | 1045 | 311 | 98.3 | 94.2 | 730 | 15 | 14 | 15 | 1850 | 0.931 | 0.036 |
| FV2_7 | 150 | 378 | 12.8 | 20.8 | 867 | 10 | 14 | 1.5 | 206 | 0.912 | 0.020 |

†cyclic swipe test

imum moment load capacity of $\frac{M}{s_u(2R)^3} \approx 0.83$. Furthermore, the interest of that study was to trace the outermost yield surface, with a size defined by $\pm V_o = \pm V_u$. As a consequence, a failure envelope for flat circular footings suggested by Taiebat and Carter (2000) was used in conjunction with upper bound solutions to obtain the moment and horizontal loads at failure $M_u$ and $H_u$. In this study interest was focused on defining the yield surface with a size $V_o$ around the installation load $V_c$, hence before a bearing capacity failure.

Swipes tests were carried out at a rotational velocity $2R\dot{\theta} = 0.01$ mm/s, resulting in partially drained conditions since $v_n = 5$ ($< 10$, according to the criterion in section §7.1.3). Figure 7.15(a) shows the moment-rotation curves of the swipe tests where the moment load has been normalised by $s_u$ and $2R$. Note the moment load peak in the curves of tests FV4_2, FV4_5 and less visible in test FV6_13. This reflects the effect of higher degree of overconsolidation of the clay sample and explain the high value of $\frac{s_u}{\sigma_{vi}'}$ shown in Table 2.4. Heavily OC soils tend to dilate, inducing suction. However, from Figure 7.15(c) zero variation of the pore pressure occurred during test FV4_2 and actually positive $\Delta u'$ occurred in tests FV4_5 and FV6_13, not giving evidence of soil dilation since the lid does not move vertically. Conversely, as the lid rotates it is expected that on the side that moves upwards $u'$ will be negative and on the side that moves downwards it will

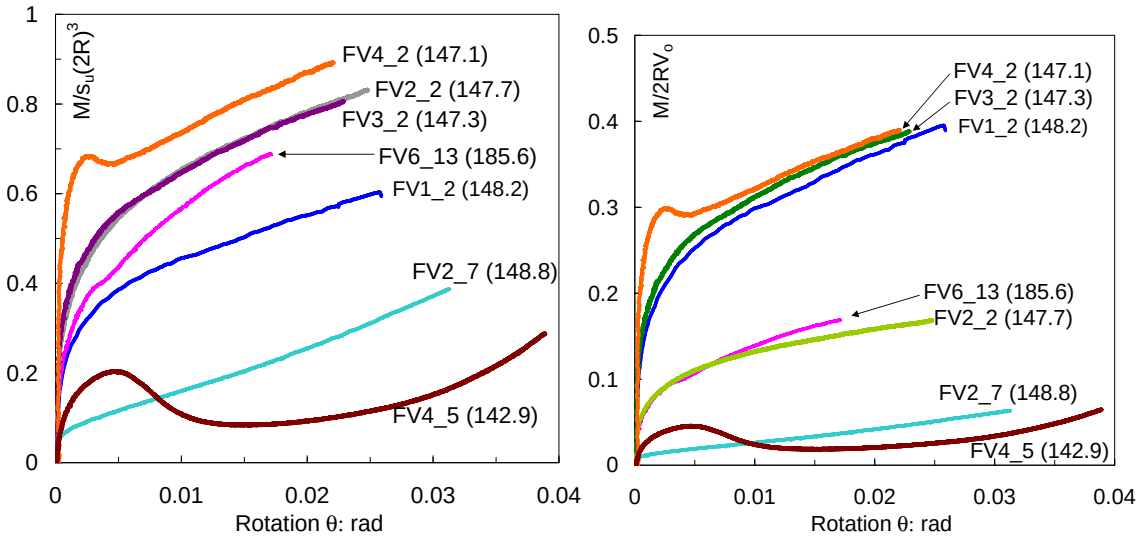


(a) Normalisation by $s_u$ (b) Normalisation by $V_o$

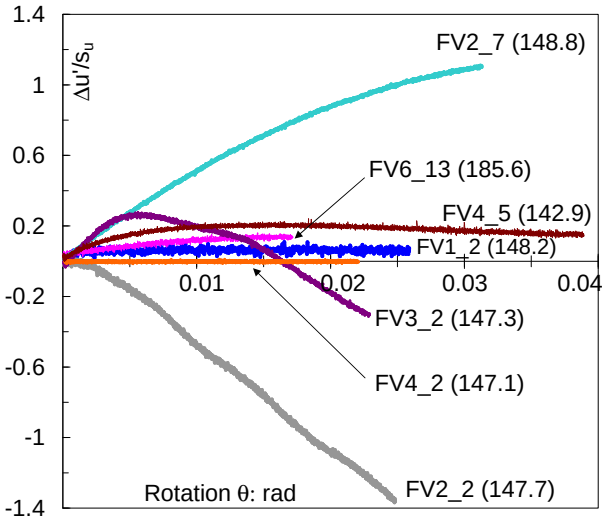


(c)

Figure 7.15: Swipe tests showing normalised moment-rotation and excess pore pressure-rotation curves (in brackets penetration $h$ in millimetres)

be positive as shown in Figure 6.17. Therefore, there is probably a situation where the pore pressure transducer recorded positive $u'$ because it was located under the lid side moving downwards, which compensates or prevails over the suction generated due to soil dilation. In addition, the passive lateral pressure on the loaded side induces suction due to soil dilation, but $u' > 0$ on that side of the soil-plug caused by water flowing outwards, whereas the opposite occurs on the other side.

Figure 7.15(b) shows the same curves as in Figure 7.15(a) but with the moment load normalised by $V_o$. In these figures the fixed caisson penetration $h$ appears in brackets and

in millimetres, where except tests FV4_5 and FV6_13, $h$ is between 147 mm and 149 mm. Figure 7.15(b) highlights that the normalisation by $V_o$ creates three groups of curves. The first group above corresponds to swipe events conducted immediately after installation without further penetration or preloading. The second group in the middle shows a lower normalised moment capacity because test FV2_2 was vertically preloaded more than three times $V_c = 316$ N, approaching the value of bearing capacity failure $V_u \approx 1.5$ kN. Test FV6_13 was conducted after a series of cyclic vertical loads. Nevertheless, the strongly remoulded soil in the interface could have been sufficient to reduce the moment capacity. In the third group at the bottom the moment capacity is the lowest. Test FV4_5 presents the effects of soil disturbance as a consequence of previous moment loading events despite showing a moment load peak. Previous loading with $V_o$ near to $V_u$ reduced considerably the moment capacity of Test FV2_7.

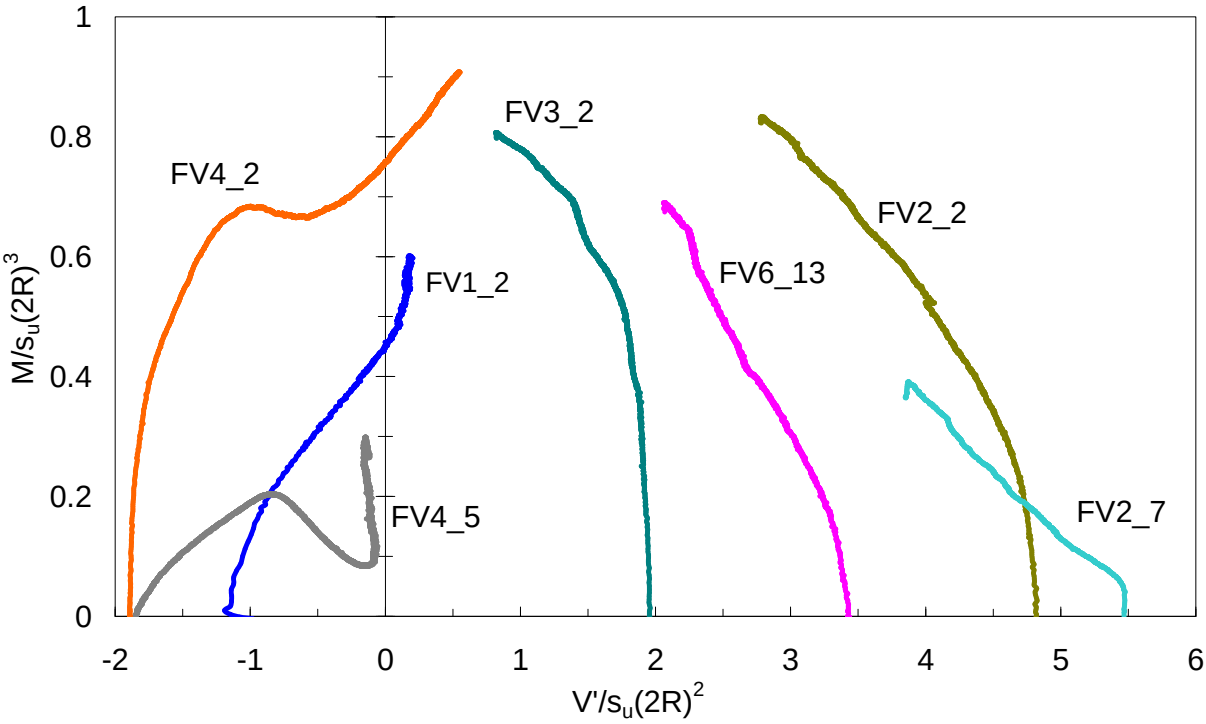


Figure 7.16: Swipe tests in the normalised moment vertical load plane

Figure 7.16 shows all the swipe tests in the strength normalised moment-vertical load plane. No moment peaks with further softening is observed in the compressive swipe tests. The shape of the yield surface traced by the swipe events can be observed as well as the increase of the size with the increase of $\left|\frac{V'}{s_u(2R)^2}\right|$. The expansion of the yield surface

towards the tension side is substantially more significant as proportion of the compressive side than in sand. This is due to the fact that in clay low permeability assures the prevalence of partially or undrained conditions, which in turn allows suction to develop even under slow loading rates. It is worth noting that an upper limit for the moment load is reached at $\frac{M}{s_u(2R)^3} \approx 0.8$, which is very close to the value reported by Cassidy *et al.* (2004). Test FV4_5 shows apart from a peak and subsequent softening previously described, a further increase of moment capacity with rotation at constant vertical load close to zero. A negative rotation was applied in this test, which returned the caisson to a centred position after positive rotations were applied in the previous three tests. It is believed that caisson contact with soil less disturbed on the opposite side as rotation progresses increased the moment capacity.

Figures 7.17(a) and 7.17(b) show the results of a cycle swipe test. A particular hysteresis loop shape appears after the fourth cycle, giving evidence of gapping. In fact, there is a point around zero rotation before which the tangential stiffness decreases and after which it increases during reloading and unloading. The cyclic swipe test FV2_14 was carried out immediately after a second installation into the same site but with the loading plane changed 90°. Full installation was completed with $V_c = 260$ N (FV2_12) and a further penetration from 147 mm to 153 mm caused $V'$ to increase up to 1100 N, which is a value near to $V_u$. Despite the increase of the normalised moment capacity with rotation (and with the decrease of $V'$), the maximum moment capacity has reduced to a half of that obtained for instance in tests FV2_2 or FV3_2. Moreover, the loading history is reflected in the high values of $u'$ as shown in Figure 7.17(c). Although $u'$ dissipates cycle after cycle, the normalised pore load represents a significant percentage of the normalised vertical load.

In section §6.1.7 cyclic swipe tests of caissons in dense saturated sand starting from tension and regardless of the rotation amplitude, the vertical load always returned to a value of tensile load close to the initial $V'$ after each cycle. On the contrary, in Figure 7.17(b) the cyclic swipe test started from a large compressive $V'$ load where $V'$ continu-

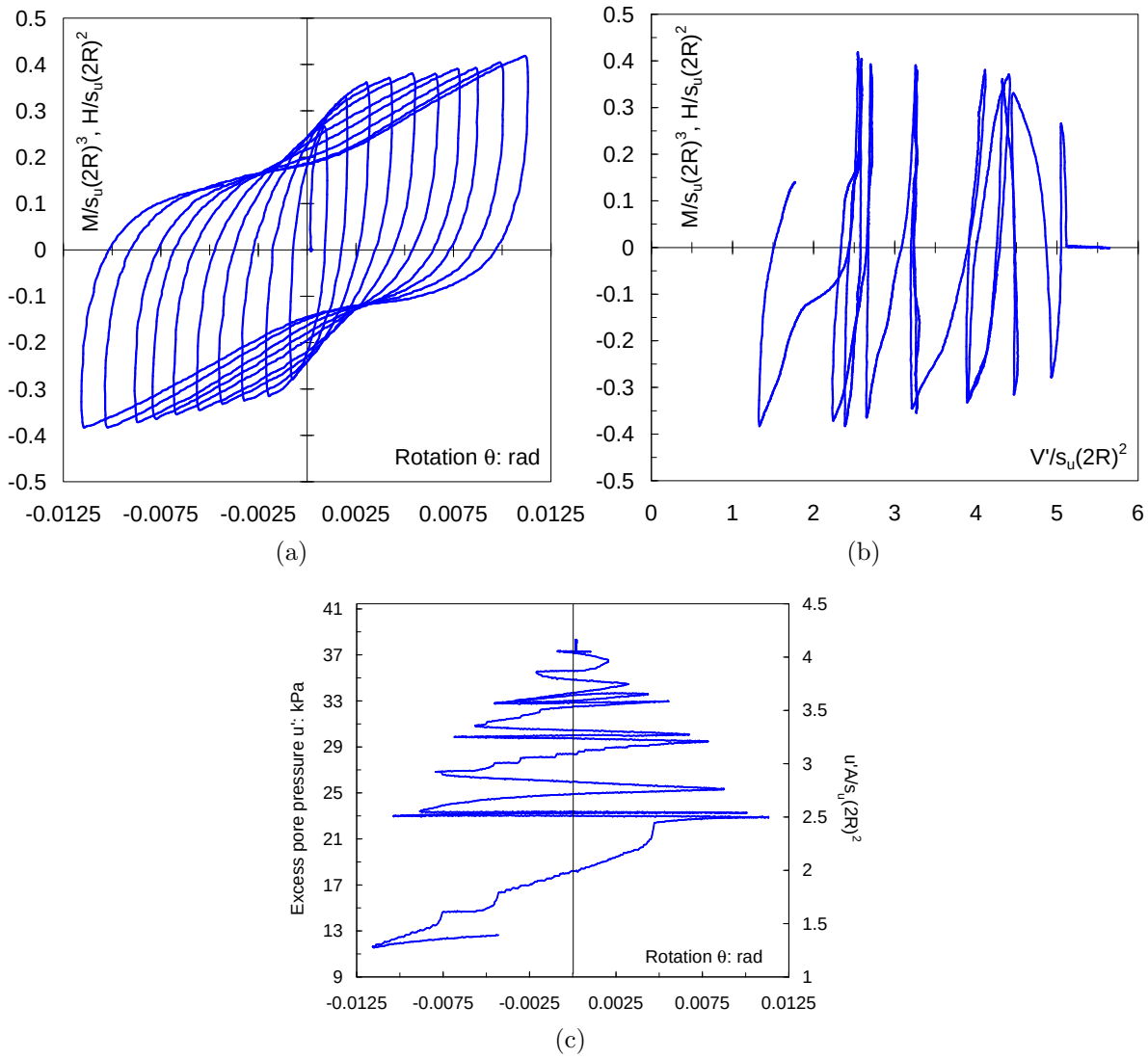


Figure 7.17: Cyclic swipe test FV2_14, $\frac{M}{2RH} = 1$, $V' = 838$ N $\mapsto$ 296 N showing normalised: (a) moment-rotation curve, (b) moment-vertical load curve, and (c) pore pressure-rotation curve

ously decreases after every cycle. It would be interesting to see if this is the case in cyclic swipe events in sand and vice versa.

### 7.3.3 Constant $V'$ moment loading tests

Moment loading tests under constant $V'$ were performed extensively for caissons in sand at various relatively low $\frac{V'}{V_o}$ values and covering a spectrum of $\frac{M}{2RH}$ values (details of experimental procedure, load path, *etc.* can be found in sections §5.3 and §6.1). A similar testing strategy to determine the yield surface and flow rule of a caisson in clay is extremely time consuming owing to the preparation of samples. Swipe tests disturb the clay sample next to caisson mostly in one direction, leaving other directions of loading

not so seriously damaged, additionally, no vertical movement occur. This offers the opportunity to perhaps obtain useful complementary data of good quality from constant $V'$ tests in the same site.

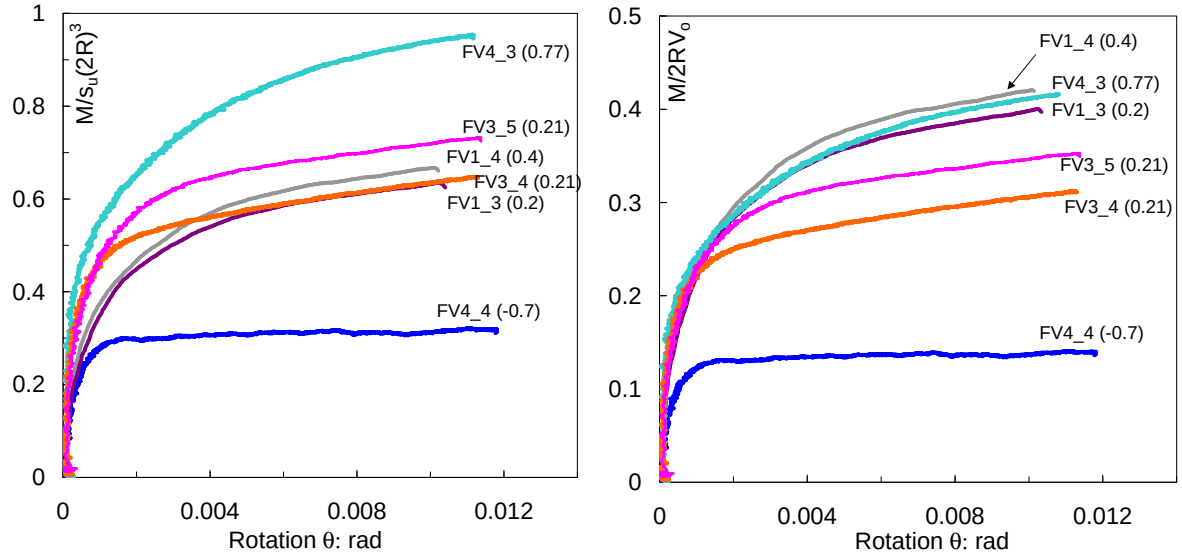


(a) Normalisation by $s_u$ (b) Normalisation by $V_o$

Figure 7.18: Normalised moment-rotation curves for tests with $\frac{V_o}{V_u} \leq 0.32$, $\frac{M}{2RH} = 1$, showing $\frac{V'}{V_o}$ values in brackets

Table 7.4 collects information of the constant $V'$ tests conducted at a rotational velocity of 0.01 mm/s, which as for the swipe tests corresponds to a partially drained condition. Moment-rotation curves of tests with low values of $\frac{V_o}{V_u}$ are shown normalised by $s_u$ in Figure 7.18(a) and normalised by $V_o$ in Figure 7.18(b); with the numbers in brackets corresponding to $\frac{V'}{V_o}$. The value of $V_u$ for series FV1 was experimentally obtained as 1.5 kN, from which a value of $N_c = 11$ was deduced and used to calculate $V_u$ for the remaining series. It is interesting to note that the curve of test FV4_4 follows a perfect elasto-plastic response, *i.e.* an initial very stiff response mostly linear until yield occurs with the development of large plastic rotations progressing under constant moment, hence with the absence of hardening. However, for the curves above test FV4_4 hardening appears after yield instead of the perfect-plastic behaviour. These curves represent a OC condition for the foundation: $|\text{OCR}| = \frac{V_o}{V'} \geq 1.3$.

The curves of plastic vertical displacement *versus* plastic rotation $\delta w^p - \delta\theta^p$ are presented in Figure 7.19(a), where two trends can be clearly identified: i) large uplift due

Table 7.4: Summary of moment loading tests under constant vertical load $V'$

| Test | $\frac{V_o}{V_u}$ | $\frac{V'}{V_o}$ | $V'$ N | $V_o$ N | $V_u$ N | $\frac{M}{2RH}$ | $h$ mm | $u'_i$ kPa | $\Delta u'_i$ kPa | $\Delta u'_f$ kPa |
|---|---|---|---|---|---|---|---|---|---|---|
| FV1_3 | 0.17 | 0.20 | 50 | 250 | 1500 | 1.00 | 148.0 | 0.2 | 0 | 0 |
| FV1_4 | 0.17 | 0.40 | 100 | 250 | 1500 | 1.01 | 148.1 | 0.2 | 0 | 0.2 |
| FV1_5 | 0.17 | 0.80 | 200 | 250 | 1500 | 1.02 | 148.8 | 0.9 | 6 | 9 |
| FV1_6 | 0.17 | 0.40 | 100 | 250 | 1500 | -0.40 | 148.5 | 0 | 1 | 9.5 |
| FV1_7 | 0.17 | 0.80 | 200 | 250 | 1500 | -1.2 | 149.0 | 8.6 | 1.4 | 7.4 |
| FV1_8 | 0.17 | 0.80 | 200 | 250 | 1500 | -0.77 | 149.0 | 14 | 1.5 | 1 |
| FV3_3 | 0.24 | 0.21 | 100 | 474 | 2000 | 1.99 | 147.4 | 1.6 | 0 | -3.2 |
| FV3_4 | 0.24 | 0.21 | 100 | 474 | 2000 | 1.00 | 147.3 | -0.8 | 0 | 0.7 |
| FV3_5 | 0.24 | 0.21 | 100 | 474 | 2000 | 1.00 | 147.3 | -2 | 0.2 | 1 |
| FV3_6 | 0.24 | 0.21 | 100 | 474 | 2000 | -0.99 | 147.4 | -2 | 0 | 0.5 |
| FV3_7 | 0.24 | 0.21 | 100 | 474 | 2000 | -0.50 | 147.4 | 0 | 0 | 0.1 |
| FV4_3 | 0.26 | 0.77 | 500 | 650 | 2500 | 1.01 | 147.0 | 6 | -2.5 | -3.5 |
| FV4_4 | 0.26 | -0.75 | -487 | 650 | 2500 | 0.96 | 146.7 | -0.4 | -4 | -4.3 |
| FV6_12 | 0.31 | 0.20 | 100 | 500 | 1600 | -0.89 | 154.4 | 0 | 0.1 | 0.25 |
| FV7_15S | 0.40 | 0.62 | 494 | 800 | 2000 | 1.02 | 151.8 | 0.6 | 0 | 1.2 |
| FV7_16S | 0.45 | 0.81 | 732 | 900 | 2000 | 1.06 | 154.7 | 4.6 | 0 | 2.4 |
| FV7_17S | 0.45 | 0.95 | 852 | 900 | 2000 | 1.04 | 156.0 | 8.3 | 0 | 2.2 |
| FV2_3 | 0.60 | 0.44 | 400 | 900 | 1500 | 1.02 | 148.0 | 20 | -2 | -3.5 |
| FV2_4 | 0.60 | 0.22 | 200 | 900 | 1500 | 1.01 | 148.0 | 12.4 | -2.4 | -6.4 |
| FV2_5 | 0.60 | 0.11 | 100 | 900 | 1500 | 1.00 | 148.0 | 3.8 | -1 | -3.5 |
| FV2_6 | 0.60 | -0.11 | -100 | 900 | 1500 | 0.98 | 147.9 | -3 | -2 | -1.5 |
| FV2_9 | 0.60 | 0.22 | 200 | 900 | 1500 | 0.50 | 149.2 | 14.4 | -3.5 | -3.5 |
| FV2_10 | 0.60 | 0.00 | 3 | 900 | 1500 | 0.47 | 148.8 | 6 | 0 | -1.4 |

| Test | $K_{mi}$ N/mm | $K_{hi}$ N/mm | $\frac{M_y}{2R}$ N | $H_y$ N | $K_{mf}$ N/mm | $K_{hf}$ N/mm | $G_M$ MPa | $\frac{\delta u^p}{2R\delta\theta^p}$ | $\frac{\delta w^p}{2R\delta\theta^p}$ |
|---|---|---|---|---|---|---|---|---|---|
| FV1_3 | 776 | 300 | 86.1 | 82.5 | 13 | 11 | 10 | 1.240 | 0.001 |
| FV1_4 | 776 | 251 | 87.7 | 85.1 | 16 | 11 | 10 | 1.264 | 0.121 |
| FV1_5 | 503 | 129 | 37.6 | 37.1 | 39 | 23 | 10 | 1.450 | 0.122 |
| FV1_6 | 588 | -258 | 23.5 | -69.0 | -333 | 500 | 0.6 | 0.460 | -0.310 |
| FV1_7 | 1503 | -128 | 126.3 | -80.0 | 120 | -263 | 2.5 | 0.570 | 0.402 |
| FV1_8 | 800 | -500 | 53.2 | -200.0 | 52 | 179 | 2 | 0.300 | -0.080 |
| FV3_3 | 2500 | 150 | 187.5 | 91.6 | 41 | 23 | 25 | 1.115 | 0.035 |
| FV3_4 | 1800 | 350 | 118.8 | 116.5 | 18 | 16 | 30 | 1.107 | -0.008 |
| FV3_5 | 1599 | 450 | 138.8 | 137.3 | 18 | 16 | 25 | 1.091 | 0.015 |
| FV3_6 | 1750 | -215 | 54.2 | -50.0 | 165 | -323 | 2.5 | 0.633 | 0.399 |
| FV3_7 | 550 | -377 | 110.4 | -190 | 165 | 328 | 0.5 | -1.993 | 0.900 |
| FV4_3 | 2824 | 500 | 225.9 | 218.3 | 38 | 31 | 50 | 1.158 | 0.061 |
| FV4_4 | 1029 | 349 | 89.0 | 87.8 | 4 | 7 | 10 | 0.850 | -0.808 |
| FV6_12 | 824 | 2034 | 51.1 | -46.0 | 140 | -606 | 2 | 0.300 | 0.080 |
| FV7_15S | 800 | 800 | 38.0 | 36.0 | 25 | 33 | 10 | 0.760 | 0.330 |
| FV7_16S | 1200 | 1000 | 38.4 | 36.0 | 28 | 36 | 20 | 0.730 | 0.610 |
| FV7_17S | 2000 | 1850 | 47.0 | 48.1 | 22 | 24 | 30 | 0.675 | 2.019 |
| FV2_3 | 1263 | 404 | 132.8 | 131.4 | 15 | 13 | 20 | 0.971 | 0.038 |
| FV2_4 | 1370 | 400 | 143.9 | 140.0 | 12 | 13 | 20 | 0.943 | 0.001 |
| FV2_5 | 1085 | 312 | 143.9 | 139.1 | 13 | 15 | 26 | 0.942 | 0.021 |
| FV2_6 | 1500 | 320 | 106.7 | 106.5 | -7 | -8 | 23 | 0.800 | -0.400 |
| FV2_9 | 700 | 900 | 59.5 | 118.4 | 12 | 21 | 12 | 0.940 | -0.061 |
| FV2_10 | 1000 | 1200 | 38.0 | 78.0 | 98 | 151 | 18 | 1.007 | -0.170 |

S: caisson installed by suction

to the application of a tensile load (test FV4_4), and ii) very small or simply no vertical movement for $\frac{V'}{V_o} = 0.2$, 0.4 and 0.77. Note that the concept of parallel point or parallel

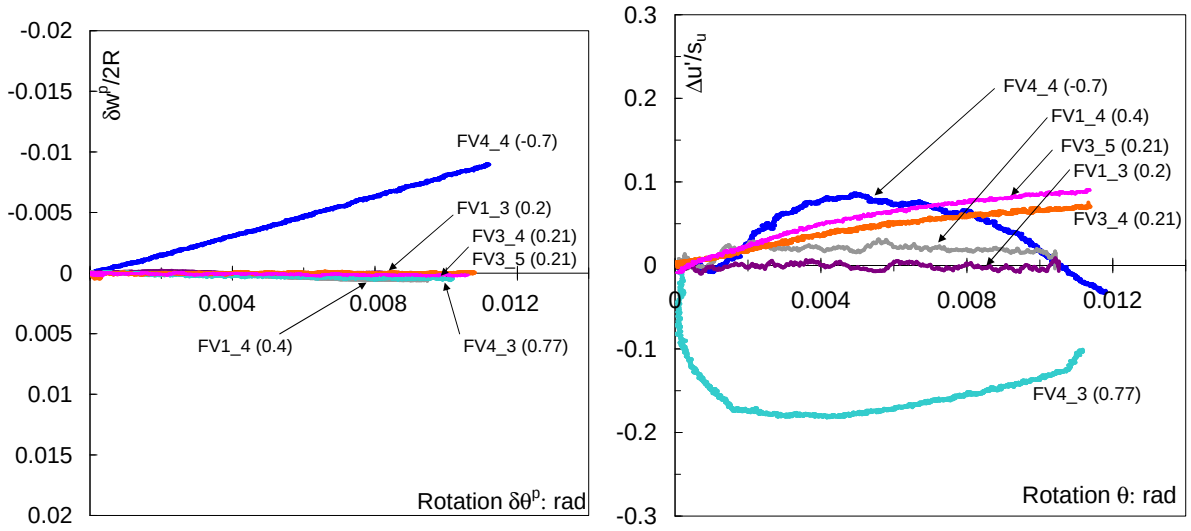


(a) (b)

Figure 7.19: Tests with $\frac{V_o}{V_u} \leq 0.32$, $\frac{M}{2RH} = 1$ and $\frac{V'}{V_o}$ values in brackets, showing normalised: (a) plastic vertical displacement *versus* plastic rotation, and (b) excess pore water pressure variation *versus* rotation

line introduced in Chapters 5 and 6 for caissons in sand seems to apply for a range of values since in ii) $\delta w^p \cong 0$ for five tests with $0.2 < \frac{V'}{V_o} < 0.77$. In test FV4_3 the initial negative $\Delta u'$ was due to the double effect of previous inclination of the caisson caused by a swipe event and the PPT location at the rising side of the lid. Nevertheless, once those initial effects disappear the $\Delta u'$ trend switched from negative to positive due to the slight settlement of the caisson. In tests FV3_4 and FV3_5 the $u' - \theta$ curves tend to a zero absolute value of $u'$. In general the level of $\Delta u'$ was much higher in the swipe tests because of the larger caisson rotations and also the larger variation in $V'$ seems to affect more than the $w$ variation. The two trends are linked with the curves of pore water pressure variation with rotation $\Delta u' - \theta$ as shown in Figure 7.19(b) (with the exception of the initial part of tests FV4_4 and FV4_3 owing to the location of the *ppt* under the lid).

Tests with high values of $\frac{V_o}{V_u}$ are shown in Figures 7.20(a) and 7.20(b), representing a 'normally loaded' condition ($|\text{OCR}| \leq 1.1$). It can be observed that the order of magnitude of $\frac{M}{s_u(2R)^3}$ in these curves are fairly similar to the curves in Figure 7.18(a). Conversely, the effect of a different range of $V_o$ values is obviously evident comparing Figures 7.20(b) and 7.18(b) since $V_o$ is used in the normalisation of the moment load. Although larger $V_o$ values cause an increase in the moment capacity (compare for example tests under similar

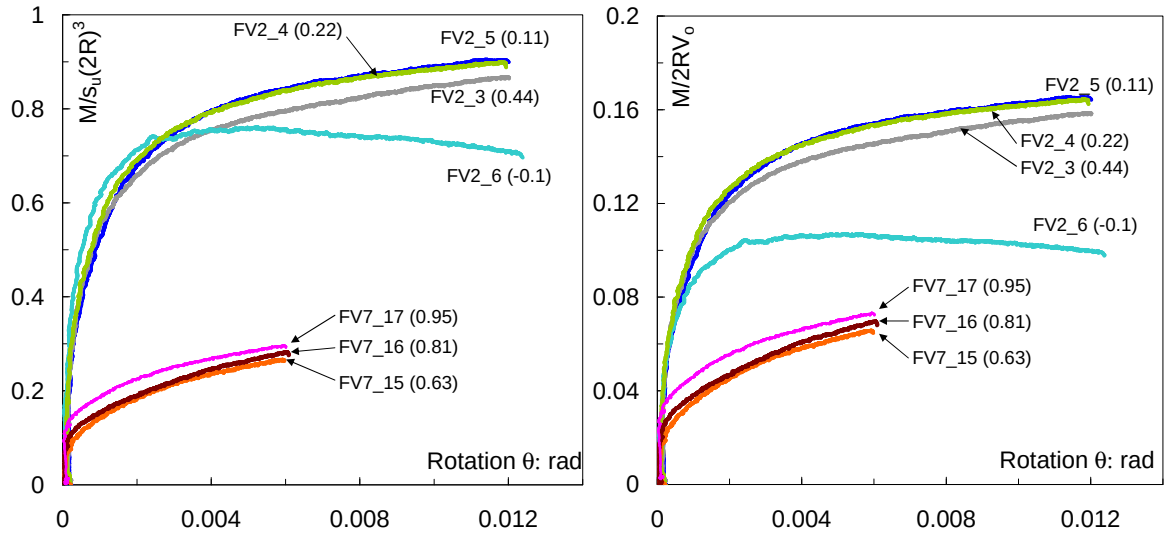


(a) Normalisation by $s_u$ (b) Normalisation by $V_o$

Figure 7.20: Tests with $\frac{V_o}{V_u} \geq 0.4$, $\frac{M}{2RH} = 1$ and $\frac{V'}{V_o}$ values in brackets showing normalised moment-rotation curves

$\frac{V'}{V_o}$; FV1_3 with FV2_4 and FV1_4 with FV2_3 in Table 7.4), the increase in moment load capacity does not compensate the increase of $V_o$, resulting in a reduction of $\frac{M}{2RV_o}$ from 0.4 to 0.16.

Three trends of plastic vertical displacement can be identified in Figure 7.21(a). The two first trends were found and described in Figure 7.19(a). The third trend corresponds

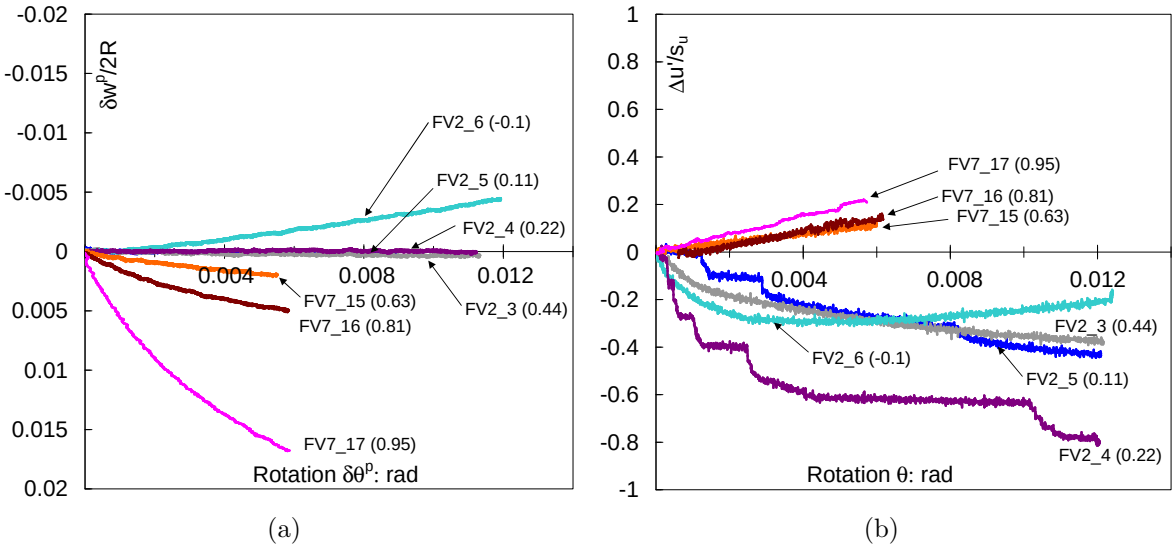


(a) (b)

Figure 7.21: Tests with $\frac{V_o}{V_u} \geq 0.4$, $\frac{M}{2RH} = 1$, and $\frac{V'}{V_o}$ values (numbers in brackets) showing: (a) plastic vertical displacement *versus* rotation, and (b) pore water pressure variation *versus* rotation

to the increasing caisson settlement with $\frac{V'}{V_o}$. Figure 7.21(b) shows that suction appeared under the caisson lid for values of $\frac{V'}{V_o} < 0.45$. This reveals that during the caisson rotation the underside of the lid and the top of the soil plug kept in contact. Full contact during uplift is a strong assumption made in numerical analysis of undrained moment capacity of skirted footings (Gouvernec and Randolph, 2003; Gouvernec, 2003).

### 7.3.4 Yield surface and flow vectors

The results of constant $V'$ tests are shown in Figure 7.22 as yield points (values listed in Table 7.4) in the normalised moment *versus* horizontal load. In the same figure two calculated yield surfaces are included based on the yield surface formulation presented in Chapter 5. Despite the lack of data for load ratios different to one, two major groups can be identified regardless of the value of $\frac{V'}{V_o}$: one group with high deviatoric load capacity forming an exterior boundary, and a second group with low deviatoric load capacity forming an interior boundary. The yield surfaces were estimated relying mainly on the few yield points with negative load ratios. The parameters $h_o$, $m_o$ and $e$ obtained from these estimations are summarized in Table 7.5. Obviously, more data for a wider variety of load ratios is required to confirm or not these tentative values. However, in the next stage of this analysis these values will be validated using a three dimensional yield surface formulation (expression (5.43) or (6.3)).

Figure 7.23 coalesces the results from swipe tests and from constant $V'$ tests in the $\frac{M}{2RV_o} - \frac{H}{V_o}$ plane. The data is divided according to the $\frac{V_o}{V_u}$ ratio, from where two groups can be recognized as well, at least for the data with load ratio of one. Based on the values of $h_o$, $m_o$ and $e$ estimated from Figure 7.22 two yield surfaces were calculated for $\frac{V_o}{V_u} \geq 0.4$ and for $\frac{V_o}{V_u} \leq 0.32$, as shown in Figure 7.23. Table 7.5 presents the values of the parameters $\beta_1$ and $\beta_2$ determined by fitting the experimental results. In the light of these results, it appears a third group of data above the yield surface for data with $\frac{V_o}{V_u} \leq 0.32$. This reflects that larger capacities were obtained owing to higher degree of OC (samples 4 and 3 had the highest values of $s_u$). In addition, series of tests FV3 and FV4 had $V_o$

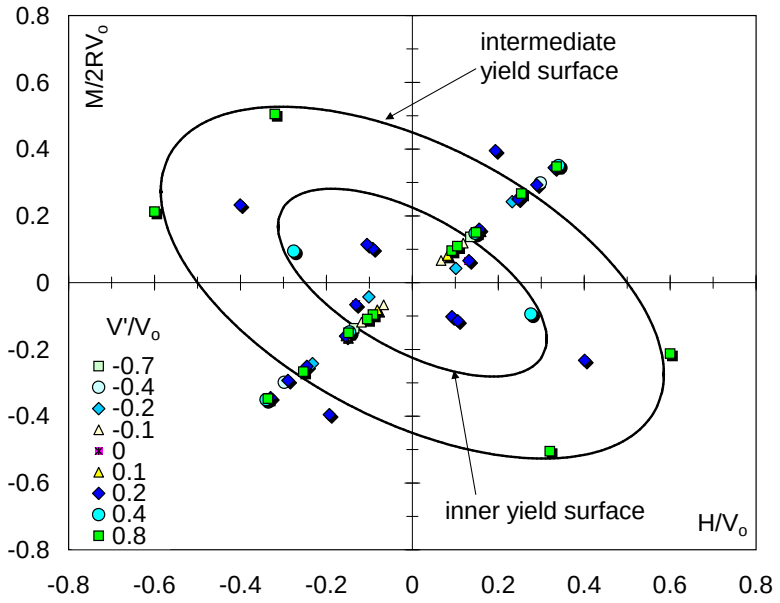


Figure 7.22: Normalised yield points in the $\frac{M}{2RV_o} - \frac{H}{V_o}$ plane and fitted yield surfaces

values much closer to $V_c$ rather than $V_u$. The set of parameter values estimated for this outer yield surface are presented in Table 7.5.

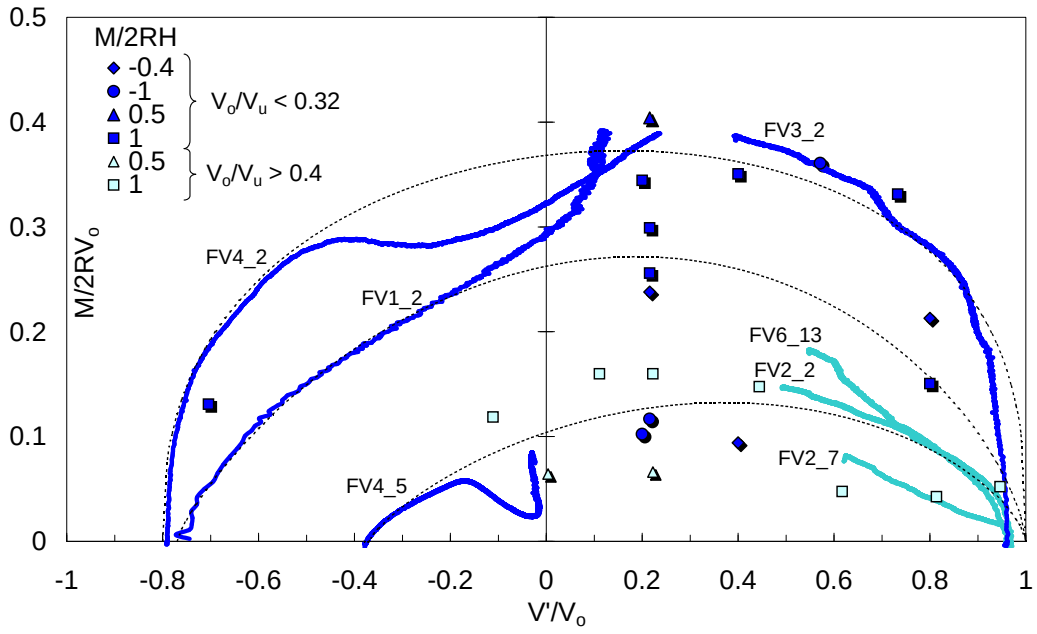


Figure 7.23: Normalised yield points in the $\frac{M}{2RV_o} - \frac{V'}{V_o}$ plane and fitted yield surfaces

The study of the flow rule follows the analysis of section §5.4.3. Associated flow has been assumed in the calculations, hence the association factors are equal $a_M = a_H$. The theoretical flow rule is compared with the experimental results in Figure 7.24(a) using the parameter values summarized in Table 7.5. Although associated flow may hold for the

Table 7.5: Parameter values of the yield surface

| Yield surface for $\frac{V_o}{V_u}$ | $m_o$ | $h_o$ | $t_o$ | $e$ | $\beta_1$ | $\beta_2$ |
|---|---|---|---|---|---|---|
| $\leq 0.32$ † | 0.7 | 0.6 | 0.8 | -0.5 | 0.4 | 0.35 |
| $\leq 0.32$ | 0.5 | 0.45 | 0.77 | -0.52 | 0.8 | 0.675 |
| $\geq 0.4$ | 0.25 | 0.225 | 0.37 | -0.6 | 0.8 | 0.675 |

†clay heavily overconsolidated with the highest values of $s_u$

results presented more data (with different load ratios and load histories) is required for a definitive conclusion. Experimental and theoretical predictions of the vertical plastic displacement increments are shown in Figure 7.24(b), where associated flow has been assumed, making the association factors $a_{V_1} = a_{V_2} = 1$. The study of the flow rule becomes more complex not only for the variation of the flow vector directions with $\frac{V'}{V_o}$ and $\frac{M}{2RH}$ as presented in section §5.4.3, but also due to the different load history $\frac{V_o}{V_u}$ and pore pressure variations. The development of suction can modify substantially the vertical displacement of the caisson. Some of the larger values of $\Delta u'$ are shown in Figure 7.24(b) next to each point.

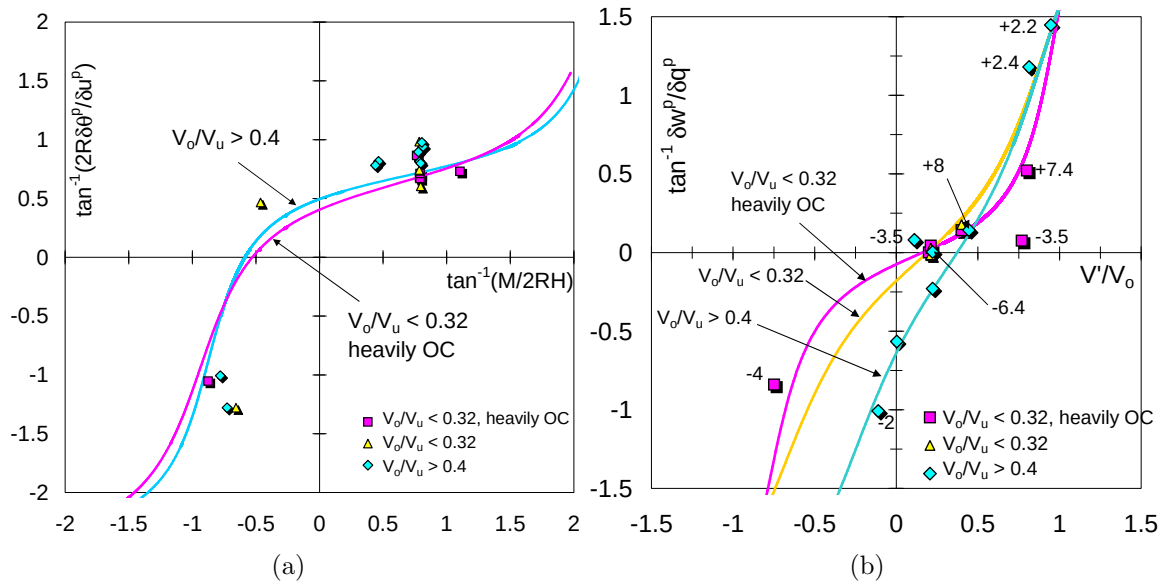


Figure 7.24: Experimental and theoretical predictions of incremental plastic displacement ratios in the $\pi$ plane assuming normality (numbers in (b) refer to $u'$ and points without numbers imply $u' \approx 0$ kPa)

### 7.3.5 Cyclic moment loading tests

The cyclic rotational response of suction caissons in clay is a fundamental issue owing to the cyclic nature of the offshore environmental loads as mentioned in Chapter 1. Pre-

Table 7.6: Summary of cyclic moment loading tests. Field test taken from Houlsby *et al.* (2005)

| Test | 2R m | $\frac{L}{2R}$ | $s_u$ kPa | $V_o$ kN | $\frac{V'}{V_o}$ | $\frac{V'}{s_u(2R)^2}$ | $\frac{M}{2RH}$ | $w_t$ mm |
|---|---|---|---|---|---|---|---|---|
| FV7_12S | 0.15 | 1 | 9.9 | 0.75 | -0.13 | -0.44 | 1 | -5 |
| FV6_10 | 0.15 | 1 | 8.4 | 0.5 | 0.20 | 0.45 | 1 | -0.2 |
| Field trial | 3 | 0.5 | 14.4 | 200 | 0.21 | 0.33 | 1 | 5 |

vious research of cyclic combined loading has concentrated on suction caissons as anchors for deep water floating structures, which include eccentric vertical cyclic loading in tension leg platforms TLP (Andersen *et al.*, 1993; Clukey *et al.*, 1995) and laterally moored systems (House, 2002). Therefore, it was regarded as important to investigate the cyclic moment loading response of monopod suction caisson foundations due to the differences prevalent in offshore wind turbines as pointed out in section §7.3.1. Recently, results from cyclic moment loading tests with large scale caissons at the Bothkennar site have been reported by Houlsby *et al.* (2005) for offshore wind turbine applications. Consequently, comparisons of laboratory results with field results will be pursued.

Cyclic moment loading tests FV7_12S and FV6_10 were performed using caisson D under the soil and loading conditions listed in Table 7.6. Both tests were conducted after a series of cyclic vertical loading events, for that reason it was thought that the clay samples were not so seriously damaged in the lateral direction. Figure 7.25(a) shows the moment-rotation curve of test FV6_10 with the strength normalisation by $s_u$ on the left hand side and the load normalisation by $V_o$ on the right hand side of the plot. The first four cycles present the typical growing hysteresis loops with increasing rotation amplitude. But beyond the fourth cycle a hysteresis loop constriction appears added to the fact that the moment capacity stabilizes and even decreases slightly with larger rotation amplitudes. This modification in the hysteresis loop shape is not considered in the Masing rules, in which cycles are reproduced following the first loading curve. This issue may cause modifications in the modelling.

Figure 7.25(b) shows the curve response of test FV7_12S, with the caisson installed by suction and experiencing tension. It is noteworthy that the onset of a hysteresis loop con-

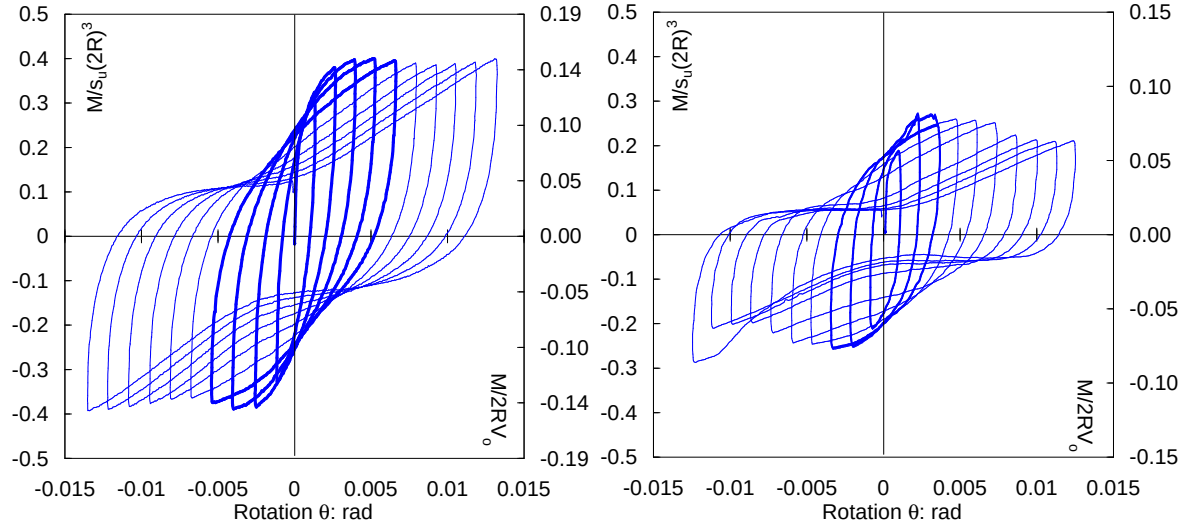


(a) Test FV6_10, $\frac{V'}{V_o} = 0.2$ (b) Test FV7_12S, $\frac{V'}{V_o} = -0.13$

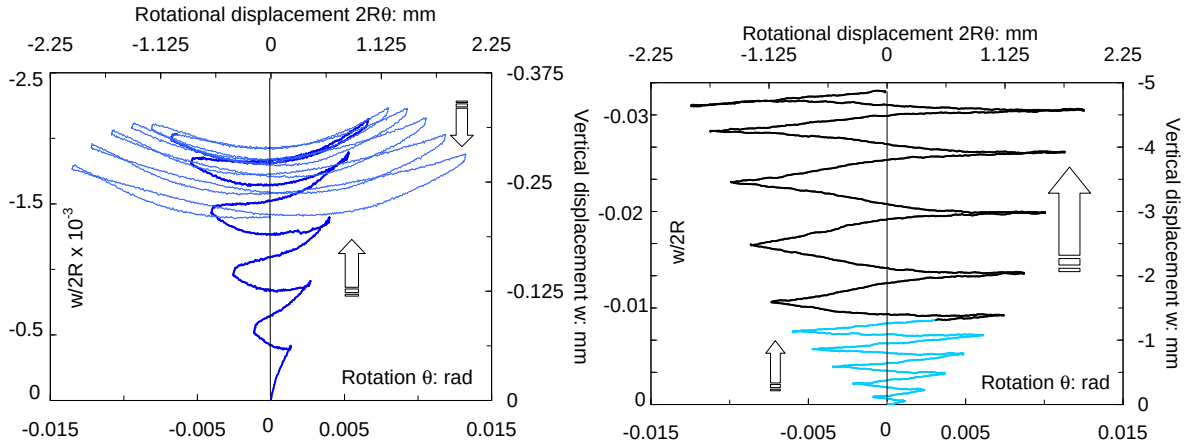


(c) Test FV6_10, $\frac{V'}{V_o} = 0.2$ (d) Test FV7_12S, $\frac{V'}{V_o} = -0.13$

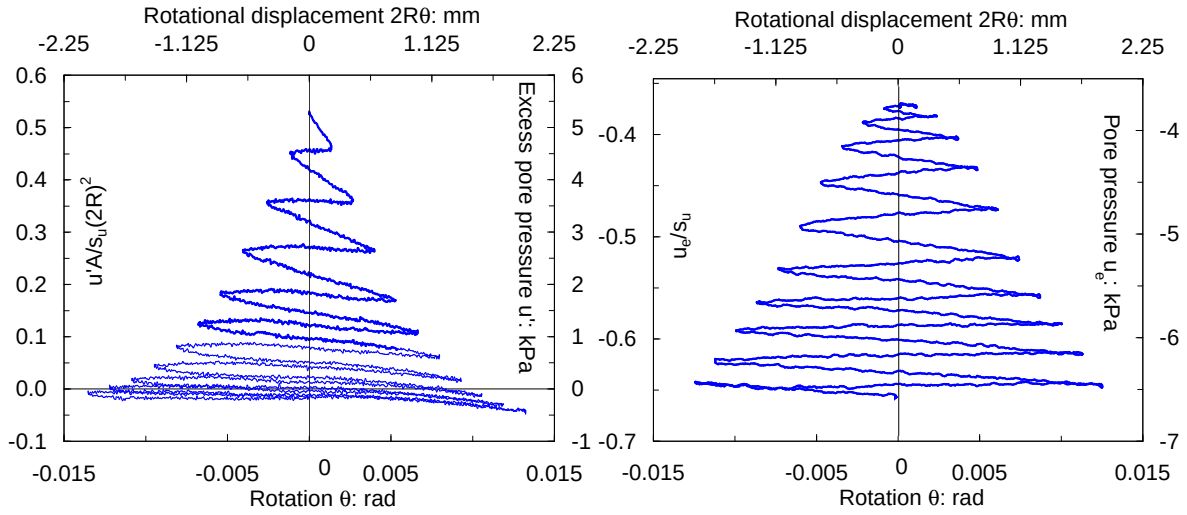


(e) Test FV6_10, $\frac{V'}{V_o} = 0.2$ (f) Test FV7_12S, $\frac{V'}{V_o} = -0.13$

Figure 7.25: Results from two cyclic moment loading tests

striction starts earlier (third cycle) and is much more pronounced than in test FV6_10, causing a considerable moment capacity decrease. Constriction of the hysteresis loops is the result of gaps simultaneously opening and closing from top to bottom, and vice versa, next to the skirt during each rotational cycle. This phenomenon is also found when cracks appear in cyclic shear loading of reinforced concrete elements. Then the onset of gapping is an indication of foundation failure and further opening of the gaps reveals the level of damage.

The resulting vertical displacement evolution in test FV6_10 is shown in Figure 7.25(c), where the arrows indicate the direction of the vertical displacement. It is interesting to note that initially the caisson moves upwards, but when it reaches the fourth cycle the caisson rocks with a small vertical movement during three cycles. Thereafter, the caisson rocks moving downwards although it was not able to return to the initial point. This pattern of vertical displacement evolution does not agree with the monotonic tests with $\frac{V'}{V_o} = 0.2$, in which zero vertical displacement was observed. However, it is similar to the behaviour observed in test FV80_13_1B with also a caisson aspect ratio of one but in dry loose sand (section §5.5.3). This agreement leads to the same conclusion related to the transition or parallel point being reached between uplift and settlement. Conversely, Figure 7.25(d) shows that in test FV7_12 there was not a transition point since the uplift increased steadily with the amplitude of rotation due to the tensile load being applied.

Figure 7.25(e) shows the pore pressure variation during cyclic rotation in test FV6_10. A significant reduction of $u'$ in the first four cycles from an initial value of 5 kPa to a value close to 1 kPa is seen. In the next cycles $u'$ reduces even more although at a lower rate since the caisson is not moving upwards any more. Nevertheless, suction appears in the last three cycles. By comparison, in Figure 7.25(f) the tensile load causes the appearance of suction from the beginning and the onset of rotational cycles increases the suction even more.

In a moment *versus* vertical displacement plot the pattern followed by the curve of test

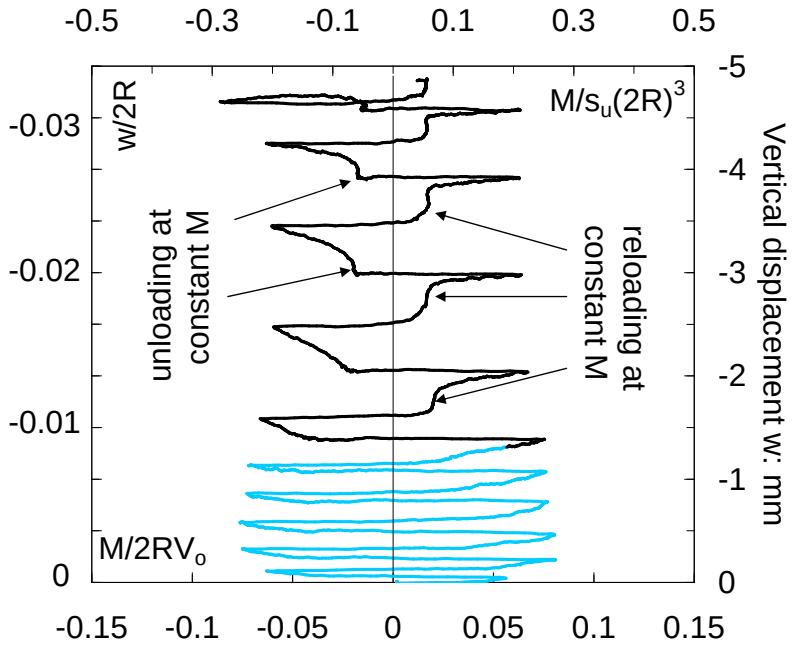


Figure 7.26: Effect of hysteresis loop constriction on the higher rate of uplift during moment reloading and unloading (test FV7_12S)

FV6_10 (not shown) in the last cycles is identical to that shown in Figure 5.34. The caisson settles smoothly during reloading and unloading, whereas uplift occurs when reaching the maximum positive and negative moment load in each cycle. Conversely, in Figure 7.26 it is clear that only uplift occurs with a pattern totally different to that mentioned above. The largest uplifts occur not near the maximum moment load, but at a lower and almost constant value which is reached during constriction or gapping. This indicates that under tension the reduction of moment capacity induced by gapping also increases the rate of caisson uplift.

Houlsby *et al.* (2005) undertook a series of large scale tests under load-controlled conditions at the Bothkennar site using a suction caisson with the dimensions and loading conditions listed in Table 7.6. The Bothkennar clay is an estuarine clay with an OCR $\leq$ 1.6 (Hight *et al.*, 1992). Results from the field offer an invaluable opportunity for comparison with laboratory results. In this context, Kelly *et al.* (2006) reproduce the same normalised cyclic rotational displacement paths (and normalised $V'$) in the laboratory to those in the field with the intension of studying effects of scale on the moment capacity. Although the purpose of the present study was not to replicate the conditions of the

Bothkennar tests, it is very interesting to see whether similar patterns and trends exist or not. Figure 7.27(a) reproduces the moment-rotation curve from the field, which can be compared with test FV6_10 owing to closeness in the normalised vertical load (although the caisson aspect ratios are different). The normalised moment capacity for the first cycles in both tests is comparable (around $\frac{M}{s_u(2R)^3} \approx 0.3$) as well as for the final cycles (around $\frac{M}{s_u(2R)^3} \approx 0.4$). This agreement reveals that the effect of higher level of stresses in the field is not as important in clay as it is in sand. In terms of the normalisation by $V_o$ test FV6_10 exhibits less moment capacity because of the larger $V_o$ value caused by the further penetration during the cyclic vertical loading.

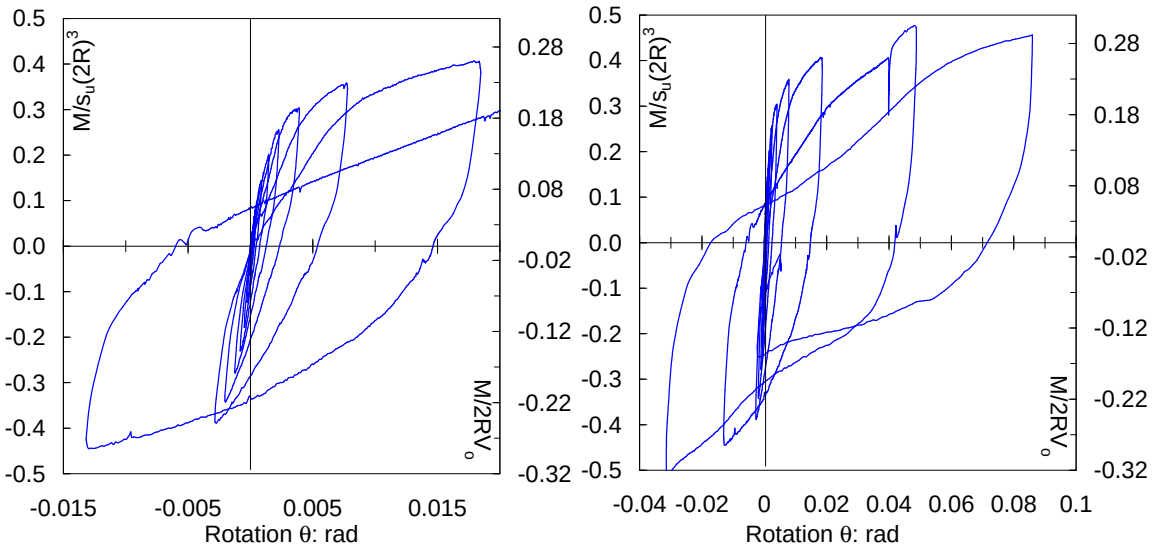


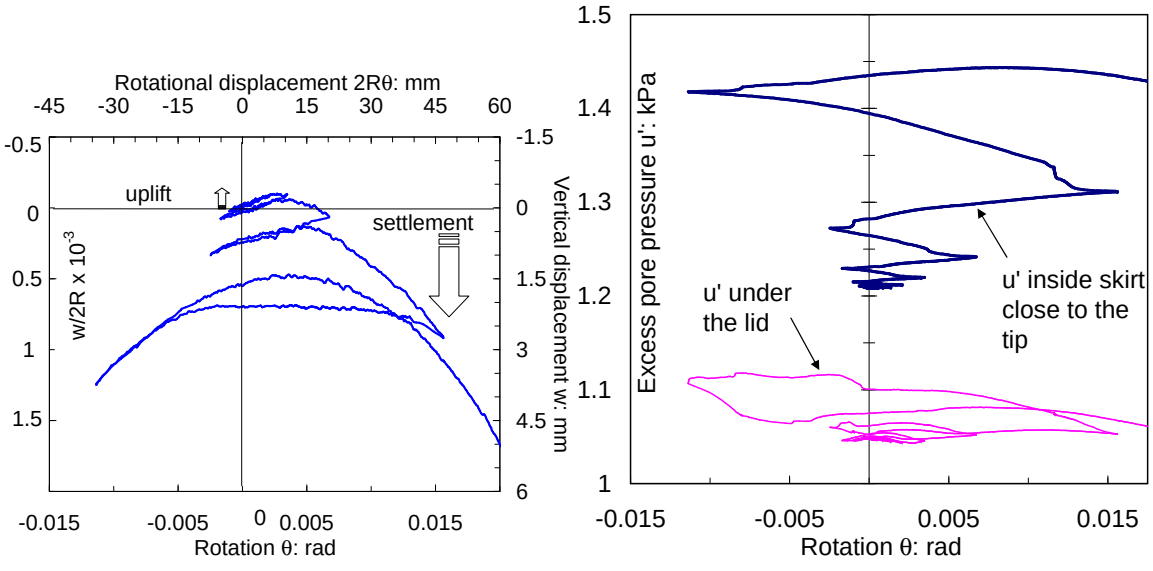


Figure 7.27: Large scale test results (adapted from Houlsby *et al.*, 2005)

It is worth noting the influence of the loading control mode in Figures 7.27(a) and 7.25(a). The load-controlled mode applied in the field forces the caissons to reach in each cycle an increased moment load target, to cope with that the rotation in each cycle should recover from the previous cycle. With the appearance of plastic rotations, larger rotations will develop in order to complete the cycle as it can be observed in the last cycle shown in Figure 7.27(a), where for a minor increase in moment load a very large rotation results. Even much larger rotations will develop to achieve a very small increase in moment load in the next two cycles as shown in Figure 7.27(b). Conversely, the displacement-controlled tests performed in the laboratory target rotations instead, therefore the moment load is free to increase, decrease or stay the same. The gapping response obtained in the laboratory under small rotations ($\theta \geq 0.005$ rad) also occurred in the field, but for rotations one order of magnitude less ($\theta \geq 0.04$ rad) as shown in Figure 7.27(b).

By comparing Figures 7.27(c) and 7.25(c) it can be observed that the normalised vertical displacement obtained in the field shows initially a four times smaller upward movement of the caisson than the obtained in the laboratory. Afterwards, the caisson moves downwards with the largest settlements occurring at reversals. Although the laboratory result also shows a switch from upward to downward movement, normalised settlements in the field are three times larger. In addition, in the laboratory the largest settlements occur around $\theta = 0$ rad and the minimum settlements at reversals, hence opposite to the field. Figure 7.28 depicts the rotation mechanism of the caisson in the field occurring around the centre and the rotation mechanism of the caisson in the laboratory lifting up on the edges.

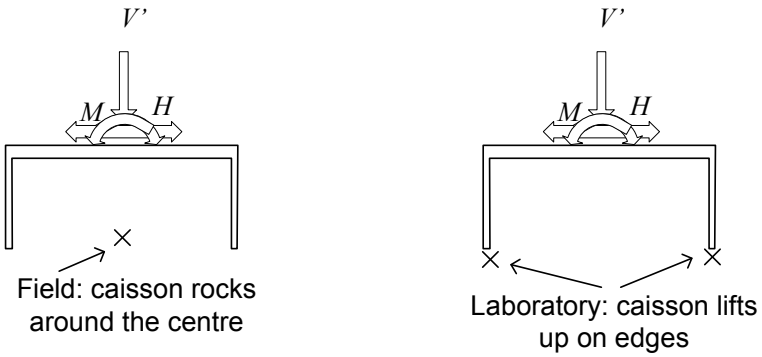


Figure 7.28: Rotation mechanisms observed in the field and in the laboratory

Figure 7.27(d) shows the variation of the pore pressure underneath the caisson lid and inside the caisson skirt near the tip. It is interesting to observe that there is a minor variation of $u'$ under the lid, not agreeing with the laboratory results, whereas a small increase of $u'$ develops close to the tip.

## 7.4 CONCLUSIONS

The results of an experimental study of suction caisson foundations in clay for offshore wind turbines have been described. This study was necessary to obtain the data to determine the parameters required to model the response of suction caisson foundations. A suction caisson with an aspect ratio of 1 was tested in heavily overconsolidated kaolin clay. This study considered three stages. Firstly, installation and pullout capacity, secondly, cyclic vertical loading, and thirdly, the monotonic and cyclic moment capacity.

### 7.4.1 Installation and pullout

The calculation procedure proposed by Houlsby and Byrne (2005) was used to back-analysed the inside and outside adhesion factors. Similarly, remoulded $s_u$ values obtained from shear vane tests provided reliable values of adhesion factors as the inverse of the clay sensitivity following Andersen and Jostad (2002). This allowed the prediction of the penetration resistance for caissons installed by pushing. However, the prediction of the suction for suction assisted penetration should account for a diminished adhesion factor due to non-dissipated pore pressures. No substantial difference was found between the net vertical load required to install a caisson by pushing and by suction, agreeing with previous findings for normally consolidated kaolin clay found in the literature.

A reverse $N_c = 8.6$ was determined from a pullout test, value that is slightly lower than the lower bound solution for smooth skirts. Furthermore, an even lower $N_c = 6.4$ was determined from a large scale pullout test.

### 7.4.2 Cyclic vertical loading

Results of cyclic vertical loading tests are relevant for applications of multiple-caisson foundations. The cyclic vertical loading around a mean vertical load equal to the maximum installation load induced permanent settlement of the caisson, whereas the cycling around a mean vertical load equal to zero induced permanent uplifting of the caisson, although for large load amplitudes temporary settlements were observed during compressive loading.

It was found that in the short term substantial difference occurred in the vertical cyclic loading response between a caisson installed by pushing and a caisson installed by suction. The large magnitude of non dissipated pore water pressure generated during the suction installation influences the load-displacement response, diminishing substantially the amount of caisson uplift and increasing the bearing capacity failure in 50%.

### 7.4.3 Moment loading

Results from cyclic moment loading tests revealed hysteresis loop constriction at small level of rotation, reducing the caisson moment capacity and increasing the rate of uplifting under tensile load. This was caused by the opening and closing of gaps next to the skirt amidst the reloading and unloading. Recently, this phenomenon has been reported in the literature for large scale caisson tests, but for rotations one order of magnitude higher. Furthermore, the parallel point or transition from uplift to settlement was found to occur at the onset of the hysteresis loop constriction.

Swipe and constant $V'$ tests were performed to determine the yield surface. It was found that the size and shape of the yield surface depend on the caisson load history and bearing capacity, expressed as the ratio $\frac{V_o}{V_u}$. For values of $\frac{V_o}{V_u} \geq 0.4$ the yield surface size was found to reduce, whilst for $\frac{V_o}{V_u} \leq 0.32$ the yield surface size increased.

The parallel point was found to extend for a wide range of $\frac{V'}{V_o}$ values, namely from 0.2 to

0.77 for low $V_o$ and from 0.11 to 0.44 for high $V_o$. Despite the acceptable agreement of the associated flow assumed with the experimental results, more data is required to confirm the assumption of associated flow.

### 7.4.4 Discussion and recommendations

The majority of tests concentrated on $\frac{M}{2RH} = 1$ at different $V'$ values, with only few tests with $\frac{M}{2RH} \neq 1$. As a consequence, these series of combined loading tests carried out are not sufficient to cover exhaustively other load paths needed to define accurately the size and shape of the yield surface, hence the parameters for modelling. The preparation of kaolin samples is time consuming and is not possible to obtain more than two fresh sites per specimen. Therefore, further experiments in undisturbed samples are required to increase the data base, using not only a caisson with $\frac{L}{2R} = 1$, but also including caissons with other geometries. Moreover, a study of the effect of the installation method on the caisson moment capacity is necessary. It has been confirmed that no significant difference exists, whether the caisson is installed by pushing or by suction. However, this similarity accounts only for the penetration resistance and not for the subsequent moment capacity. Furthermore, such a study should consider the case of combined loading immediately after suction installation (no dissipated pore pressures) and cases accounting for some degree of consolidation (dissipation of pore pressures).

# Chapter 8

# CONCLUSIONS

This thesis has presented the study of an experimental research programme of suction caisson foundations for offshore wind turbines. The results were interpreted within the framework of force-resultant plasticity models. From the analysis of the results, it was possible to estimate the parameter values needed to apply hyperplasticity formulations to the modelling of suction caissons. Conclusions and discussions of each part of this research programme have been included in the previous chapters. In this chapter the principal conclusions are summarized and suggestions for future research are proposed.

## 8.1 CONCLUDING REMARKS

In this investigation a variety of testing conditions were used: i) different caisson geometries, ii) five type of soils: two dry sands - loose and dense, two dense saturated sands - water-saturated and oil-saturated, and a heavily overconsolidated Kaolin clay, and iii) different loading systems and regime: pure vertical and combined loading and monotonic and cyclic loading. From these conditions valuable comparisons between tests were possible using normalised expressions, which also allow preliminary estimations of the scaling of prototype load capacity, displacements, pressures and stiffnesses.

### 8.1.1 Main findings

The study of monotonic vertical loading in sand revealed that once the full bearing capacity is mobilised, caisson stiffness reduced considerably, nevertheless, permanent softening did not occur as in flat footing, on the contrary, in loose sands the vertical load increased further with penetration. In dense sands hardening occurred after a sequence of peak response followed by relaxation and softening. A new formulation for the hardening law was proposed for this observed response.

The results from caisson installation tests showed considerable reduction of the net vertical load when suction was used to assist the penetration, owing to the creation of hydraulic gradients. Krynine's expression (Handy, 1985) was used to calculate the passive earth lateral pressure coefficient for caisson penetration and the active pressure for caisson drained pullout. The calculation procedure proposed by Houlsby and Byrne (2005b) to estimate the suction was found to be very sensitive to the permeability ratio, which is the soil permeability inside the caisson divided by the soil permeability outside the caisson. Good estimations of the suction were obtained with values of the permeability ratio between 2 and 4. However, for rapid penetrations of a caisson with large thickness ratio high values of the permeability ratio were required to obtain good estimations of the suction.

The yield surface was determined from moment loading tests under low constant vertical loads. A yield surface expression including tensile loads was fitted to the experimental results, which allowed the estimation of the parameters required to construct plasticity models. The flow rule formulation was derived from the yield surface expression rather than from a potential function. The flow rule was found to be associated in the plane of radial plastic displacement increments. Moment and horizontal association factors $a_M$, $a_H$ were found to be identical. Conversely, a strongly non-associated flow rule was found in the radial-vertical load plane, leading to the vertical association factor $a_{V_1}$ to be different to the other association factors. From symmetric and non-symmetric cyclic moment loading tests under constant $V'$ it was found that Masing's rules were obeyed. However,

from cyclic swipe tests Masing's rules were not obeyed.

In the analysis of moment and lateral loading under drained, partially drained and undrained conditions the effect of the installation method has been considered. Under drained conditions and in the short term, the moment resistance of a suction caisson depends on the method of installation. However, the ratio of plastic radial displacement increments was independent of the installation method. Conversely, the suction installation reduced the caisson uplift during rotation. Under partially drained conditions the caisson resistance diminished with the build-up of excess pore pressures in comparison with that under drained conditions. However, the caisson rotational stiffness was similar to that under drained conditions. To model in the laboratory the wave periods of extreme waves, and the range of permeabilities of the seabed and prototype caisson diameters, the scaled rotation velocities applied to the caisson to induce undrained conditions were determined. Moment loading tests under low constant vertical loads simulating those conditions revealed a dramatic reduction of the caisson resistance and stiffness. Without a substantial increase of the constant vertical load, the caisson moment capacity and stiffness did not recover.

In the study of cyclic vertical loading of suction caissons in clay it was found that in the short term negative excess pore pressures, induced by suction installation, reduced the caisson uplift compared with that from a caisson installed by pushing. Cyclic moment loading showed the effect of gapping at smaller normalised rotations than in the field. The change of hysteresis loop shape due to gapping cannot be reproduced using only the Masing rules. From moment swipe and constant vertical load tests it was found that the moment capacity diminished with the increase of the ratio between the preload $V_o$ and the ultimate bearing capacity load $V_u$. Since for suction caissons for offshore wind turbines this ratio is low, $\frac{V_o}{V_u} \approx 0.2$, it is expected that the caisson moment capacity will be high.

## 8.2 SUGGESTIONS FOR FURTHER RESEARCH

The bearing capacity of skirted footings in sand was determined using the bearing capacity factors for flat footings. Therefore, bearing capacity factors $N_q$ and $N_\gamma$ considering the geometry of skirted footings are necessary.

It was found that high values of permeability ratio were necessary to obtain a good estimations of the suction in rapid caisson penetrations. It is suggested that suction installation experiments using the same caisson aspect ratio but with different thickness ratios, soil densities as well as different penetration rates should be carried out. Calculation procedures including penetration rates related to the field would be necessary to estimate the suction.

A series of moment loading tests under high constant vertical loads is necessary to complete the analysis of the flow rule, so as to estimate the value of the association factor $a_{V_2}$ and $\beta_2$, which have been assumed in this study equal to 1 and 0.99 respectively.

There was not great difference between results of moment loading tests performed 48 hours after suction installation and moment loading tests of caissons installed by pushing. This proved that soil strength was recovered. It is suggested that subsequent moment loading tests should consider different consolidation times, *i.e.* after suction installation. It is well established that fine-grained soils and clays have strength properties and behaviour that change over time as a result of consolidation. The way in which the strength of the soil, disturbed by the flow induced by the suction, changes with time is not known. However, it is known that ageing effects can include the contribution of creep processes, continuous viscous rearrangement of particles (no densification as in secondary consolidation). Therefore, the effect of the suction on the soil strength should be considered in the study of caisson moment capacity.

Research that includes the long term effect of small ocean wave loading amplitude, where

the period is much lower than 12 s is required (between 2 s and 7 s). Although, this loading train has small loading amplitude, their period is closer to the period of the structure, which may induce resonance. Furthermore, it is the prevalent regime of loading offshore, which accounts for millions of cycles per year (from 1 to up to 5 millions). This unexplored condition needs experiments that consider saturated sandy and clayey soils to measure possible build-up of excess pore pressure. It is also of fundamental importance to know if the cyclic response encountered in this investigation continues for larger number of cycles or stabilizes. Vertical loading as well as combined loading should be studied.

Offshore loading of a wind turbine is three dimensional. Therefore, the extension of this study from two dimension to three dimensions is necessary to account for simultaneous loadings along different axes and the inclusion of torsion.

The effect of anisotropy has not been included in the estimation of elastic displacements, since a unique value of elastic shear modulus has been assumed in the calculations. Research to find out whether anisotropy is important or not is suggested. It would be necessary to know the sensitivity of the displacement calculations to the different shear modulus values in each direction to assess whether is worth to include different shear moduli.

In combined loading tests the vertical load has been kept constant. However, moment loading tests where the vertical load varies during rotation could be carried out. For instance, the vertical load could be reduced or increased keeping the ratio between the moment load and vertical load constant. For instance, this would reflect the combined loading occurring in a multiple caisson foundation. It would be interesting to find out whether, through different load paths with all the loads varying, the same yield surface is reached and the same flow vectors are obtained or not.

It has been found that the pore pressure is a key parameter. However, the measurement of the pore pressure at one point on the caisson lid limits the analysis, since variations across

the lid as well as along the skirt occur during caisson rotation. Therefore, it is suggested that model suction caissons be instrumented with at least two pore pressure transducers on the lid and at least two at the skirt. At the skirt the use of miniature PPT will be required. Additionally, knowing in advance the final caisson penetration PPT could be located from below within the soil to measure pore pressures during and after installation.

Further experiments are necessary in clay to confirm or not the parameter values of the yield surface and flow rule expressions presented in this investigation. In particular, experiments with load ratios different to one should be considered. The evaluation of the effect of different consolidation times on the moment response of suction caissons is also suggested.

Finally, research that integrates the experimental results with hyperplasticity formulations is necessary. It is suggested that a parametric calibration study of hyperplasticity models with experimentally obtained parameter values should be pursued to use those models with confidence in the design of suction caisson foundations for offshore wind turbines.

# REFERENCES


Aldwinckle, C. G. (1994). The installation of offshore plated foundation for oil rigs. Final Year Project Report, Department of Engineering Science, University of Oxford

Allersma, H.G.B., Kirstein, A.A., Brinkgreve, R.B.J. and Ferres, B. (1999). Centrifuge and numerical modelling of methods to optimise the horizontal bearing capacity of suction piles. *International Offshore Mechanics and Arctic Engineering Conference* OMAE, St. Johns

Allersma, H.G.B., Kirstein, A.A., Brinkgreve, R.B.J. and Simon, T. (1999b). Centrifuge and numerical modelling of horizontally loaded suction piles. *Proceedings of the* $9^{th}$ *International Symposium on Offshore and Polar Engineering Conference*, Brest, 711-717

Allersma, H.G.B., Hogervorst, J.R. and Pimoulle, M. (2001). Centrifuge modelling of suction pile installation using a percussion technique. *Proceedings of the* $11^{th}$ *International Offshore and Polar Engineering Conference* ISOPE, Stavanger, 2: 260-265

Andersen, K., Dyvik, R., Schrøder, K., Hansteen, O. and Bysveen, S. (1993). Field tests of anchors in clay II: Predictions and interpretation. *Journal of the Geotechnical Engineering Division* ASCE **119**, No 10, 1532-1549

Andersen, K. and Jostad, H. P. (1999). Foundation design of skirted foundations and anchors in clay. *Offshore Technology Conference*, Houston, Paper 10824

Andersen, K. and Jostad, H. P. (2002). Shear strength along outside wall of suction anchors in clay after installation. *Offshore and Polar Engineering Conference*, ISOPE, Kitakyushu, 785-794

Andersen, K.H., Murff, J.D., Randolph, M.F., Clukey, E.C., Erbrich, C.T., Jostad, H.P., Hansen, B., Aubeny, C., Sharma, P. and Supachawarote, C. (2005). Suction anchors for deepwater applications. *International Symposium on Frontiers in Offshore Geotechnics*, ISFOG, Perth, 3-30

Aubeny, C. and Murff, J. (2003). Simplified limit solutions for the capacity of suction anchors under undrained conditions. *Ocean Engineering* **32**, 864-877

Aubeny, C., Han, S. and Murff, J. (2003). Suction caisson capacity in anisotropic, purely cohesive soil. *International Journal of Geomechanics*, Vol.3, No. 2, 225-235

Ausilio, E. and Conte, E. (2005). Influence of groundwater on the bearing capacity of shallow foundations. *Canadian Geotechnical Journal* **42**, 663-672

Bell, R.W. (1991). The analysis of offshore foundations subjected to combined loading. *MSc thesis*, University of Oxford

Beresford, J.M. (2003). Economic comparison and laboratory simulation of field scale tests of foundations for offshore wind energy structures. Final Year Project Report, Department of Engineering Science, University of Oxford

Bienen, B., Byrne, B.W., Houlsby, G.T. and Cassidy, M.J. (2006). Investigating six degree of freedom loading of shallow foundations on sand. *Géotechnique* **56**, No 6, 367-379

Bolton, M.D. (1986). The strength and dilatancy of sands. *Géotechnique* **36**, No 1, 65-78 and discussion *Géotechnique* **37**, No 2, 219-226

Bolton, M.D. and Lau, C.K. (1993). Vertical bearing capacity factors for circular and strip footings on Mohr-Coulomb soil. *Canadian Geotechnical Journal* **30**, 1024-1033

Boulbibane, M. and Ponter, A.R.S. (2005). Linear matching method for limit load problems using the Drucker-Prager yield condition. *Géotechnique* **55**, No 10, 731-739

Boussinesq, J. (1878). Équilibre d'élasticité d'un solide isotrope sans pesanteur, supportant différents poids. *Compte Rendus à l'Académie des Sciences Paris* **86**, 1260-1263

Bowden, R.K. (1988). Compression behaviour and shear strength characteristics of a natural silty clay sedimented in the laboratory. *DPhil thesis*, University of Oxford

Bowles, J.E. (1996). *Foundation Analysis and Design.* McGraw-Hill

Bowman, E. T., Soga, K., and Drummond, W. (2001). Particle shape characterisation using Fourier descriptor analysis. *Géotechnique* **51**, No 6, 545-554

Bransby, M.F. and Randolph, M.F. (1998). Combined loading of skirted foundations. *Géotechnique* **48**, No 5, 637-655

Bransby, P.L. (1973). Cambridge contact stress transducers. Report No. CUED/C-SOILS/LN2, Engineering Department, University of Cambridge

Brinch Hansen, J. (1970). A revised and extended formula for bearing capacity. Bulletin No 28, Danish Geotechnical Institute, Copenhagen, 5-11

British Geological Survey (2004). Seabed sediments in the Irish Sea. Walney Offshore Windfarm. Scoping Report, Consortia Dong and Statkraft

Brown, G. A. and Nacci, V. A. (1971). Performance of hydrostatic anchors in granular soils. *Offshore Technology Conference*, Houston, Paper 1472

Butterfield, R. and Ticof, J. (1979). Design parameters for granular soils, discussion contribution. *Proceedings $7^{th}$ International Conference of Soil Mechanics and Foundation Engineering*, Brighton, Vol. 4, 259-261

Butterfield, R. (1980). A simple analysis of the load capacity of rigid footings on granular materials. *Journée de Géotechnique*, ENTPE, Lyon, 128-134

Butterfield, R. and Gottardi, G. (1994). A complete tree-dimensional failure envelope for shallow footings on sand. *Géotechnique* **44**, No 1, 181-184

Butterfield, R., Houlsby, G.T. and Gottardi, G. (1997). Standardized sign conventions and notation for generally loaded foundations. *Géotechnique* **47**, No 5, 1051-1054

Byrne, B.W. (2000). Investigations of suction caissons in dense sand. *DPhil thesis*, University of Oxford

Byrne, B.W. and Houlsby, G.T. (2001). Observations of footing behaviour on loose carbonate sands. *Géotechnique* **51**, No. 5, 463-466

Byrne, B.W. and Cassidy, M.J. (2002). Investigating the response of offshore foundations in soft clay soils. *International Offshore Mechanics and Arctic Engineering Conference* OMAE, Oslo, paper 28057

Byrne, B.W., Houlsby, G.T., Martin, C.M. and Fish, P.M. (2002). Suction caisson foundations for offshore wind turbines. *Journal of Wind Engineering* **26**, No 3, 145-155

Byrne, B.W. (2003). Personal communication

Byrne, B.W. and Houlsby, G.T. (2003). Foundation for offshore wind turbines. *Phil. Trans. of the Royal Society of London*, Series **A 361**, 2909-2300

Byrne, B.W., Villalobos, F., Houlsby, G.T. and Martin, C.M. (2003). Laboratory testing of shallow skirted foundations in sand. *Proceeding BGA International Conference on Foundations*, Newson ed., Thomas Telford, Dundee, 161-173

Byrne, B.W. and Houlsby, G.T. (2005). Investigating six degree-of-freedom loading on shallow foundations. *International Symposium on Frontiers in Offshore Geotechnics*, ISFOG, Perth, 477-482

Byrne, B.W. and Houlsby, G.T. (2006). Assessing novel foundation options for offshore wind turbines. *World Maritime Technology Conference*, London

Cao, J., Audibert, J. and Al-Khafaji, Z. (2002). Excess pore pressure induced by installation of suction caissons in NC clay. *Proceedings of the Society for Underwater Technology SUT Conference*, London, 405-412

Cassidy, M.J. (1999). Non-linear analysis of jack-up structures subjected to random waves. *DPhil thesis*, University of Oxford

Cassidy, M.J. and Houlsby, G.T. (2002). Vertical bearing capacity factors for conical footings on sand. *Géotechnique* **52**, No. 9, 687-692

Cassidy, M.J., Byrne, B.W. and Houlsby G.T. (2002). Modelling the behaviour of circular footings under combined loading on loose carbonate sand. *Géotechnique* **52**, No. 10, 705-712

Cassidy, M.J., Byrne, B.W. and Randolph, M.F. (2004). A comparison of the combined load behaviour of spudcan and caisson foundations on soft normally consolidated clay. *Géotechnique* **54**, No. 2, 91-106

Cerato, A. B. and Lutenegger A. J. (2006). Bearing capacity of square and circular footings on a finite layer of granular soil underlain by a rigid base. *Journal of Geotechnical and Geoenvironmental Engineering* **132**, 1496-1501

Charles S. (1994). The design and installation of plated foundation for offshore structures. Final Year Project Report, Department of Engineering Science, University of Oxford

Chaudhary, S.K. and Kuwano, J. (2003). Anisotropic multiple yielding of dense Toyoura sand in $p$'-constant shear plane. *Soils and Foundations* **43** (4), 59-69

Chen, W. and Randolph, M. (2004). Radial stress changes around caissons installed in clay by jacking and by suction. *International Offshore and Polar Engineering Conference*, ISOPE, Toulon, 493-499

Clukey, E.C., Morrison, M.J., Garnier, J. and Corté, J.F. (1995). The response of suction caissons in normally consolidated clays to cyclic TLP loading conditions. *Offshore Technology Conference*, Houston, Paper 7796

Clukey, E.C., Aubeny, C.P. and Murff, J.D. (2003). Comparison of analytical and centrifuge model tests for suction caissons subjected to combined loads. *International Conference on Offshore Mechanics and Arctic Engineering*, Cancún, Paper OMAE 2003-37503

Colliat, J.L. and Dendani, H. (2002). Girassol: Geotechnical design analyses and installation of the suction anchors. *Proceedings of the Society for Underwater Technology SUT Conference*, London, 107-119

Collins, I.F. and Houlsby, G.T. (1997). Application of thermomechanical principles to the modelling of geotechnical materials. *Proceedings Royal Society of London* Series **A 453**, 1975-2001

Coop, M.R., Sorensen, K.K., Bodas Freitas, T. and Georgoutsos, G. (2004). Particle breakage during shearing of a carbonate sand. *Géotechnique* **54**, No. 3, 157-163

Craig, R.F. (2001). *Soil Mechanics*. Sixth edition, Spon Press

Das, B.M. (2003). *Principles of Foundation Engineering*. Fifth edition, Thomson

Davis, R.O. and Selvadurai, A.P.S. (1996). *Elasticity and Geomechanics*. Cambridge University Press

De Beer, E.E. (1965). Influence of the mean normal stress on the shearing strength of sand. *Proceeding 6$^{th}$ International Conference of Soil Mechanics and Foundation Engineering*, Montreal **1**, 165-169

de Nicola, A. and Randolph, M.F. (1997). The plugging behaviour of driven and jacked piles in sand. *Géotechnique* **47**, No. 4, 841-856

de Santa Maria, P.E.L. (1988). Behaviour of footings for offshore structures under combined loads. *DPhil thesis*, University of Oxford

Dean, E.T.R., James, R.G., Schofield, A.N., Tan, F.S.C. and Tsukamoto, Y. (1992). The bearing capacity of conical footings on sand in relation to the behaviour of spudcan footings of jackups. *Proceedings of the Wroth Memorial Symposium, Predictive Soil Mechanics*, Oxford, 230-253. London, Thomas Telford

Deng, W. and Carter, J.P. (2000). A theoretical study of the vertical uplift capacity of suction caissons. *International Offshore and Polar Engineering Conference*, ISOPE, Seattle, 342-349

Department of Trade and Industry (2003). Energy White Paper; our energy future - creating a low carbon economy. DTI, London. Available at www.dti.gov.uk/files/file10719.pdf

Doherty, J.P. and Deeks, A.J. (2003). Elastic response of circular footings embedded in a non-homogeneous half-space. *Géotechnique* **53**, No. 8, 703-714

Doherty, J.P., Houlsby, G.T. and Deeks, A.J. (2005). Stiffness of flexible caisson foundations embedded on nonhomogeneous elastic soil. *Journal of Geotechnical and Geoenvironmental Engineering* ASCE **131**, No. 12, 1498-1508

Dyvik, R., Andersen, K., Hansen, S.B. and Christophersen, H.P. (1993). Field tests of anchors in clay I: Description. *Journal of the Geotechnical Engineering Division*, ASCE,

**119**, No 10, 1515-1531

Edwards, D.H., Zdravkovic, L. and Potts, D.M. (2005). Depth factors for undrained bearing capacity. *Géotechnique* **55**, No 10, 755-758

Einav, I. (2005). Energy and variational principles for piles in dissipative soil. *Géotechnique* **55**, No 7, 515-525

El-Gharbawy, S.L. (1998). The pullout capacity of suction caisson foundations for tension leg platforms. *PhD thesis*, University of Texas at Austin

Erbrich, C.T. and Tjelta, T.I. (1999). Installation of bucket foundations and suction caissons in sand - Geotechnical performance. *Offshore Technology Conference*, Houston, Paper 10824

Evans, K.M. (1987). A model study of the end bearing capacity of piles in layered calcareous soils. *DPhil thesis*, University of Oxford

Feld, T., Rasmussen, J.L. and Sørensen, P.H. (1999). Structural and economic optimization of offshore wind turbine support structure and foundation. *International Offshore Mechanics and Arctic Engineering Conference* OMAE, New Foundland

Feld, T. (2001). Suction buckets, a new innovative foundation concept, applied to offshore wind turbines. *PhD thesis*, Aalborg University

Ferguson, M. (1998). Support structure concepts for offshore wind turbines. *Proceedings of the twentieth British Wind Energy Association Conference*, BWEA, Cardiff

Finnie, I.M.S. (1993). Performance of Shallow Foundations in Calcareous Soil. *PhD thesis*, University of Western Australia

Flemming, W.G.K., Weltman, A.J., Randolph, M.F. and Elson, W.K. (1994). *Piling engineering*. Blackie & Sohn Ltd

Fuglsang, L.D. and Steensen-Bach, J.O. (1991). Breakout Resistance of Suction Piles in Clay. *Proceedings of the International Conference Centrifuge 91*, Ko and Mclean eds, Balkema, Rotterdam, 153-159

Georgiadis, M. and Butterfield, R. (1988). Displacements of footings on sand under eccentric and inclined loads. *Canadian Geotechnical Journal* **23**, 199-212

Goodman, L.J., Lee, C.N. and Walker, F.J. (1961). The feasibility of vacuum anchorage in soil. *Géotechnique* **11**, No. 4, 356-359

Gottardi, G. and Butterfield, R. (1993). On the bearing capacity of surface footings on sand under general planar loads. *Soils and Foundations* **33**, No. 3, 68-79

Gottardi, G. and Butterfield, R. (1995). The displacement of a model rigid surface footing on dense sand under general planar loading. *Soils and Foundations* **35**, No. 3, 71-82

Gottardi, G., Houlsby, G.T. and Butterfield, R. (1999). The plastic response of circular footings on sand under general planar loading. *Géotechnique* **49**, No. 4, 453-470

Gourvenec, S. (2003). Alternative design approach for skirted footings under general combined loading. *Proceeding BGA International Conference on Foundations*, Newson ed., Thomas Telford, Dundee, 341-349

Gourvenec, S. and Randolph, M. (2003). Effect of strength non-homogeneity on the

shape of failure envelopes for combined loading of strip and circular foundations on clay. *Géotechnique* **53**, No 6, 575-586

Gourvenec, S., Randolph, M. and Kingsnorth, O. (2006). Undrained bearing capacity of square and rectangular footings. *International Journal of Geomechanics* **6**, 147-157

Graham, J., Pinkney, R.B., Lew, K.V. and Trainor, P.G.S. (1982). Curve-fitting and laboratory data. *Canadian Geotechnical Journal* **19**, 201-205

Gue, S.S. (1984). Ground heave around driven piles in clay. *DPhil thesis*, University of Oxford

Handy, R.L. (1985). The arch in soil arching. *Journal of the Geotechnical Engineering Division*, ASCE, **111**, No 3, 302-318

Handy, R.L. (2004). Anatomy of an error. *Journal of Geotechnical and Geoenvironmental Engineering* **130**, No. 7, 768-771

Hardin, B.O. and Richart, F.E. (1963). Elastic wave velocities in granular soils. *Journal of the soil mechanics and foundation division* ASCE, Vol. **89**, No. SM1 33-65

Helfrich, S. C., Brazill R. L., and Richards, A. F. (1976). Pullout characteristics of a suction anchor in sand. *Offshore Technology Conference*, Houston, Paper 2469

Hight, D.W., Bond, A.J. and Legge, J.D. (1992). Characterization of the Bothkennar clay: an overview. *Géotechnique* **42**, No. 2, 303-347

Hight, D.W., Lawrence, D.M., Farquhar, G.B., Milligan, G.W.E., Gue, S.S. and Potts, D.M. (1996). Evidence of scale effects in the end bearing capacity of open-ended piles in sand. *Offshore Technology Conference*, Houston, Paper 7975

Hjiaj, M., Lyamin, A. and Sloan, S. (2004). Bearing capacity of a cohesive-frictional soil under non-eccentric inclined loading. *Computers and Geotechnics* **31**, No. 6, 491-516

Hjiaj, M., Lyamin, A. and Sloan, S. (2005). Numerical limit analysis solutions for the bearing capacity factor $N_\gamma$. *International Journal of Solids and Structures* **42**, 1681-1704

Honjo, Y. and Amatya, S. (2005). Partial factors calibration based on reliability analyses for square footings on granular soils. *Géotechnique* **55**, No 6, 479-491

Houlsby, G.T. (1981). A study of plasticity theories and their applicability to soils. *PhD thesis*, University of Cambridge

Houlsby, G.T. and Martin, C.M. (1992). Modelling of the behaviour of foundations of jack-up units on clay. *Proceedings of the Wroth Memorial Symposium, Predictive Soil Mechanics*, Oxford, 339-358. London, Thomas Telford

Houlsby, G.T. and Byrne, B.W. (2000). Suction caisson foundations for offshore wind turbines and anemometer masts. *Journal of Wind Energy* **24**, No. 4, 249-255

Houlsby, G.T. and Puzrin, A.M. (2000). A thermomechanical framework for constitutive models for rate-independent dissipative materials. *International Journal of Plasticity* **16**, No. 9, 1017-1047

Houlsby, G.T. and Byrne, B.W. (2001). Discussion on: Sieffert, J.-G. and Bay-Gress, Ch. (2000). Comparison of European bearing capacity calculation methods for shallow foundations. *Proceedings of the ICE, Geotechnical Engineering*, **143**, 65-74, *Geotechnical*

*Engineering* **149**, 63-64

Houlsby, G.T. and Cassidy, M.J. (2002). A plasticity model for the behaviour of footings on sand under combined loading. *Géotechnique* **52**, No. 2, 117-129

Houlsby, G.T. (2003). Modelling of shallow foundations for offshore structures. BGA *International Conference on Foundations*, Newson ed., Thomas Telford, Dundee, 11-26

Houlsby, G.T. and Byrne, B.W. (2005a). Design procedures for installation of suction caissons in clay and other materials. *Proceedings of the ICE, Geotechnical Engineering* **158**, No. 2, 75-82

Houlsby, G.T. and Byrne, B.W. (2005b). Design procedures for installation of suction caissons in sand. *Proceedings of the ICE, Geotechnical Engineering* **158**, No. 3, 135-144

Houlsby, G.T., Kelly, R.B., Huxtable, J. and Byrne, B.W. (2005a). Field trials of suction caissons in clay for offshore wind turbine foundations.*Géotechnique* **55**, No 4, 287-296

Houlsby, G.T., Amorosi, A. and Rojas, E. (2005b). Elastic moduli of soils dependent on pressure: a hyperelastic formulation. *Géotechnique* **55**, No 5, 383-392

Houlsby, G.T., Kelly, R.B. and Byrne, B.W. (2005c). The tensile capacity of suction caissons in sand under rapid loading. *International Symposium on Frontiers in Offshore Geotechnics*, ISFOG, Perth, 405-410

Houlsby, G.T., Kelly, R.B., Huxtable, J. and Byrne, B.W. (2006). Field trials of suction caissons in sand for offshore wind turbine foundations. *Géotechnique* **56**, No 1, 3-10

House, A. (2002). Suction caisson foundations for buoyant offshore facilities. *PhD thesis*, University of Western Australia

House, A. R. and Randolph, M. F. (2001). Installation and pull-out capacity of stiffened suction caissons in cohesive sediments. $11^{th}$ *International Offshore and Polar Engineering Conference* ISOPE, Stavanger, 2: 574-580

HR Wallingford (2004). Scour assessment of suction caisson founded wind turbines. Project report: Future energy solutions, the application of suction caissons foundations to offshore wind turbines. DTI

Ibsen, L.B., Schakenda, B. and Nielsen, S.A. (2003). Development of the bucket foundation for offshore wind turbines, a novel principle. *Proceeding US Wind Energy Conference*, Boston (in 'Foundation Engineering Papers', no. 20, 1398-6465, paper no. R0308)

Ibsen, L.B., Liingaard, M. and Nielsen, S.A. (2005). Bucket foundation, a status. *Copenhagen offshore wind conference and exhibition*

Ishihara, K. (1996). *Soil behavior in earthquake geotechnics*. Clarendon Press, Oxford

Jardine, R., Chow, F., Overy, R. and Standing, J. (2005). *ICP Design Methods for Driven Piles in Sands and Clays*. Thomas Telford

Johnson, K. (1999). Partially drained loading of shallow foundations. Final Year Project Report, Department of Engineering Science, University of Oxford

Kelly, R.B., Byrne, B.W., Houlsby, G.T. and Martin, C.M. (2003). Pressure chamber testing of model caisson foundations in sand. *Proceeding BGA International Conference on Foundations*, Newson ed., Thomas Telford, Dundee, 421-431

Kelly, R.B., Byrne, B.W., Houlsby, G.T. and Martin, C.M. (2004). Tensile loading of model caisson foundations for structures on sand. *International Offshore and Polar Engineering Conference*, ISOPE, Toulon, 638-641

Kelly, R.B., Houlsby, G.T. and Byrne, B.W. (2006a). A comparison of field and laboratory tests of caisson foundations in sand and clay. *Géotechnique* **56**, No. 9, 617-626

Kelly, R.B., Houlsby, G.T. and Byrne, B.W. (2006b). Transient vertical loading of model suction caissons in a pressure chamber. *Géotechnique*, **56**, No. 10, 665-675

Kim, Y., Kim, S., Park, J., Kim, S., Kim, H. and Kim, K. (2001). A centrifuge study of suction pile installation in sand. $11^{th}$ *International Offshore and Polar Engineering Conference* ISOPE, Stavanger, 2: 615-619

Kobayashi, S. (2005). Hybrid type rigid plastic finite element analysis for bearing capacity characteristics of surface uniform loading. *Soils and Foundations* **45**, No 2, 17-27

Kühn, M. (2002). Offshore wind farms. *Wind Power Plants: Fundamentals, design, construction and operation*, Gasch and Twele eds., 365-384

Kumar, J. (2003). $N_\gamma$ for rough strip footing using the method of characteristics. *Canadian Geotechnical Journal* **40**, No. 3, 669-674

Larsen, P. C. (1989). Suction anchors as an anchoring system for floating offshore constructions. *Offshore Technology Conference*, Houston, Paper 6029

Lau, C.K. (1988). Scale effects in tests on footings. *PhD thesis*, University of Cambridge

Lee, J., Salgado, R. and Kim, S. (2005). Bearing capacity of circular footings under surcharge using state-dependent finite element analysis. *Computers and Geotechnics* **32**, No. 6, 445-457

Lee, J. and Salgado, R. (2005). Estimation of bearing capacity of circular footings on sand based on cone penetration test. *Journal of Geotechnical and Geoenvironmental Engineering* **131**, No. 4, 442-452

Lehane, B.M., Gaudin, C. and Schneider, J.A. (2005). Scale effects on tension capacity for rough piles buried in dense sand. *Géotechnique* **55**, No. 10, 709-719

Lings, M.L. and Dietz, M.S. (2005). The peak strength of sand-steel interfaces and the role of dilation. *Soils and Foundations* **45**, No. 6, 1-14

Luzzani, L. and Coop, M.R. (2002). On the relationship between particle breakage and the critical state of sands. *Soils and Foundations* **42**, No. 2, 71-82

Mangal, J.K. (1999). Partially drained loading of shallow foundations on sand. *DPhil thesis*, University of Oxford

Martin, C.M. (1994). Physical and numerical modelling of offshore foundations under combined loads. *DPhil thesis*, University of Oxford

Martin, C.M. and Houlsby, G.T. (1999). Jackup units on clay: structural analysis with realistic modelling of spudcan behaviour. *Offshore Technology Conference*, Houston, Paper OTC 10996

Martin, C.M. and Houlsby, G.T. (2000). Combined loading of spudcan foundations on clay: laboratory tests. *Géotechnique* **50**, No. 4, 325-337

Martin, C.M. and Houlsby, G.T. (2001). Combined loading of spudcan foundations on clay: numerical modelling. *Géotechnique* **51**, No. 8, 687-699

Martin, C.M. (2001). Vertical bearing capacity of skirted circular foundations on Tresca soil. *Proceedings 15$^{th}$ International Conference on Soil Mechanics and Geotechnical Engineering*, Istanbul, Vol. 1, 743-746

Martin, C.M. (2003). User guide for ABC - Analysis of Bearing Capacity. Report No. OUEL 2261/03, Department of Engineering Science, University of Oxford

Martin, C.M. (2003b). New software for rigorous bearing capacity calculations. *International BGA Conference on Foundations*, Newson ed., Thomas Telford, Dundee, 581-592

Martin, C.M. (2004). Discussion of "Calculations of bearing capacity factor $N_\gamma$ using numerical limit analyses" by Ukritchon *et al. Journal of Geotechnical and Geoenvironmental Engineering* **130**, No. 10, 1106-1107

Martin, C.M. (2005). Exact bearing capacity calculations using the method of characteristics. *Proc. 11$^{t}$h International Conference of IACMAG*, Turin, Vol. 4, 441-450

Masing, G. (1926). Eigenspannungen und Verfestigung beim Messing. Proceedings of the 2$^{nd}$ International Congress of Applied Mechanics, Zurich

McCarthy, D.F. (1998). *Essentials of Soil Mechanics and Foundations. Basic Geotechnics*. Fifth edition, Prentice Hall

McDowell, G.R. (2002). On the yielding and plastic compression of sand. *Soils and Foundations* **42**, No. 1, 139-145

Meyerhof, G.G. (1951). The ultimate bearing capacity of foundations. *Géotechnique* **2**, No 4, 301-332

Meyerhof, G.G. (1963). Some recent research on the bearing capacity of foundations. *Canadian Geotechnical Journal* **1**, 16-26

Mitchell, J.K. and Soga, K. (2005). *Fundamentals of soil behavior*. Third edition, John Wiley & Sons, New Jersey

Montrasio, L. and Nova, R. (1997). Settlements of shallow foundations on sand: geometrical effects. *Géotechnique* **47**, No 1, 49-60

Muir Wood, D. (2004). *Geotechnical modelling*. London, Spon Press

Ngo-Tran, C.L. (1996). The Analysis of Offshore Foundations Subjected to Combined Loading. *DPhil thesis*, University of Oxford

Nguyen-Sy, L. and Houlsby, G.T. (2005). The theoretical modelling of a suction caisson foundation using hyperplasticity theory. *International Symposium on Frontiers in Offshore Geotechnics*, ISFOG, Perth, 417-423

Nguyen-Sy, L. (2006). The theoretical modelling of circular shallow foundations for offshore wind turbines. *DPhil thesis*, University of Oxford

Nova, R. and Montrasio, L. (1991). Settlements of shallow foundations on sand. *Géotechnique* **41**, No 2, 243-256

Nova, R. and di Prisco, C. (2003). The macro-element concept and its application in geotechnical engineering. *Proceeding International Symposium FONDSUP 2003*, J.-P.

Magnan and N. Droniuc eds., Paris, Presse ENPC,1, 389-396

Nutt, N.R.F. (1993). Development of the cone pressuremeter. *DPhil thesis*, University of Oxford

Office of Public Sector Information (2002). The Renewables Obligation Order 2002. Statutory Instrument 2002 no. 914, London. The Stationery Office. Available at www.opsi.gov.uk/si/si2002/20020914.htm

Osman, A.S. and Bolton, M.D. (2005). Simple plasticity-based prediction of the undrained settlement of shallow circular foundations on clay. *Géotechnique* **55**, No 6, 435-447

Ovesen, N.K. (1979). The use of physical models in design. *Proceedings 7th International Conference of Soil Mechanics and Foundation Engineering*, Brighton, Vol. 4, 318-323

Poorooshasb, H.B., Holubec, I. and Sherbourne, A.N. (1967). Yielding and flow of sand in triaxial compression: Part I. *Canadian Geotechnical Journal* **4**, No 4, 376-388

Poulos, H.G. and Davis, E.H. (1974). *Elastic soultions in soil and rock mechanics.* Wiley, New York

Prandtl, L. (1920). Über die Härte plastischer Körper. *Nachrichten Gesellshaft Wissenschaft*, Göttingen, math.-phys. Klasse, 74 - 85

Przewlócki, J. (2005). A stochastic approach to the problem of bearing capacity by the method of characteristics. *Computers and Geotechnics* **32**, No. 5, 370-376

Puzrin, A.M. and Houlsby, G.T. (2000). A Thermomechanical Framework for Rate-Independent Dissipative Materials with Internal Functions. *International Journal of Plasticity* **17**, 1147-1165

Puzrin, A.M. and Houlsby, G.T. (2001). Fundamentals of Kinematic Hardening Hyperplasticity. *International Journal of Solids and Structures* **38**, No. 21, 3771-3794

Puzrin, A.M. and Houlsby, G.T. (2003). Rate Dependent Hyperplasticity with Internal Functions. *Journal of the Engineering Mechanics Division* **129**, No. 3, 252-263

Rao, S. N., Ravi, R. and Ganapathy, C. (1997). Pullout behaviour of model suction anchors in soft marine clay. *International Offshore and Polar Engineering Conference*, ISOPE, Honolulu 740-744

Randolph, M.F., Leong, E.C. and Houlsby, G.T. (1991). One-dimensional analysis of soil plugs in pipe piles. *Géotechnique* **41**, No 4, 587-598

Randolph, M.F., O'Neill, M.P., Stewart, D.P. and Erbrich, C.T. (1998). Performance of suction anchors in fine-grained calcareous soils. *Offshore Technology Conference*, Houston, OTC paper 8831

Randolph, M.F. and House, A.R. (2002). Analysis of suction caisson capacity in in clay. *Offshore Technology Conference*, Houston, OTC paper 14236

Rauch, A.F., Olson, R.E., Luke, A.M. and Mecham, E.C. (2003). Measured response during laboratory installation of suction caissons. *International Offshore and Polar Engineering Conference*, ISOPE, Honolulu, 780-787

Reissner, H. (1924). Zum Erddruckproblem. *Proceedings 1st International Congress on Applied Mechanics*, Delft, 295-311

Richards, N.P. and Barton, M.E. (1999). The Folkestone Bed sands: microfabric and strength. *Quarterly Journal of Engineering Geology*, **32** 21-44

Roscoe, K.H. and Schofield, A.N. (1957). The stability of short pier foundations in sand. *Discussion. British Welding Journal*, 12-18

Salgado, R., Lyamin, A.V., Sloan, S.W. and Yu, H.S. (2004). Two- and three-dimensional bearing capacity of foundations in clay. *Géotechnique* **54**, No 5, 297-306

Sanham, S.C. (2003). Investigation into the installation of suction assisted caisson foundations. Final Year Project Report, Department of Engineering Science, Oxford University

Sassa, S. and Sekiguchi, H. (2001). Analysis of wave-induced liquefaction of sand beds. *Géotechnique* **51**, No 2, 115-126

Schnaid, F. (1990). A study of the cone pressuremeter test in sand. *DPhil thesis*, University of Oxford

Senpere, D. and Auvergne, G.A. (1982). Suction anchor piles - a proven alternative to driving or drilling. *Offshore Technology Conference*, Houston, OTC paper 4206

Sentenac, P., Lynch, R. J., and Bolton, M.D. (2001). Measurement of a side-wall boundary effect in soil columns using fibre-optics sensing. *International Journal of Physical Modelling in Geotechnics* **4**, 35-41

Sills, G. and Bartholomeeusen, G. (2001). Consolidation and strength measurements on Dibden Bay soil. Report SM18101, Department of Engineering Science, University of Oxford

Skempton, A.W. and Northey, R.D. (1952). The sensitivity of clays. *Géotechnique* **3**, No 1, 30-53

Smith, M.G. (1993). A laboratory study of the Marchetti dilatometer. *DPhil thesis*, University of Oxford

Smith, C. C. (2005). Complete limiting stress solutions for the bearing capacity of strip footings on a MohrCoulomb soil. *Géotechnique* **55**, No 8, 607-612

Sowers, G.F. (1979). *Introductory soil mechanics and foundations: geotechnical engineering.* Fourth edition, New York, Macmillan Publishing

Sparrevik, P. (2002). Suction pile technology and installation in deep waters. *Offshore Technology Conference*, Houston, paper 14241

Steensen-Bach, J.O. (1992). Recent model tests with suction piles in clay and sand. *Offshore Technology Conference*, Houston, Paper 6844

Taiebat, H.A. and Carter, J.P. (2000). Numerical studies of the bearing capacity of shallow foundations on cohesive soil subjected to combined loading. *Géotechnique* **50**, No 4, 409-418

Tan, F.S.C. (1990). Centrifuge and numerical modelling of conical footings on sand. *PhD thesis*, University of Cambridge

Terzaghi, K. (1943). *Theoretical soil mechanics.* New York, John Wiley & Sons

Terzaghi, K. and Peck, R. (1967). *Soil Mechanics in Engineering Practice.* New York, John Wiley & Sons

Ticof, J. (1977). Surface footing on sand under general planar loads. *PhD thesis*, University of Southampton

Tjelta, T.I., Guttormsen, T.R. and Hermstad, J. (1986). Large-scale penetration test at deepwater site. *Offshore Technology Conference*, Houston, Paper 5103

Tjelta, T.I. (1994) Geotechnical aspects of bucket foundations replacing piles for the Europipe 16/11-E jacket. *Offshore Technology Conference*, Houston, Paper 7379

Tjelta, T.I. (1995) Geotechnical experience from the installation of the Europipe jacket with bucket foundations. *Offshore Technology Conference*, Houston, Paper 7795

Tomlinson, M.J. (1999). *Foundation design and construction.* Sixth edition, Longman

Tran, M.N., Randolph, M.F. and Airey, D.W. (2004). Experimental study of suction installation of caissons in dense sand. *International Conference on Offshore Mechanics and Arctic Engineering*, Vancouver, Paper No OMAE2004-51076

Tran, M.N., Randolph, M.F. and Airey, D.W. (2005). Study of sand heave formation in suction caissons using particle image velocimetry (PIV). *International Symposium on Frontiers in Offshore Geotechnics*, ISFOG, Perth, 259-265

Tsukamoto, Y. (2005). Evaluating superposition errors in bearing capacity factors from Sokolovski's method of characteristics. *Soils and Foundations* **45**, No 3, 161-165

Uesugi, M. and Kishida, H. (1986). Frictional resistance at yield between dry sand and mild steel. *Soils and Foundations* **26**, No. 4, 139-149

Ukritchon, B., Whittle, A.J. and Klangvijit, C. (2003). Calculations of bearing capacity factor $N_\gamma$ using numerical limit analyses. *Journal of Geotechnical and Geoenvironmental Engineering* **129**, No. 6, 468-474

Vesic, A. S. (1975). Bearing capacity of shallow foundations. In *Foundation Engineering Handbook*, Winterkorn, H.F. and Fang, H.Y. eds., Van Nostrand, New York, 121-147

Villalobos, F., Byrne, B.W., Houlsby, G.T. and Martin, C.M. (2003a). Bearing capacity tests of scale suction caisson footings on sand: Experimental data. Report FOT0005/1, Department of Engineering Science, University of Oxford

Villalobos, F., Byrne, B.W., Houlsby, G.T. and Martin, C.M. (2003b). Moment loading tests of scale suction caisson footings on sand: Experimental data. Report FOT015/1, Department of Engineering Science, University of Oxford

Villalobos, F.A. (2004). An experimental study of cyclically loaded monopod suction caisson foundations for offshore wind turbines. *Eighth Young Geotechnical Engineer's Symposium*, BGA, Birmingham

Villalobos, F., Byrne, B.W., Houlsby, G.T. and Martin, C.M. (2004a). Cyclic moment loading tests of suction caisson footings on sand: Experimental data. Report FOT020/1, Department of Engineering Science, University of Oxford

Villalobos, F.A., Houlsby, G.T. and Byrne, B.W. (2004b). Suction caisson foundations for offshore wind turbines. *Proceedings $5^{th}$ Chilean Conference of Geotechnics (Congreso Chileno de Geotecnia)*, SOCHIGE, Santiago

Villalobos, F.A., Byrne, B.W. and Houlsby, G.T. (2005). Moment loading of caissons installed into saturated sand. *International Symposium on Frontiers in Offshore Geotech-*

*nics*, ISFOG, Perth, 411-416

Wang, M. C., Demars, K.R. and Nacci, V.A. (1977). Breakout capacity of model suction anchors in soil. *Canadian Geotechnical Journal* **14**, 246-257

Watson, P.G. (1999). Performance of skirted foundations for offshore structures. *PhD thesis*, University of Western Australia

Whittle, A.J, Germaine, J.T. and Cauble, D.F. (1998). Behavior of miniature suction caissons in clay. *Offshore site investigation and foundation behavious '98*, SUT, London, 279-300

Wroth, C.P. (1984). The interpretation of in situ soil tests. *Géotechnique* **34**, No 4, 449-484

Zeevaert, L. (1983). *Foundation engineering for difficult subsoil conditions*. Second edition, van Nostrand Reinhold

Ziegler, H. (1977). *An introduction to Thermodynamics*. North Holland, Amsterdam

Ziegler, H. (1983). *An introduction to Thermodynamics*. Second edition, North Holland, Amsterdam

Zhu, D., Lee, C. and Law, K. (2003). Determination of bearing capacity of shallow foundations without using superposition approximation. *Canadian Geotechnical Journal* **40**, 450-459

Zhu, M. and Michalowski, R.L. (2005). Shape factors for limit loads on square and rectangular footings. *Journal of Geotechnical and Geoenvironmental Engineering* **131**, No.2, 223-231

# Index